Spring 2019

A Miniaturized Phased Array Antenna Based on Novel Switch Line Phase Shifter Module

Rudra Lal Timsina
University of New Hampshire, Durham

A MINIATURIZED PHASED ARRAY ANTENNA BASED ON NOVEL SWITCH LINE PHASE SHIFTER MODULE

BY

RUDRA TIMSINA

Bachelor of Science in Electrical Engineering
University of New Hampshire, 2014

THESIS

Submitted to the University of New Hampshire
in Partial Fulfillment of the
Requirements for the Degree of

MASTER OF SCIENCE
IN
ELECTRICAL ENGINEERING

May 2019

This thesis has been examined and approved in partial fulfillment of the requirements for the degree of Master of Science in Electrical Engineering by:

Thesis Director, Dr. Richard A. Messner, Associate Professor of Electrical and Computer Engineering, University of New Hampshire

Dr. Michael J. Carter, Associate Professor of Electrical and Computer Engineering, University of New Hampshire

Dr. Wayne Smith, Senior Lecturer of Electrical and Computer Engineering, University of New Hampshire

On April 12, 2019

ACKNOWLEDGEMENTS

I would like to acknowledge my advisor Professor Richard Messner for his support and guidance to execute this project. He provided me an opportunity to carry out the graduate level research work at the University of New Hampshire. His advice was very influential in completing this project. I like to thank Northrop Grumman for sponsoring this work. I would also like to thank my thesis committee members, Dr. Michael Carter and Dr. Wayne Smith for accepting my request to be in my committee. I would like to thank the department chair, Dr. Kent Chamberlin for guiding me through problems and financially supporting me to attend a conference in Singapore related to this project.

I can't help without thanking James Abare, who assisted me with antenna fabrication. I also like to thank my fellow graduate student Jean Lambert Kubwimana for his help with test setup in the anechoic chamber and discussions with various problems while working on this project. Lastly, I would like to thank my family members, and friends who supported me continuously throughout my education process.

Rudra Timsina

TABLE OF CONTENTS

LIST OF FIGURES

LIST OF TABLES

ABSTRACT

A Miniaturized Phased Array Antenna based on Novel Switch Line Phase Shifter Module

By

Rudra Timsina

A miniaturized phased array antenna with a uniquely designed switch line phase shifter to obtain a steerable beam pattern is presented. A 1x4 phased array patch antenna is designed at 5 GHz using Rogers dielectric material with a relative permittivity of 6.15 and a thickness of 1.524 mm. Each element of the probe fed PAA are connected to a phase shifter on a different dielectric substrate. The phase shifter has four equal length microstrip lines placed in a circular fashion around a via that connects to the antenna at the center. The addition of each microstrip line is designed to provide a phase shift of 90º. This design provides the ability to place the phase shifter and feed to the antenna in space constrained locations.

The maximum steering angle obtained was ±45º. This design is appropriate for Wi-Fi applications that requires directional beam pattern, Multiple Input Multiple Output (MIMO) communications, scanning radars, and other applications requiring steerable beam pattern. This design is patent pending.

CHAPTER 1: INTRODUCTION

1.1 Problem Statement

There are many problems which would benefit from an antenna capable of transmitting and receiving signals from a desired known direction. Before cable television, the directional Yagi antennas used had to bemanually adjusted at the right direction to receive a strong signal. Until 2016, 21 percent of US households depended on antenna reception for at least one televison in their home [1]. The antenna thus needed to be positioned at the right direction to maximize received signal strength from a desired broadcast station.

Human exposure to electromagnetic radiation due to cell phone use has shown effects on human health [2]. The uses of omnidirectional antenna inside a cell phone transmits the signal with equal strength in all directions. As a result, a part of signal energy is transmitted to the user's body as shown in *Figure 1*.

Figure 1: Cellphone radiation [3].

Other problems which arise include call failure in large crowds due to base station signal issues. The use of Single Input Single Output (SISO) antenna systems has limited

capacity. Similarly, the onmidirectoinal antennas used in WiFi routers for home use, trasmit signals with equal strength in all directions. The signal is also transmitted outside of the house where no one is using the WiFi service thus wasting signal energy. A directional antenna would reduce this signal spillage, at least from one direction.

A part of these problems exist due to the lack of affordable and compact antenna arrays. The realization of a compact antenna array capable of transmitting and receiving signals to and from a desired direction that supports multipath propagation can partially mitigate many problems.

Phased Array Antennas (PAA) are widely used for various applications requiring fixed or steerable beam patterns. These antennas provide control over the direction and beam pattern without mechanically adjusting the antenna position. The beam produced by the antenna can be steered in a desired angle by changing the excitation phase and amplitude of individual antenna elements. The PAA provides flexibility to receive a signal from a direction where the signal path is not obstructed and transmit a signal in any preferred direction. The applications of the traditional PAA were limited to aerospace and military use due to high cost, complexity, and the size of the antenna. The use of such antennas is found mostly in space-based applications [4] and military radars [5]. To obtain a directional antenna pattern, each antenna element in an array must be fed through a phase shifter. The realization of a mechanical phase shifter on each antenna element makes an antenna costly and bulky. Therefore, the implementation of such antennas on a small electronic device is difficult due to area constraints.

To reduce the size and bulkiness of an antenna, electrical phase shifters are more desirable than mechanical phase shifters. A Butler Matrix [6] and switch-line phase shifter

are some of the popular electrical phase shifters used in antenna arrays. To reduce the size of an antenna, a dual band Butler matrix is implemented on a phased array [6]. As the number of antenna elements increases, the number of such phase shifters must increase, and as a result, the size of the antenna gets larger. The number of input and output ports in a Butler matrix is equal. Excitation of each input port provides a specific directional beam pattern of an antenna. The direction of an antenna beam can be controlled using this method; however, the phase shift on each antenna element cannot be controlled independently. Therefore, a broadside beam cannot be obtained using this method. A Butler matrix can be formed with 4, 8 or 16 input/output ports. Hence, an antenna array with a different number of antenna elements cannot be realized. The Butler matrix must be stacked up if it is used to feed a planar array, thus increasing space and complexity of the design.

1.2 Objectives

The research advancement in patch antenna and microstrip-based phase shifters makes it possible to realize antenna arrays for a wide range of applications. Today, antenna arrays are employed on Wi-Fi, LTE technology [7], and health care applications [8]. In this project, we design a phase shifter for a four-element linear patch antenna array. The antenna is designed at 5 GHz; however, the concept of the phase shifter can be applicable for diverse applications in other frequency bands. Our goal is to design a phase shifter small enough to fit within the antenna element spacing so that its realization is possible under each antenna unit.

In a switch-line phase shifter, the input signal is routed through different length transmission lines so that the signal reaches the antenna at different times. A true time delay

is obtained using a switch-line phase shifter as in [9] and [10]. A four-bit switch-line phase shifter is realized in [9] using Micro-electro-mechanical switches (MEMS) where different length transmission lines are switched to obtain desired phase shifts. In [10], a constant phase shift is produced by switching a reference transmission line with a phase shifting line. In current designs, the length of the transmission lines switched to obtain phase shifts are longer and do not fit within antenna element spacing. In our proposed design, the phase shift is provided by extending a transmission line using RF switches along a circular path around the via that feeds the antenna. If the circular traces are branched at four equal lengths to feed the coaxial fed antenna at the center, four phases of 0º, 90º, 180º, and 270º is expected to be achieved. The uses of the Butler matrix in modern wireless communications [11] and 5G technologies [12] can be substituted with the proposed design to reduce the overall antenna array dimensions.

The initial goal of this project was to find an application for US patent US5912606A [13] granted to UNH. This is a patent owned by Northrop Grumman and granted to UNH for application development. The usefulness of this patent will be discussed later in design section.

1.3 Organization of the Thesis

The chapters of this thesis are organized as follows:

- Chapter 2 provides background information necessary to carry out this project. This chapter explains theory on transmission lines, microstrip antennas, phased array antennas and provides a brief explanation of antenna terminology used throughout the thesis.

- Chapter 3 explains in detail on how the antenna is designed. This chapter also describes the steps carried out in High Frequency Structural Simulator (HFSS) to perform antenna simulation. The simulation results are also presented in this chapter.
- Chapter 4 shows how the antennae are fabricated. This chapter presents pictures of all fabricated antennae.
- Chapter 5 presents a comparison of both anechoic chamber tests and simulated radiation pattern results for the antenna.
- Chapter 6 provides some conclusions of this project.

CHAPTER 2: BACKGROUND

This chapter contains the background material necessary to interpret the work presented in this thesis. The concepts of antenna theory that supported the realization of a phased array antenna are explained in brief.

2.1 Antenna Terminology

The antenna terminology explained below will be used throughout the thesis. Each of the terms are briefly explained below.

2.1.1 Radiation Pattern

The radiation pattern depicts the power emitted by an antenna as a function of spatial coordinates. The power emitted in the far-field region is usually considered to determine the radiation pattern of an antenna. The radiation pattern is called a field pattern, if an electric or a magnetic field is visualized on a spatial coordinate system. If the distribution of power density is represented as a radiation pattern, it is called the power pattern [14]. The electric and magnetic field are perpendicular to each other in the far field, and hence, they produce the elevation and azimuth in a radiation pattern for a horizontally polarized antenna. The field parallel to the antenna plane is called azimuth and the field normal to the antenna is called elevation.

Radiation patterns are used to visualize the antenna's response to an input radio frequency signal. To better visualize the response of the antenna, a radiation pattern is usually normalized by its maximum value. The normalized field pattern is obtained by dividing the obtained electric or magnetic field by the maximum value. The normalized

field pattern is dimensionless. The equation of normalized field pattern is shown in equation (1).

$$E_\theta(\theta,\phi)_n = \frac{E_\theta(\theta,\phi)}{E_\theta(\theta,\phi)_{\max}} \tag{1}$$

On a spherical coordinate system, if we assume the main lobe has its maximum in z direction (θ= 0), the θ component of an electric field is given by $E_\theta(\theta,\phi)$ [15].

Power patterns are expressed in terms of Poynting vector $S(\theta,\phi)$. The normalized power pattern is obtained by diving the Poynting vector by its maximum value. Equation (2) shows the normalized power pattern. Both field patterns and power patterns can also be expressed in the decibel units relative to field maximum value. [15]

$$P_n(\theta,\phi) = \frac{S(\theta,\phi)}{S(\theta,\phi)_{\max}} \tag{2}$$

The *Figure 2* shows a radiation pattern of a patch antenna placed on xy plane. A radiation pattern of a directional antenna has a narrow width and is pointed to a desired direction with a dominant main lobe.

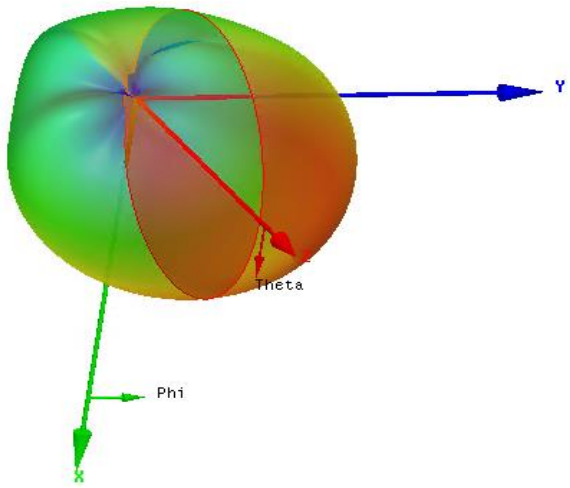

Figure 2 : Radiation Pattern of a Patch Antenna showing elevation and azimuth planes.

2.1.2 Radiation Intensity

The Radiation Intensity is defined as the power radiated from an antenna per unit solid angle. The unit of radiation intensity is watts per steradian [15]. Steradian is the angle at the center of a sphere subtended by a spherical surface area equal to one radius square. The radiation intensity is measured in the far-field region of the antenna.

2.1.3 Beamwidth

Beamwidth is the angular width of an antenna radiation pattern. The width is measured on a principal lobe of a radiation pattern. To measure the beam width, two identical points are taken on opposite sides of the main lobe. Beamwidth can be measured at any points on a radiation pattern, but most commonly used beamwidths are measured at the half power level and null points. Half Power Beamwidth (HPBW) is measured where the power level is half (-3 dB) the maximum power represented by a radiation pattern. Similarly, First-Null Beamwidth (FNBW) is measured between first nulls of the principal radiation pattern. The *Figure 3* illustrates the measurement of HPBW and FNBW.

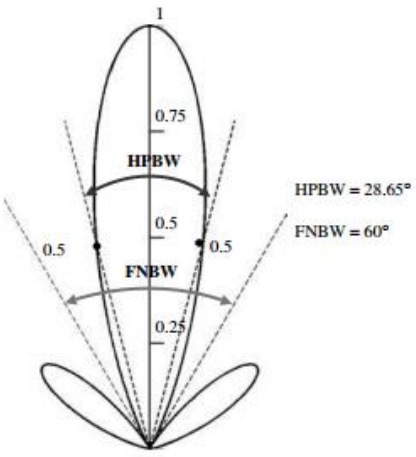

Figure 3: 2D Radiation pattern showing half power beamwidth and first-null beamwidth [14].

2.1.4 Directivity

The directivity of an antenna is the ratio of the radiation intensity to the average radiation intensity of an antenna. The directivity can also be defined as the ratio of maximum to average Poynting vector [15]. A higher value of directivity implies a relatively stronger main lobe and very few minor lobes. Greater directivity is obtained if the solid angle of the main-lobe is small. The unit of directivity is dimensionless. The equation (3) shows the ratio of directivity.

$$D = \frac{U(\theta,\phi)_{\max}}{U_{average}} = \frac{S(\theta,\phi)_{\max}}{S_{average}} \tag{3}$$

Where, D is the directivity, $U(\theta,\phi)_{\max}$ is the maximum radiation intensity and $U_{average}$ is the average radiation intensity. *S* denotes the Poynting vector.

2.1.5 Antenna Gain

Antenna performance is also measured in terms of gain. The gain of the antenna is defined as the ratio of intensity measured in a given direction to that of an isotropic antenna. A conceptual isotropic antenna radiates energy uniformly in all directions. Isotropic antennas are a useful abstraction, but it is used as a reference "antenna" to compare real antenna gain. The radiation intensity of an isotropic antenna is equal to the input power to the antenna divided by 4π steradians [14]. Thus, the equation for antenna gain is shown in equation (4).

$$Gain = 4\pi \frac{U(\theta,\phi)}{P_{in}} \tag{4}$$

The gain of an antenna is usually measured in dBi or dBd. When the gain is measured in reference to an isotropic radiator, the unit of dBi is used. When the gain is measured in reference to a dipole antenna, the unit of dBd is used.

2.1.6 Antenna Efficiency

Antenna efficiency is the ratio of the power radiated from the antenna to the input power of the antenna. The isotropic antenna is the ideal antenna and has efficiency of 1. Efficiency of 1 cannot be obtained practically. The efficiency of the antenna is affected by the conduction and dielectric losses. A part of energy received or transmitted by an antenna is converted into heat. Same energy is lost due to finite conductivity of the material used in the antenna. The equation (5) shows the formula to obtain efficiency of the antenna.

$$Efficiency = \frac{P_{radiated}}{P_{in}} \tag{5}$$

2.1.7 Bandwidth

The bandwidth of an antenna is the range of frequencies over which the antenna performance is acceptable. The bandwidth is taken as the range of frequencies around the design center frequency over which acceptable performance is obtained. The range is chosen based on the application the antenna is designed for. The bandwidth can be measured using antenna parameters like Voltage Standing Wave Ratio (VSWR), return loss, antenna gain or antenna impedance. These antenna parameters vary over the range of frequencies. The desired frequency range is the bandwidth where the chosen antenna parameters has acceptable values.

2.1.8 Polarization

The polarization of an antenna is defined as the orientation of the transmitted electric field in the far field region. The time-varying electric field vector traces a locus in a direction that determines the antenna polarization. Therefore, polarization provides the direction of propagation of instantaneous electric field for transverse waveforms. The most common types of wave polarization are, linear, circular, and elliptical. If the vector that represents the electric field propagates along a line in space, the wave is considered to be linearly polarized. Elliptical polarization occurs when the curve traced by the vector electric field is elliptical. Similarly, the circular trace of the vector field produces circular wave polarization. Linear polarization and circular polarization are special cases of elliptical polarization. The elliptical path of the vector field changes to become a line or a circle and produce linear and circular polarization respectively [14]. The circular or elliptical polarized wave can either traces a curve in clockwise or a counter-clockwise direction. The curve with clockwise instantaneous fields is right-handed. The curve with counter-clockwise instantaneous fields are left-handed [14]. The circularly polarized wave field is shown in *Figure 4*.

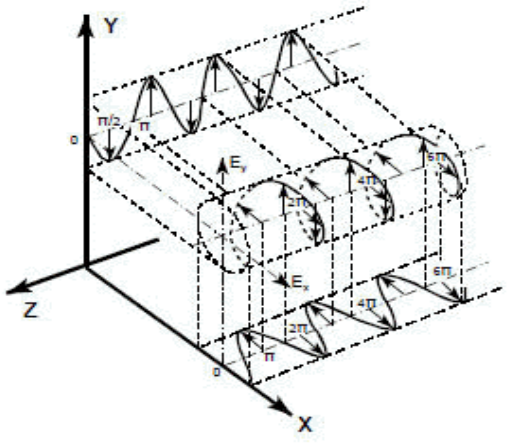

Figure 4: Circularly polarized electric field [16].

2.2 Transmission Line

When dealing with high frequency design, transmission line theory must be incorporated. At DC, the voltage along the transmission line remains considerably uniform. The same case does not apply with radio frequency signals. As the frequency increases, the wavelength of the signal decreases. At high frequency, the wavelength of the signal can be comparable to the size of the electronic components used. When the components used are of few wavelengths long, it causes a variation of voltage along the transmission line [17]. Voltage variation is caused due to loss in the transmission line. The loss is introduced due to resistance, capacitance and inductance on the line. A microstrip trace on a dielectric substrate must be carefully designed to minimize the losses to ensure maximum power transfer. The topics associated with transmission lines are discussed below. The formulae that follow are very useful to carry out the design.

2.2.1 Transmission Line Types

There are two types of transmission lines incorporated in this project. Each types are described below.

2.2.1.1 Coaxial Line

Coaxial cables are widely used in many RF applications. This cable is designed to minimize the interference and radiation loss. Coaxial cables are made with an inner conductor, dielectric layer, and outer conductor. The dielectric layer lies between the inner conductor and outer conductor. For maximum power transfer, the cable characteristic impedance must match the input impedance of the equipment to which it connects. The

antenna designed in this project is for 50 Ω applications. The formula shown in equation (6) and (7) determines the characteristic impedance of a coaxial cable [18].

$$Z_0 = \frac{1}{2\pi}\sqrt{\frac{\mu}{\varepsilon}}\ln\left(\frac{a}{b}\right) \tag{6}$$

$$Z_0 \approx \frac{138}{\sqrt{\varepsilon_r}}\log_{10}\left(\frac{a}{b}\right) \tag{7}$$

Where, μ = Permeability of dielectric medium

ε = Permittivity of dielectric medium.

ε_r = relative permittivity

a = Inner radius of the outer conductor of coaxial cable.

b = Radius of the inner conductor of coaxial cable

2.2.1.2 Microstrip Line

Microstrip lines are conducting traces on a dielectric substrate. The other side of the substrate has a ground plane. The dimension of the conducting traces must be carefully determined to obtain an optimal result. At higher frequencies, microstrip lines suffers radiation, conduction, and dielectric losses [17]. To ensure maximum power transfer, the impedance of the transmission line must be matched to the RF circuit.

Due to the presence of a dielectric substrate, the microstrip line suffers from fringing effects at the edge of the patch [14]. *Figure 5* shows the electric field lines on a microstrip transmission line. Due to the presence of two dielectrics, air and the substrate, the field lines look nonhomogeneous. Most of the electric field lines reside inside the dielectric substrate and part of it remains in the air. As the ratio of width of the transmission

line to the height of the dielectric substrate is much greater than 1 and the relative permittivity of the substrate is much greater than 1, the field lines mostly remains inside the substrate. Due to the presence of some field lines in the air, the width of the transmission line looks electrically wider than its actual width. To account for the fringing effect, an effective dielectric constant is introduced [14].

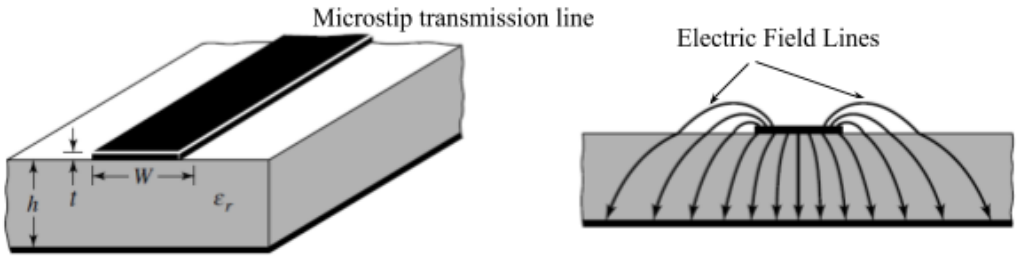

Figure 5: Microstrip transmission line and the electric field lines [14].

The effective dielectric constant when *w/h <1*, is calculated using equation (**8**) [17].

$$\varepsilon_{eff} = \frac{\varepsilon_r + 1}{2} + \frac{\varepsilon_r - 1}{2}\left[\left(1 + 12\frac{h}{w}\right)^{-1/2} + 0.04\left(1 - \frac{w}{h}\right)^2\right] \tag{8}$$

Where, h = height of the dielectric substrate

w = width of the transmission line

Thus, the impedance of the transmission line is given by equation (9).

$$Z_0 = \frac{Z_f}{2\pi\sqrt{\varepsilon_{eff}}}\ln\left(8\frac{h}{w} + \frac{w}{4h}\right) \tag{9}$$

Where Z_f = wave impedance in free space (377 ohms)

Similarly, for a transmission line having *w/h* > 1, the effective dielectric constant is given by equation (10).

$$\varepsilon_{eff} = \frac{\varepsilon_r + 1}{2} + \frac{\varepsilon_r - 1}{2}\left[\left(1 + 12\frac{h}{w}\right)^{-1/2}\right] \tag{10}$$

The characteristic impedance of the line is then given by equation (11).

$$Z_0 = \frac{Z_f}{\sqrt{\varepsilon_{eff}}\left(1.393 + \frac{w}{h} + \frac{2}{3}\ln\left(\frac{w}{h} + 1.444\right)\right)} \tag{11}$$

2.2.2 Voltage Reflection Coefficient (Γ)

The voltage reflection coefficient is an important parameter when designing microstrip transmission lines. It is measured when the transmission line is terminated with a load impedance. The reflection coefficient is measured in terms of the characteristic impedance of the transmission line and the load impedance. The equation (12) below is used to calculate the reflection coefficient [17].

$$\Gamma_0 = \frac{Z_L - Z_0}{Z_L + Z_0} \tag{12}$$

Where, Z_L= load impedance of the transmission line

Z_0= characteristic impedance of the transmission line

When the transmission line is open, the load impedance is infinity and hence the reflection coefficient is 1. The reflected wave has the same polarity as the input wave. When the line is shorted, the load impedance is 0, and therefore the reflection coefficient is -1. The input energy to a transmission line is reflected if it encounters a short in the transmission line.

To obtain maximum power transfer, the impedance of the load must match the characteristic impedance.

2.2.3 Voltage Standing Wave Ratio (VSWR)

Reflection in the transmission line is caused by an impedance mismatch in the line. The VSWR shows the amount of mismatch in the transmission line. The value of VSWR ranges from 1 to infinity. If there is minimum reflection on a transmission line, the value of VSWR tends to be near 1. A complete reflection of a signal in a transmission line has value of VSWR reaching infinity. Mismatch is measured in terms of amplitude of the signal. The ratio of the maximum voltage to the minimum voltage along the line determines the VSWR [17]. It is also represented in terms of reflection coefficient. Equation (13) shows VSWR as a function of reflection coefficient.

$$VSWR = \frac{1+|\Gamma_0|}{1-|\Gamma_0|} \tag{13}$$

2.2.4 Input Impedance

Input impedance allows us to determine how the load impedance is transferred along a transmission line. The input impedance of a lossless transmission line with characteristic impedance of Z_0 at a distance d away from the load Z_L, is given by equation (14) [17].

$$Z_{in}(d) = Z_0 \frac{Z_L + jZ_0 \tan(\beta d)}{Z_0 + jZ_L \tan(\beta d)} \tag{14}$$

Where, d = distance away from load

β = wave number given by $\frac{2\pi}{\lambda}$, λ is a wave length

2.2.5 Return Loss and Insertion Loss

Return loss measures the amount of signal returned in the transmission line due to a fault in the line. The fault can be an impedance mismatch in the line or the load. The return loss is the ratio of reflected power to the incident power [17]. The equation for return loss is shown in equation (15). It can be measured in terms of reflection coefficient.

$$RL[dB] = -10\log\left(\frac{P_r}{P_i}\right) = -20\log|\Gamma_{in}| \tag{15}$$

Where, P_r = reflected power

P_i = incident power

Γ_{in} = Reflection coefficient at the input of the transmission line.

Similarly, the insertion loss is a ratio of transmitted power to the incident power. The equation for insertion loss is shown in equation (16).

$$IL[dB] = -10\log\left(\frac{P_t}{P_i}\right) = -10\log\left(1-|\Gamma_{in}|^2\right) \tag{16}$$

Where, P_t=transmitted power.

2.2.6 Impedance Matching

To solve the problem of reflection on the transmission line of an antenna, the impedance can be matched so that maximum power is transferred. There are two kinds of matching techniques used in this project. These methods are explained below.

2.2.6.1 Quarter Wave Transformer

A quarter wave transformer is a transmission line which is an electrical quarter wavelength long at the frequency of interest. By using this segment of the transmission

line, a desired input impedance can be achieved to match with the load impedance [17]. If the distance *d* in equation (14) is substituted with quarter wavelength, i.e. $\frac{\lambda}{4}$, the characteristic impedance of the quarter wave transformer is obtained.

$$Z_{in}(d = \frac{\lambda}{4}) = Z_0 \frac{Z_L + jZ_0 \tan\left(\frac{2\pi}{\lambda}\frac{\lambda}{4}\right)}{Z_0 + jZ_L \tan\left(\frac{2\pi}{\lambda}\frac{\lambda}{4}\right)} \quad (17)$$

Since, $\beta = \frac{2\pi}{\lambda}$

Therefore, $Z_0 = \sqrt{Z_L Z_{in}}$ (18)

2.2.6.2 Stub Matching

Using discrete components to transform the impedance in a transmission line for high frequency applications is challenging due to the size of the components. The matching is also achieved using open or shorted microstrip traces in a transmission line. Every conducting trace on a dielectric substrate possess some resistance, inductance and capacitance. To cancel out the capacitance or inductance in a transmission line, a stub is added to the line. The characteristic impedance of the stub is often the characteristic impedance of the transmission line. The impedance is made equal so that the input impedance seen by the source does not vary with load impedance. The parallel combination of the input impedance of the line and the stub are made equal to the characteristic impedance at the stub location. The mathematics involves a set of non-linear equations [19]. Two solutions each for open and shorted stubs are shown below. Equation (19) shows

the position of the stub from the load [19]. The position of the stub is valid for both open and shorted stubs.

$$d = \frac{1}{\beta}\tan^{-1}\left\{\frac{1-g_L}{b_L \pm \sqrt{g_L\left[(1-g_L)^2 + b_L{}^2\right]}}\right\} \tag{19}$$

Where, g_L = conductance, real part of admittance

b_L = susceptance, imaginary part of admittance

The length for the open stub is given by equations (20) and (21).

$$L_{stub} = \frac{1}{\beta}\tan^{-1}\left[\sqrt{\frac{g_L}{(1-g_L)^2 + b_L{}^2}}\right] \tag{20}$$

$$L_{stub} = \frac{\pi}{\beta} - \frac{1}{\beta}\tan^{-1}\left[\sqrt{\frac{g_L}{(1-g_L)^2 + b_L{}^2}}\right] \tag{21}$$

Similarly, the length of the shorted stubs is given by equations (22) and (23) .

$$L_{stub} = \frac{\pi}{\beta} - \frac{1}{\beta}\tan^{-1}\left[\sqrt{\frac{(1-g_L)^2 + b_L{}^2}{g_L}}\right] \tag{22}$$

$$L_{stub} = \frac{1}{\beta}\tan^{-1}\left[\sqrt{\frac{(1-g_L)^2 + b_L{}^2}{g_L}}\right] \tag{23}$$

2.2.7 Scattering Parameters (s-Parameters)

The scattering parameters describe the input-output relationship of waves passing through a multiport network. Not all the signal that passes through the input terminal of a system gets through to the output terminal. Some of the energy is reflected due to impedance mismatch and some of the energy is dissipated as heat. The scattering matrix is

a measure of the signal at the system's port in terms of incident and reflected power [17]. Scattering parameters are denoted by S_{ij}, which gives the response at port *i* due to an incident signal at port *j*. For a two-port network shown in *Figure 6* , four parameters – S_{11}, S_{21}, S_{12} and S_{22}, can be computed or measured.

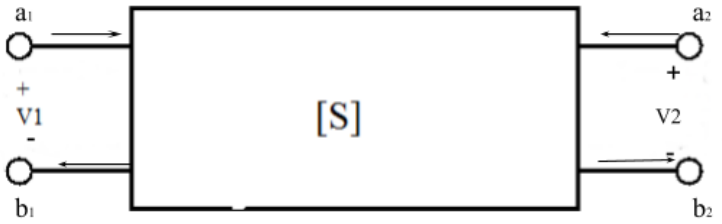

Figure 6: S-parameters in a two-port network.

The S-parameters in a matrix form are shown in equation (24) [17].

$$\begin{Bmatrix} b_1 \\ b_2 \end{Bmatrix} = \begin{bmatrix} S_{11} & S_{12} \\ S_{21} & S_{22} \end{bmatrix} \begin{Bmatrix} a_1 \\ a_2 \end{Bmatrix} \tag{24}$$

Where

$$S_{11} = \left.\frac{b_1}{a_1}\right|_{a_2=0} = \frac{\text{reflected power at port 1}}{\text{incident power at port 1}} \tag{25}$$

$$S_{21} = \left.\frac{b_2}{a_1}\right|_{a_2=0} = \frac{\text{transmitted power at port 2}}{\text{incident power at port 1}} \tag{26}$$

$$S_{22} = \left.\frac{b_2}{a_2}\right|_{a_1=0} = \frac{\text{reflected power at port 2}}{\text{incident power at port 2}} \tag{27}$$

$$S_{12} = \left.\frac{b_1}{a_2}\right|_{a_1=0} = \frac{\text{transmitted power at port 1}}{\text{incident power at port 2}} \tag{28}$$

S-Parameters provide many useful measurements in RF circuits. S_{11} is a reflection coefficient at the input terminal of the system. The return loss is measured in terms of S_{11}. As shown in equation (15), the return loss is obtained by taking the logarithm of the

magnitude of the input reflection coefficient. The insertion loss is measured in terms of S_{21}. It is obtained by taking the logarithm of the magnitude of S_{21} [17]. Similarly, S_{22} is the reflection coefficient at the output port. The return loss at the output port can be obtained using this parameter. Insertion loss at the output port can be computed using S_{12}.

2.2.8 Impedance Parameters (Z-parameters)

Similar to the s-parameters, impedance parameters or z-parameters provide the input-output impedance relationship in a two-port network. The impedance parameters can also be expressed in terms of reflection coefficients. Impedance parameters are obtained by keeping the input or output terminals of the system open circuited. Hence, the z-parameters are also called open-circuit impedance parameter. The z-parameter matrix for a two-port network is shown in equation (29).

$$[Z] = \begin{bmatrix} Z_{11} & Z_{12} \\ Z_{21} & Z_{22} \end{bmatrix} \tag{29}$$

Where, Z_{11} = Open circuit input impedance

Z_{12} = Open circuit transfer impedance from port 1 to port 2

Z_{21} = Open Circuit transfer impedance from port 2 to port 1

Z_{22} = Open circuit output impedance

2.3 Microstrip Antenna

A microstrip antenna consist of a metallic patch on a dielectric substrate. The other side of the dielectric substrate may contain a ground plane. The antenna is excited through a feeding network attached to the antenna. The size of the antenna, dielectric material,

substrate thickness and other antenna parameters are chosen to obtain maximum radiation at the desired frequency. Microstrip patch antennas are very appropriate for electronics that have size and weight constraints and that require low cost antennas. The size of the antenna reduces as the frequency increases; therefore, patch antennae are very suitable for high frequency applications. This antenna can be manufactured inexpensively using printed circuit board technology [14]. For low frequencies, the size of the antenna is too big to be fabricated on a circuit board. Patch antennas can be easily designed and developed for any shape and size based on the system requirements. There are also some disadvantages of using patch antennas. Patch antennas are not suitable for wide-band applications. This antenna has low efficiency, operates at low power and has poor scan performance [14]. The desired polarization, radiation pattern, resonant frequency and impedance can be easily achieved by altering the antenna parameters. For instance, a thicker dielectric can be used to obtain wide bandwidth [14].

2.3.1 Rectangular Patch Antenna

The size of the antenna for this project is obtained by using transmission line model analysis. Similar to the microstrip line, a patch antenna also suffers fringing effect. As shown in *Figure 5*, the electric field lines are nonhomogeneous due to the presence of air and dielectric substrates near the patch. To account for the fringing effect, an effective dielectric constant must be determined using

(8) and (10). The length of the antenna must be extended by a small length to compensate for the fringing effect. The length by which the antenna must be extended is

calculated by using the effective dielectric constant. Equation (30) is used to obtain the extension length ΔL [14].

$$\Delta L = 0.412h \frac{\left(\varepsilon_{eff} + 0.3\right)\left(\frac{W}{h} + 0.264\right)}{\left(\varepsilon_{eff} - 0.258\right)\left(\frac{W}{h} + 0.8\right)} \tag{30}$$

Where, W = width of the antenna

Each side of the patch antenna is extended by length ΔL. Thus, the effective length of the antenna is given by equation (31) [14].

$$L_{eff} = L + 2\Delta L \tag{31}$$

Where L = Nominal design length of the antenna

The effective length of an antenna is a factor of the effective dielectric constant and the resonance frequency. Thus, the effective length is calculated using equation (32) [14].

$$L_{eff} = \frac{1}{2 f_r \sqrt{\varepsilon_{eff}} \sqrt{\mu_0 \varepsilon_0}} \tag{32}$$

Where f_r = resonance frequency

μ_0 = permeability of free space (4π x 10^{-7} N/A^2)

ε_0 = permittivity of free space (8.854×10^{-12} F/m)

The equation to calculate the actual length of an antenna is obtained by substituting equation (32) in equation (31). Therefore, equation (33) gives the actual length of an antenna [14].

$$L = \frac{1}{2 f_r \sqrt{\varepsilon_{eff}} \sqrt{\mu_0 \varepsilon_0}} - 2\Delta L \tag{33}$$

The width of an antenna is a function of dielectric constant and the resonant frequency. The width is calculated using equation (34) [14].

$$W = \frac{1}{2 f_r \sqrt{\mu_0 \varepsilon_0}} \sqrt{\frac{2}{\varepsilon_r + 1}} \tag{34}$$

An antenna provides maximum radiation if the input impedance of the antenna is matched with the feed line. Typical values of impedance at the edge of a rectangular patch antenna ranges from 100 to 400 Ω [20]. For an edge fed antenna, the input impedance is given by (35) [20].

$$Z = 90 \frac{\varepsilon_r^2}{\varepsilon_r - 1} \left(\frac{L}{W} \right)^2 \Omega \tag{35}$$

The input impedance is a function of dielectric constant, length and width of the antenna. The impedance value can be reduced by increasing the width of the antenna. However, the ratio of the width to the length of the antenna must remain below 2, to keep the aperture efficiency of the antenna at a reasonable level. As the ratio increases over 2, the efficiency starts dropping [14]. The impedance can also be adjusted by choosing appropriate feeding methods and feed locations.

2.3.2 Feeding Methods

There are many ways to feed a microstrip patch antenna. Feeding methods are classified into three different kinds; directly coupled, electromagnetically coupled and aperture coupled [20]. Different techniques are applied to each feeding method to obtain the desired input impedance at the antenna port. *Figure 7* shows the various kinds of feeding techniques.

The edge feed and the coaxial feed are different kinds of direct feed. Edge feed are directly attached to the edge of the patch antenna. The feed line is printed on the same layer as the antenna. Edge feed can be realized either with a quarter wave transformer or an inset. The input impedance of the antenna can be matched to the feed line with a quarter wavelength long transmission line. The characteristic impedance of the quarter wavelength transmission line is determined using equation (18).

For an inset fed antenna, the feedline distance into the antenna is adjusted to achieve the needed impedance. For a high permittivity substrate, the inset depth may be not practical to realize as it affects cross polarization and radiation pattern [20]. The inset feed scales the input impedance in (35) as shown in

(36) [20].

$$Z(\Delta x_i) = \cos^2\left(\frac{\pi \Delta x_i}{L}\right) Z\left(\Delta x_i = 0\right) \tag{36}$$

Where, Δx_i = inset depth from the edge of the antenna.

In this project, the antenna is fed by a combination of coaxial feed and a corporate feed. The idea of quarter wave transformer is used to realize the corporate feed network. The detail of this feeding method will be explained in the design section.

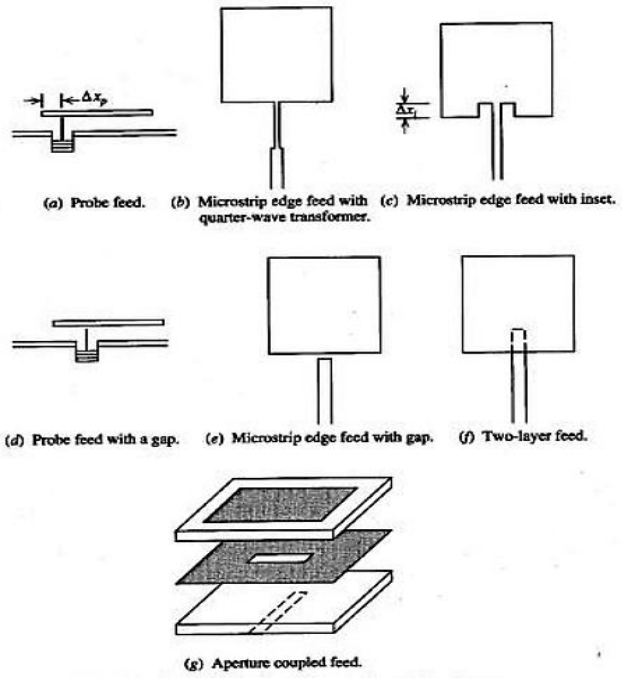

Figure 7: Different feeding techniques on a patch antenna [20].

The coaxial feed is another kind of direct coupled feed method. The inner conductor of the coaxial cable is probed through the dielectric substrate and is connected with the antenna patch. The outer conductor of the coaxial cable is connected to the ground on the other side of the dielectric substrate. The impedance is adjusted by changing the feed location. The distance between the edge of the antenna and the feed location is changed to obtain the desired impedance. As the distance from the edge of the antenna is increased, the impedance in equation (35) is scaled as shown in

(37) [20].

$$Z(\Delta x_p) = \cos^2\left(\frac{\pi \Delta x_p}{L}\right) Z\left(\Delta x_p = 0\right) \tag{37}$$

The coaxial feed and the edge feed can also be implemented by keeping a small gap between the feedline and the antenna. These are the types of electromagnetically coupled feeds. The signal from the feedline is transferred to the antenna with a coupling effect. This

feeding method is sometime advantageous over the probe feed. The gap between the feedline and the antenna will introduce some capacitance. The reactance part of the impedance is minimized, as the capacitance introduced from the gap cancels out the probe inductance [20].

In an aperture feed, two different dielectric substrates are used for an antenna and the feed line. The two substrates are separated by a ground plane. The feedline lies at the bottom of the lower dielectric substrate. The signal from the feed line is coupled with the antenna through a slot on a ground plane separating two substrates. The upper substrate is typically thicker and has low dielectric constant. The lower substrate has higher dielectric constant [14]. The thicker dielectric is very useful for wide-band applications. The antenna also possesses less spurious radiation since the ground plane between the substrate partially isolates the feed from the radiating element.

2.4 Phased Array Antenna

A single antenna is limited to a fixed gain and directivity. A single antenna element produces a wide radiation pattern, and the direction of the radiation beam cannot be controlled. A communication system, that requires high directivity and gain requires a directional antenna. One way to achieve high directivity is to use multiple antenna elements. Antenna elements can be arranged in a linear or planar geometry to form an array. In a phased array antenna, the amplitude and phase of the signal that feeds the antenna elements can be controlled to obtain a radiation pattern in a desired direction. The electric field strength of an antenna array is the sum of the electric fields of the individual antenna elements. The distance between the antenna elements, the phase and amplitude excitations of individual elements, and the array geometry determines the shape of

radiation pattern [14]. Phased array antennas are widely used for applications that require fixed or steerable beam patterns. These antennae provide control over the direction and beam pattern without mechanically adjusting the antenna position. The phased array antenna provides flexibility to receive signals from a direction where the signal path is obstructed and transmit signals in any desired direction.

In this project a four-element linear array of patch antennas is designed and realized. The distance between each antenna element is uniform. The derivation of the electric field that contributes to shape the radiation pattern is shown below.

Let us assume the separation between the antenna elements is *d*. As shown in *Figure 8*, *x* is a distance of delay between adjacent antennas. R is the far-field distance of the antenna. The delay distance can be calculated as shown in equation (38).

$$x = d\cos\theta \tag{38}$$

Where θ = direction of the main beam

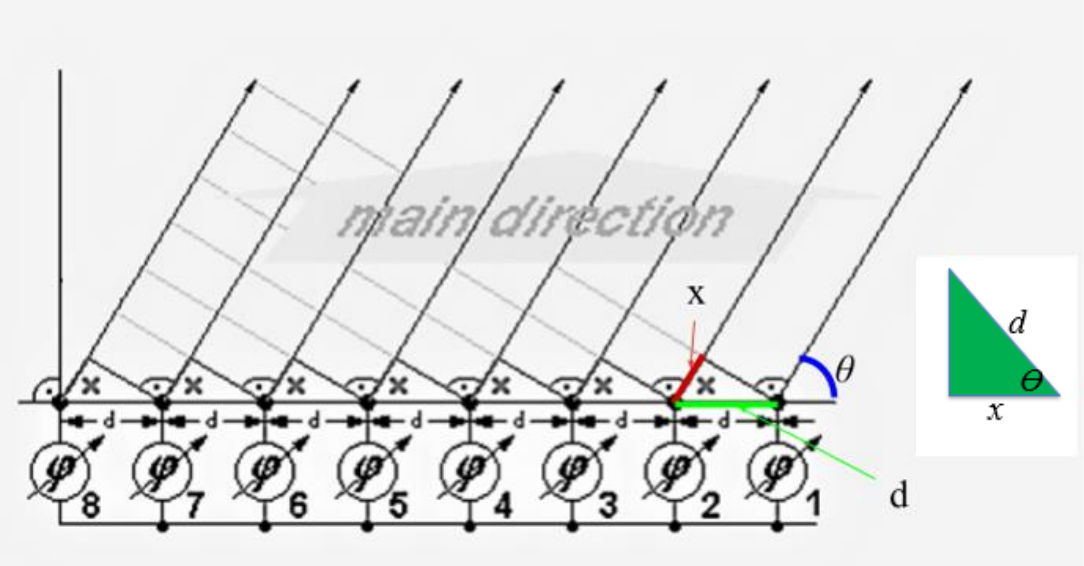

Figure 8: Geometry of a linear antenna array [21]

Now let us calculate a small phase change due to antenna separation. The ratio of delay distance to the wavelength is proportional to the ratio of phase change over 360°.

$$\frac{2\pi}{\Delta\phi} = \frac{\lambda}{x} \tag{39}$$

$$\Delta\phi = \frac{2\pi}{\lambda} x = \beta x \tag{40}$$

Substituting *x* in equation (40) from (38), the change in phase due to antenna element separation is obtained as shown below in equation (41).

$$\Delta\phi = \beta d \cos\theta \tag{41}$$

To obtain beam steering, the signal going to each antenna element will have some phase excitation. In this calculation, the phase change on consecutive antenna element are assumed to be uniform. If the input current to the first antenna element is I_o, then the input current to other antenna element is given by equations below.

$$I_1 = I_0 \tag{42}$$

$$I_2 = I_0 e^{j\phi} \tag{43}$$

$$I_3 = I_0 e^{j2\phi} \tag{44}$$

$$I_N = I_0 e^{j(N-1)\phi} \tag{45}$$

Where ϕ = input current phase shift.

Now, the electric field on each antenna element can be calculated using the input current to the antenna. The electric field on the first antenna element is given by equation (46). The mutual coupling between antenna elements is not considered while developing the electric field equations at far field region.

$$E_1 = I_0 \frac{e^{-j\beta R}}{4\pi R} = E_0 \tag{46}$$

The electric field for second and third element can be calculated as shown below.

$$E_2 = I_0 e^{j\phi} \frac{e^{-j\beta R + j\Delta\phi}}{4\pi R} = E_0 e^{j(\beta d\cos\theta + \phi)} \tag{47}$$

$$E_3 = I_0 e^{j2\phi} \frac{e^{-j\beta R + j2\Delta\phi}}{4\pi R} = E_0 e^{j2(\beta d\cos\theta + \phi)} \tag{48}$$

Similarly, the far electric field for N^{th} antenna element is given by equation (49).

$$E_N = I_0 e^{j(N-1)\phi} \frac{e^{-j\beta R + j(N-1)\Delta\phi}}{4\pi R} = E_0 e^{j(N-1)(\beta d\cos\theta + \phi)} \tag{49}$$

The radiation energy in the far field of the antenna is the sum of energy radiated through the individual antenna elements. Therefore, the total electric field of an antenna array spaced in a uniform geometry and excited with uniform phase shift is given by equation (50).

$$E = E_0 + E_0 e^{j(\beta d\cos\theta + \phi)} + E_0 e^{j2(\beta d\cos\theta + \phi)} + ... + E_0 e^{j(N-1)(\beta d\cos\theta + \phi)} \tag{50}$$

$$E = E_0 \left[1 + e^{j(\beta d\cos\theta + \phi)} + e^{j2(\beta d\cos\theta + \phi)} + ... + e^{j(N-1)(\beta d\cos\theta + \phi)}\right]$$

$$E = E_0 \times AF \tag{51}$$

Where, AF = Array Factor

Therefore, the total electric field of an antenna array is the product of the electric field of a single antenna element and the array factor. The mutual coupling between the antenna elements is not accounted for in the equation. The array factor is the function of the antenna spacing, input signal phase, and the wavelength. These parameters are key in determining the antenna radiation pattern. Thus, the directivity of the antenna is shaped by the array factor. The array factor equation is simplified below.

$$AF = 1 + e^{j(\beta d \cos\theta + \phi)} + e^{j2(\beta d \cos\theta + \phi)} + ... + e^{j(N-1)(\beta d \cos\theta + \phi)} \quad (52)$$

$$AF = \sum_{N=1}^{n} e^{j(N-1)(\beta d \cos\theta + \phi)} \quad (53)$$

Where, n = number of antenna element in an array

Let, $$\psi = \beta d \cos\theta + \phi \quad (54)$$

Therefore, $$AF = \sum_{N=1}^{n} e^{j(N-1)\psi} \quad (55)$$

The equation (55) is the simplified array factor equation for a linear phased array antenna.

2.5 High Frequency Structural Simulator (HFSS) Background

The phased array antenna was designed using a three-dimensional electro-magnetic simulation tool called High Frequency Structural Simulator (HFSS). HFSS uses a computational technique called Finite Element Method (FEM) to solve for fields in an antenna structure. A mesh network is formed by dividing the antenna geometry into many small tetrahedron shapes to apply FEM analysis. The electric field for each tetrahedron geometry is solved by applying a boundary condition. The boundary condition is applied between the adjacent shapes. The vector field is calculated at each edge of the mesh element. The field vector is then interpolated within the element geometry to calculate the total field. Thus, the accuracy of the total field depends on the number of tetrahedrons in a mesh. Increasing the number of tetrahedron shapes in a mesh will decreases the size of each mesh element. The accuracy of the result increases with smaller tetrahedron size but more computational power and memory is required to perform the analysis.

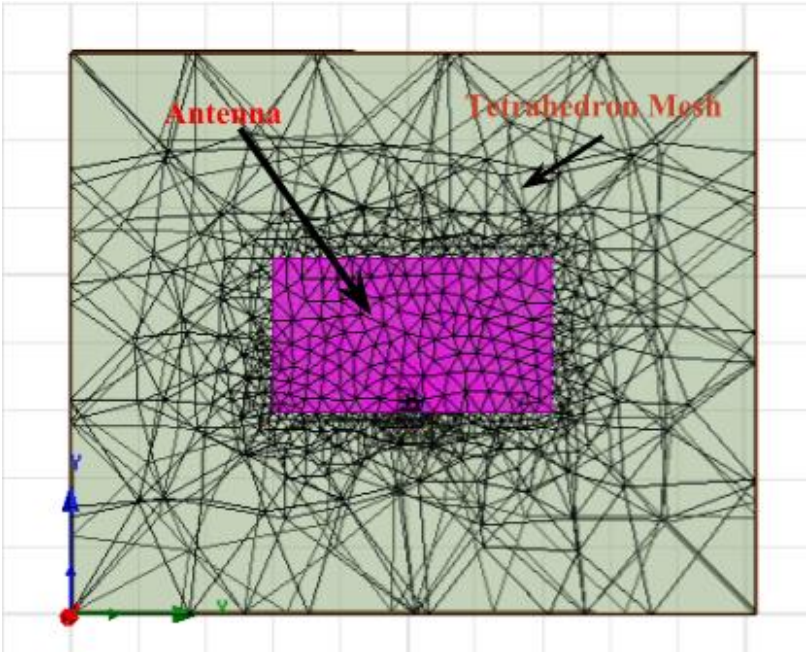

Figure 9 : Mesh network of a tetrahedron geometry on a probe fed patch antenna.

HFSS performs adaptive iterative solution to compute an accurate result. To perform iterative solution, the size of the mesh network is refined iteratively until an optimal solution is found. The vector field solution is used to calculate the scattering matrix. The amount of transmission and reflection that occurs inside the antenna geometry determines the scattering parameters [22]. *Figure 9* shows the mesh network of tetrahedron geometry on a probe fed patch antenna.

There are some conditions in HFSS that need to be established to solve an antenna structure. The software must know the antenna material, boundary condition, solution model, and excitation to perform an electromagnetic analysis. Some of the HFSS parameters that are needed for simulation are explained in brief below.

2.5.1 Antenna Geometry

A two or three-dimensional structure of any shape and size can be formed in HFSS. The size of the antenna is determined using the equations provided in previous sections of this thesis. Complex shapes can be formed by subtracting and uniting various components together or drawing equation-based surfaces. The software also allows to import drawings from other design tools. The geometrical shapes must be assigned a material for the software to accurately compute the associated field.

2.5.2 Boundary Conditions

The boundary condition can be applied to a two-dimensional object or a surface of a three-dimensional object. Some of the boundary conditions applied in this project are: finite conductivity, lumped RLC, Radiation boundary, and Perfectly Matched Layer (PML) boundary. The boundaries are used in HFSS to simplify the solution. A boundary can create an open or closed model. A boundary for a closed model will not let energy radiate out of the boundary. The boundary condition also simplifies the geometric complexity [22]. For instance, a boundary condition applied to a geometry can replace a lumped parameter such as resistor, inductor or a capacitor.

A finite conductive boundary or a boundary with Perfect Electric Conductor (PEC) can be established on a two-dimensional object like patch antennas or microstrip traces. The PEC boundary represents a lossless conductor and is applied to traces with an infinite ground plane. The finite conductivity represents an imperfect conductor and is applied to thin radiating geometries [22].

The lumped RLC boundary is an impedance boundary that is used to replace lumped components. The RLC boundary uses resistor, capacitor, and an inductor in parallel. To obtain a series combination of the lumped component, two different geometries must be placed in series and assigned a lumped RLC boundary. The RLC values assigned to the boundary provide ideal behavior of the components [22].

The radiation boundary creates a space for radiating objects like an antenna to radiate waves into infinite space. This boundary is placed one-quarter wavelength away from the antenna. Each surface of a radiation box is assigned a boundary so that the wave does not propagate outside the box. The wave is absorbed at the radiating boundary [22]. Similar to the radiation boundary is a PML boundary. This boundary is also applied outside the radiating surface. The wave reaching the radiation boundary is absorbed perfectly if the wave is incident normal to the radiating surface. For a phased array antenna, the radiated energy is steered at different angles. The wave is not absorbed as desired if the wave is incident at an angle. Therefore, the PML boundaries are used while simulating antenna structures that produces radiation pattern at an angle. *Figure 10* shows the absorption of a wave at the boundary when the wave is incident normally and at an angle.

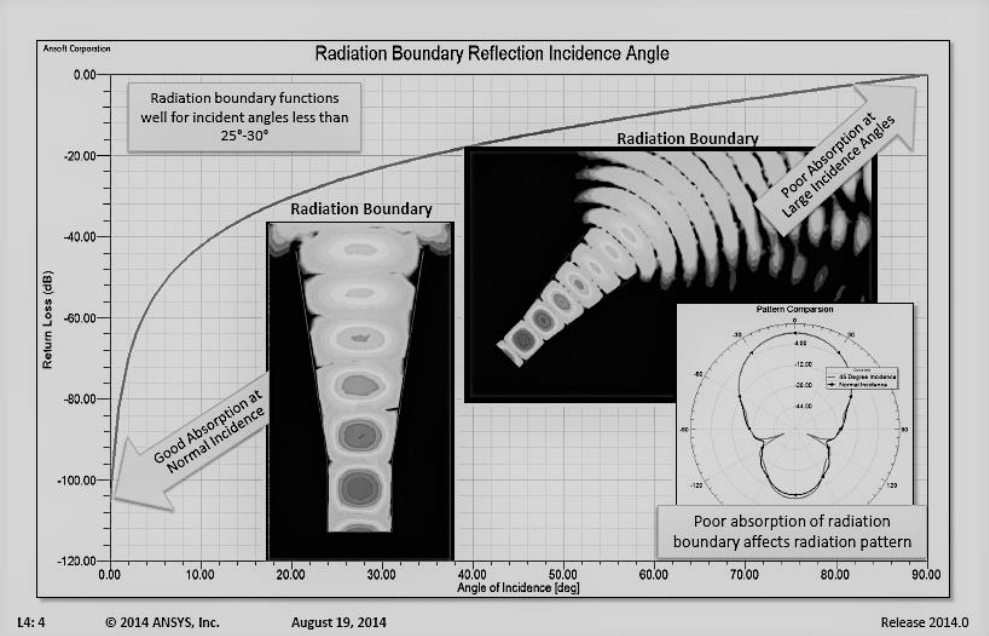

Figure 10: Wave absorption at the radiation boundary at different angle of incidence

A PML boundary has an additional layer of anisotropic material that absorbs the electromagnetic field reaching the surface.

Figure 11 shows a PML boundary.

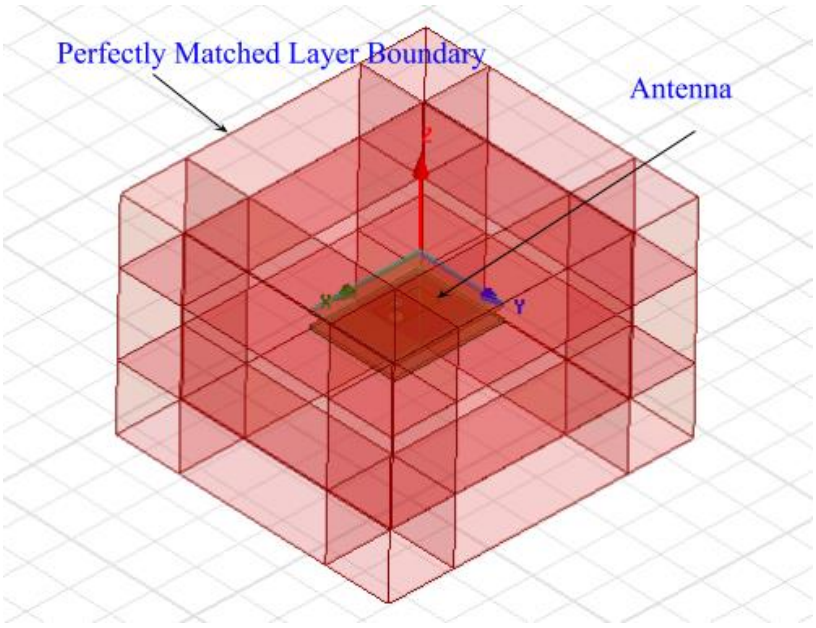

Figure 11: Perfectly Matched Layer (PML) boundary

2.5.3 Excitation

Antennas are excited with a source of current, voltage, or field at the antenna port. The most common excitation types in HFSS are the wave port and the lumped port. These excitations provide field behavior of the antenna. An impedance parameter, scattering parameter, and admittance parameter can be requested if these ports are used in the simulation. Antennas are excited using a wave port at the outer surface of the solution space. This port is located at the radiation boundary. The lumped port is used when it is not relevant to use a wave port. If an antenna must be excited from within the dielectric substrate, the use of wave port is not applicable. A lumped port can be used inside the radiation boundary and within the dielectric material. In both excitation types, an integration line must be drawn from ground to the feed line.

2.5.4 Post Processing

The behavior of an antenna can be interpreted using results in HFSS after successful completion of the simulation. Some of the results that are useful in determining the antenna performance are the scattering parameter S11, impedance parameter, 2D and 3D radiation patterns, and VSWR. The calculated dimension of an antenna does not always guarantee a desired performance. Therefore, antenna dimensions must be tuned so that the desired performance of an antenna can be achieved. During solution setup, derivatives can be requested on variables responsible to affect the solution. When a derivative on a variable is requested, HFSS solves for the field when there is 10% change in dimension. After the simulation, the result can be tuned by changing the dimension of the antenna parameter.

Parametric analysis is another option in HFSS. A range of values can be assigned to a variable and HFSS will provide result for every value. The assigned values can be in linear step, linear count, decade count, octave count, and exponential count. The correct dimension of the antenna parameter that yields the desired result can be assigned to the variable after simulation.

CHAPTER 3: ANTENNA DESIGN AND SIMULATION

3.1 Single Rectangular Patch Antenna

3.1.1 Design

A probe fed rectangular patch antenna was designed in HFSS. The dimension of an antenna depends on the resonance frequency, relative permittivity of the material, and its height. The antenna is designed for a frequency of 5 GHz. A Rogers RT/Duroid 6006™ [23] and RO4360G2™ [24] is used as a dielectric material. The height of the dielectric substrate is 1.524 mm and the relative permittivity is 6.15. The higher value of dielectric constant minimizes the size of the antenna. This kind of material is very suitable for an antenna that has an area constraint. The length and the width of the antenna is calculated using equations (33) and (34), respectively. The length of the antenna is 11.66 mm and the width is 15.86 mm. The antenna is placed on a substrate of length 41.37 mm and width 50.78 mm. The free space wave length at 5 GHz is 60 mm. Therefore, the substrate is made 15 mm wider on every side of the antenna to establish a quarter-wavelength gap between the antenna and the edge of the substrate. A ground plane is placed on the other side of the dielectric substrate. The antenna and the ground plane are both assigned the finite conductivity of copper which is 5.8×10^7 Siemens/m. The antenna parameters are shown in *Table 1*.

Antenna Parameters	Dimension/Value
Center Frequency	5 GHz
Dielectric Material	Rogers RT/Duroid 6006, RO4360G2
Dielectric Constant	6.15
Dielectric thickness	1.524 mm
Finite Conductivity (Copper)	5.8×10^7 Siemens/m
Calculated Length of Patch	11.66 mm
Calculated Width of Patch	15.86 mm
Substrate Length	41.37 mm
Substrate Width	50.87 mm

Table 1: Calculated Antenna Parameters (Single Antenna)

The antenna is fed with a coaxial line connected to the center of the longer edge of the antenna. Both longer edges have horizontal the electric field in the same direction that produces a linearly polarized radiation pattern [15]. The size of the coaxial feed line is carefully chosen to obtain an impedance of 50 Ω. The radii of inner and outer conductors were calculated using equations (6) and (7) above. The radius of 0.45 mm for the inner conductor and inner radius of 1.8425 mm for the outer conductor provides 50 Ω impedance to the transmission line. Both inner and outer conductors are made from copper. Polyethylene is used as the dielectric material between the inner and outer conductor. The relative permittivity of the material is 2.25. The coaxial cable properties are shown in *Table 2*.

Coaxial cable variables	**Values**
Impedance	50 Ω
Radius (inner conductor)	0.45 mm
Inner Radius (outer conductor)	1.1425 mm
Outer Radius (outer conductor)	1.8425mm
Dielectric Material	Polyethylene
Dielectric Constant	2.25 mm

Table 2: Coaxial cable variables.

The coaxial line connects another dielectric substrate. The phase shifting network will be placed on the second dielectric substrate later. The separation between the two substrates is 5 mm. The outer conductor of the coaxial line connects the ground plane on both substrates. The inner connector connects the antenna on one substrate to the phase shifting network on the other substrate as shown in *Figure 12*.

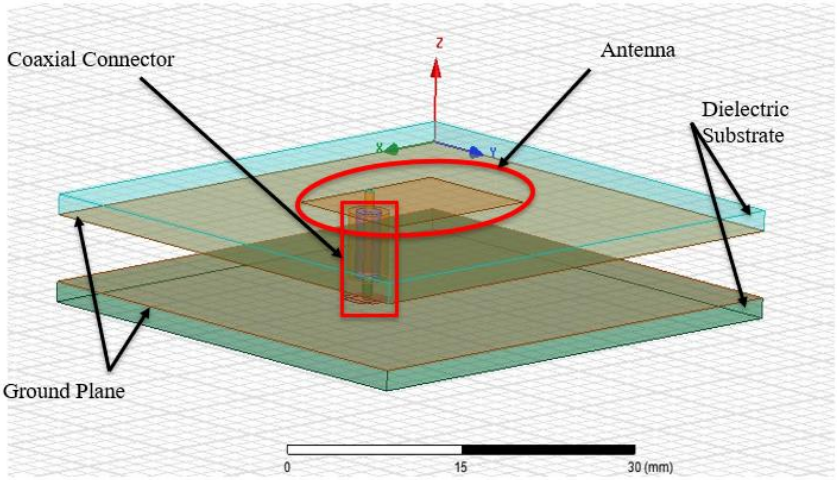

Figure 12: Single antenna design.

The phase shifting network is not included during the simulation of this antenna. However, a four-way signal trace is connected to the inner conductor of the coaxial line. Each end of the four-way signal trace will connect to a phase shifting network. These traces will affect the antenna impedance. Therefore, the antenna is simulated with a four-way trace placed at the port so that the impedance variation introduced by these traces can be compensated while tuning for antenna parameters.

3.1.2 Simulation

The designed antenna is simulated using a lumped port. To assign a lumped port excitation, an integration line is drawn from the ground plane to one of the four-way ports through the dielectric substrate. The antenna is enclosed in a PML boundary. A driven model solution type is requested. Driven Model generates S-parameters in terms of power whereas, driven terminal provides S-parameters in terms of voltage and current. To run the simulation, the resonance frequency and the values of the adaptive solution were entered

in solution setup. The frequency sweep is defined from 3 GHz to 7 GHz with a step size of 10 MHz. The results obtained from the simulation are shown below.

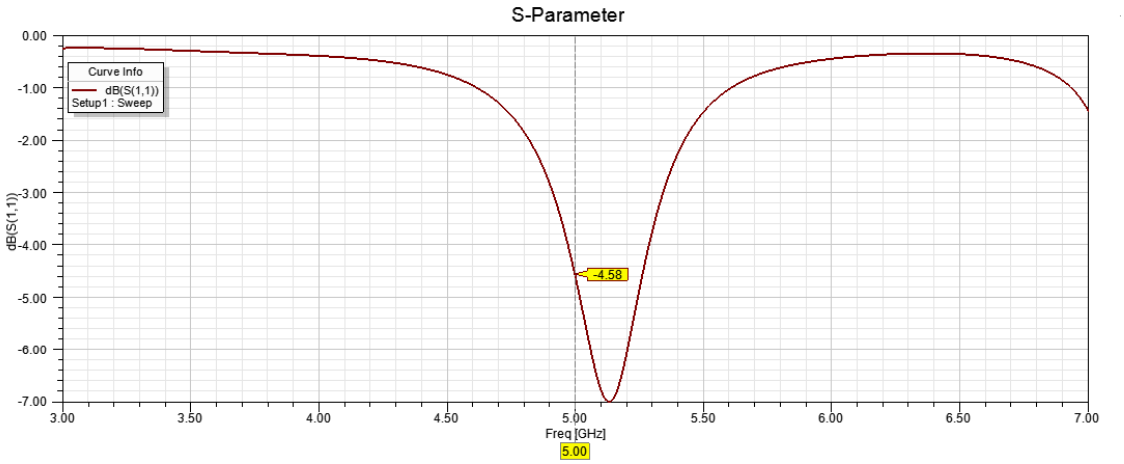

Figure 13: Return loss of untuned antenna.

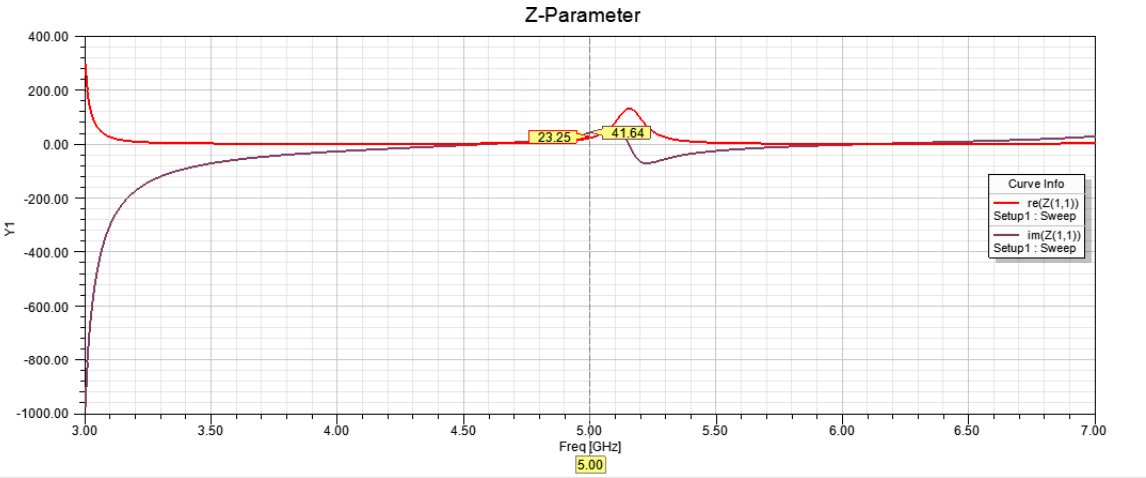

Figure 14: Impedance parameter of untuned antenna.

Figure 13 above shows that the return loss at 5 GHz is -4.58 dB. The antenna is not very efficient due to a low return loss. This is caused by an impedance mismatch in the transmission line. *Figure 14* shows the impedance at the antenna port. The impedance must be 50 Ω for a maximum power transfer. Since the antenna is not transmitting enough power, a parametric analysis is performed to tune the antenna parameters. The antenna is simulated by varying the width of the antenna from 11 mm to 25 mm with 1 mm increments. The S11 values obtained from simulation is shown in *Figure 15.*

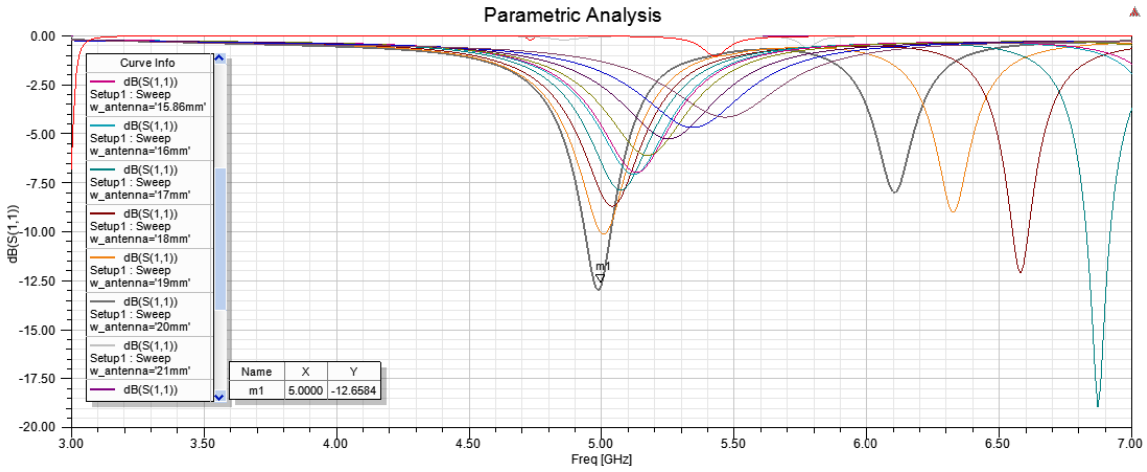

Figure 15: S – parameter for various width of the antenna.

The return loss improved from -4.58 dB to -12.66 dB, when the width is changed from 15.86 mm to 20 mm. The impedance parameter for 20 mm width is shown in *Figure 16*. A part of the input signal is reflected to the source due to mismatch in the transmission line. The parametric analysis showed an improvement in the return loss, when the width is changed to 20mm.

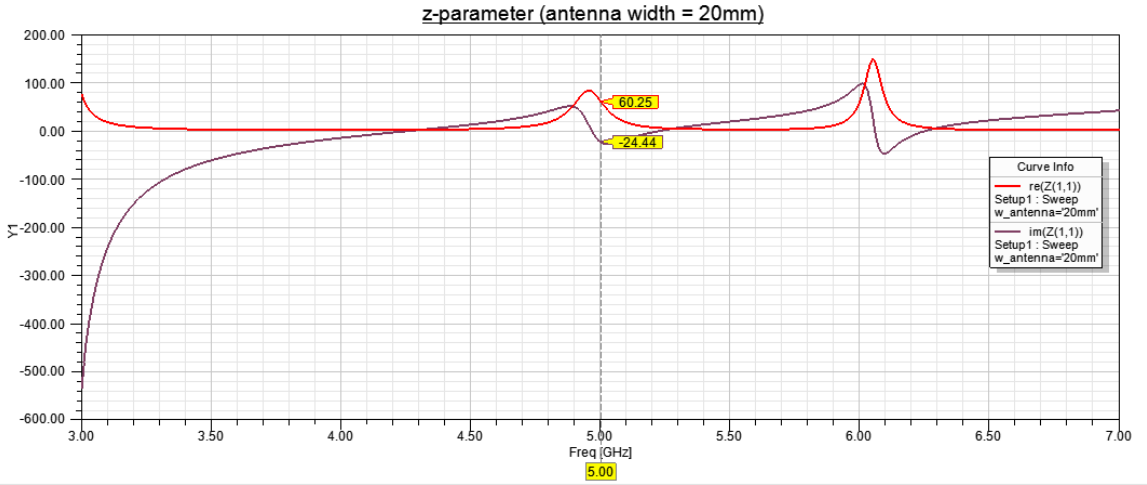

Figure 16: Impedance parameter for antenna width of 20 mm.

A derivative can be requested when simulating an antenna to fine-tune the width. When a derivative is requested, a tuning plot can be adjusted manually to produce a desired

result. After several tunings of both length and width of the antenna, a desired impedance and return loss was obtained. The length and width of the antenna was found to be 11.37 mm and 20.78 mm respectively for a desired resonance frequency. The change in antenna dimension is shown in *Table 3*.

Antenna Variables	Initial Dimension	Tuned Dimension
Length	11.66 mm	11.37 mm
Width	15.86 mm	20.78 mm

Table 3: Change in antenna dimension after tuning

3.1.3 Results

The simulation results obtained for the single antenna are shown below. A plot of return loss, impedance parameter, VSWR, 2D radiation pattern and 3D radiation pattern are included.

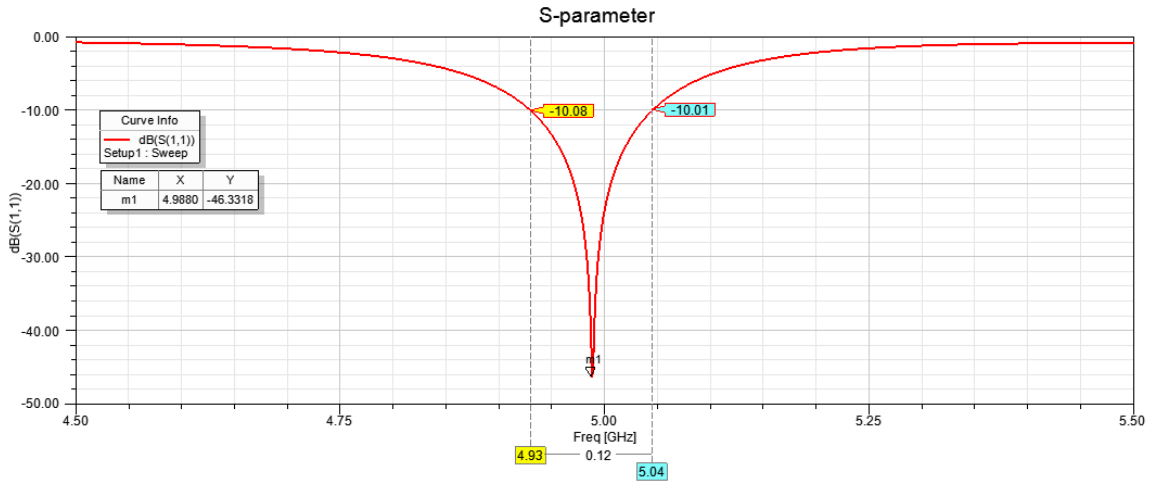

Figure 17: Single antenna return loss.

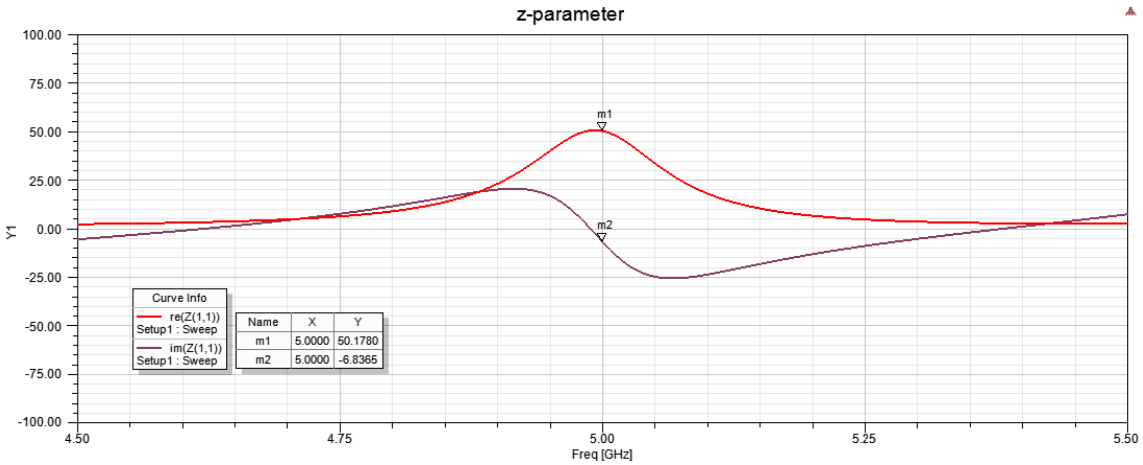

Figure 18: Single antenna Impedance parameter.

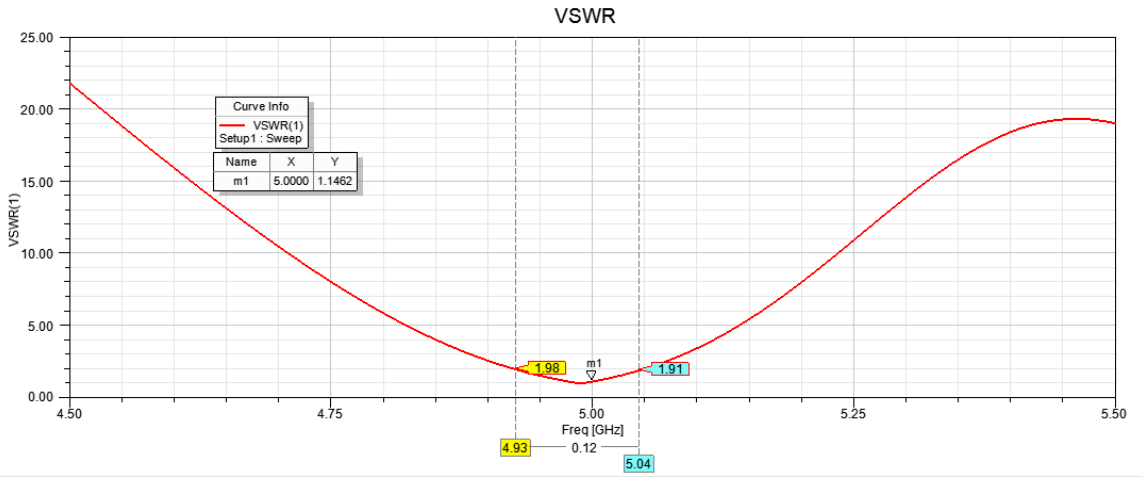

Figure 19: Single antenna VSWR.

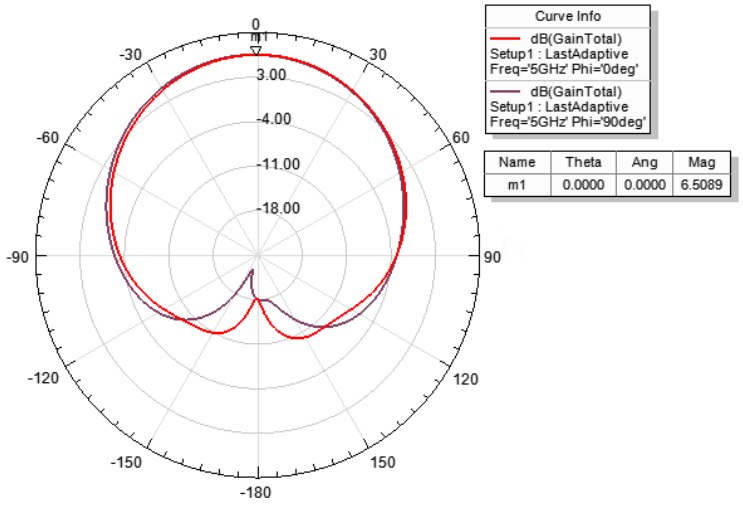

Figure 20: Single Antenna 2D radiation pattern for total field, 0º and 90º elevation view.

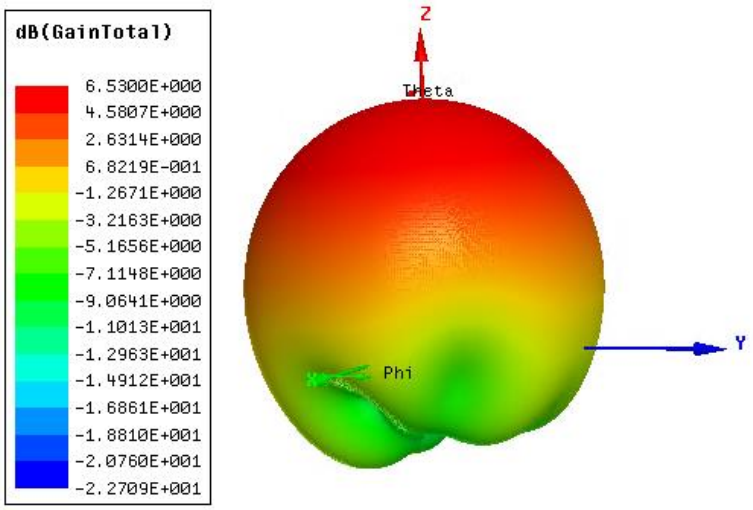

Figure 21: Single Antenna 3D radiation pattern.

The plot presented in *Figure 17* shows that the tuned antenna has a very low return loss. The minimum return loss at the center frequency is about -46 dB. *Figure 18* shows that the impedance at the antenna port is close to 50 Ω. The tuned antenna has a VSWR of less than 2 and a gain of 6.5 dBi. The change in result due to the change in antenna result is shown in *Table 4*.

Antenna Result (5 GHz)	**Untuned Antenna**	**Tuned Antenna**
Return Loss	-4.58 dB	-46 dB
Impedance	23.25+j41.64 dB	50.18-j6.84 Ω
VSWR	-	1.15
Gain (dBi	-	6.5

Table 4: Change in antenna result.

3.2 Phase shifter

3.2.1 Design

The phase shifter network and the antenna are fabricated on separate substrates. The isolation of the feeding network from the antenna substrate provides higher gain and reduces spurious effects. It also helps to suppress side lobe levels of an antenna radiation pattern. The research conducted by M. T. Ali *et al.* on two different antenna structures shows that the antenna with separate feeding substrate is more advantageous than the antenna with feeding network on the same substrate. They found the ratio of main lobe to the side lobe was -11.9 dB for an antenna with a separate feeding network, whereas, a ratio of -5.35 dB was obtained for an antenna with a feeding network on the same substrate [25]. The feeding network in our design is separate from the antenna plane to obtain a higher gain.

The input signal to the antenna is phase-shifted by providing a true time delay to the signal. The signal is routed through a different length transmission line so that the signal reaches the antenna at a different time. A true time delay is obtained using switch-line phase shifting as in [9] and [10]. A four-bit switched line phase shifter is realized in [9] using Micro-electro-mechanical switches (MEMS) where different length transmission lines are switched to obtain desired phase shift. In [10] a constant phase shift is produced by switching a reference transmission line with a phase shifting line.

In our design, a phase shift is provided by extending a transmission line using RF switches. Four phase shifts of 0º, 90º, 180º and 270º are expected to achieve by successively increasing the length of the transmission line. The transmission line traces are drawn in a circular way around the via that connects the antenna through a coaxial cable. The phase

shifter network connects to the four-way microstrip trace using switches. The design of a phase shifter network is shown in *Figure 22*.

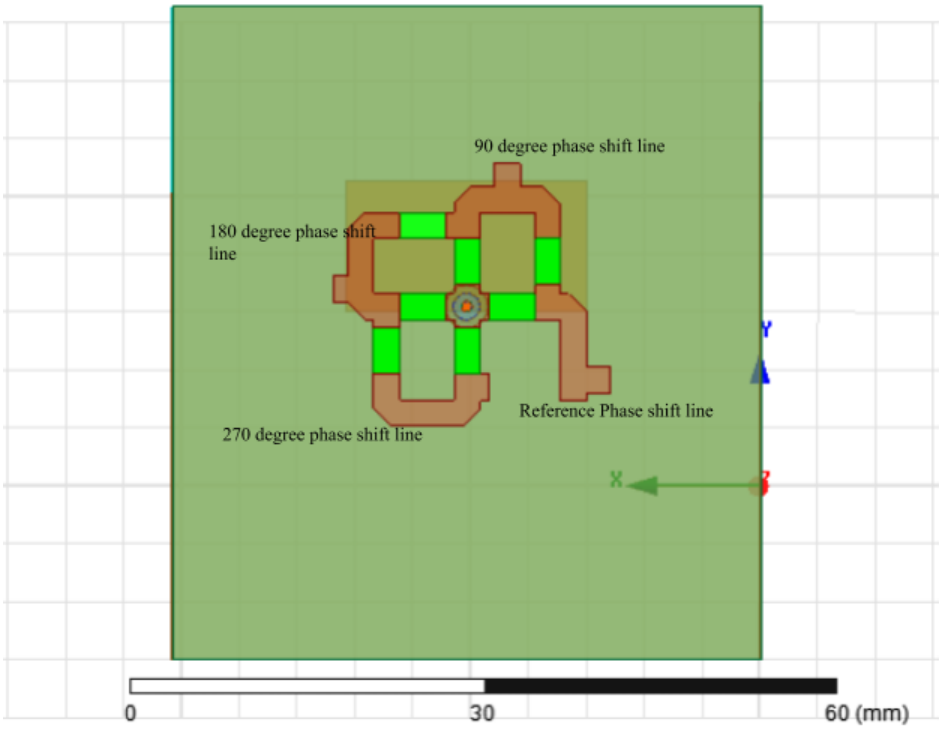

Figure 22: Switch line phase shifter network.

Each piece of a transmission line on a phase shifter network is tuned to provide a 50 Ω impedance at the port. A single-stub matching technique is applied to compensate for a mismatch in the transmission line. In *Figure 22*, the switches are placed in the empty space between the transmission lines. The switches are used to route the input signal to obtain a desired phase shift. The empty spaces between the transmission lines are assigned a lumped RLC boundary to provide an effect of switches. They are assigned a resistance of 1Ω to provide loss due to the placement of switches. The lumped RLC boundary is used only for the simulation purpose. An actual switch will be used when the antenna is fabricated.

The transmission lines are mitered to minimize the loss at the corners. A high VSWR is obtained due to a bend discontinuity. The effect of bend discontinuity increases with increasing frequency. In our design the corners are mitered as shown in *Figure 23* to compensate for the loss.

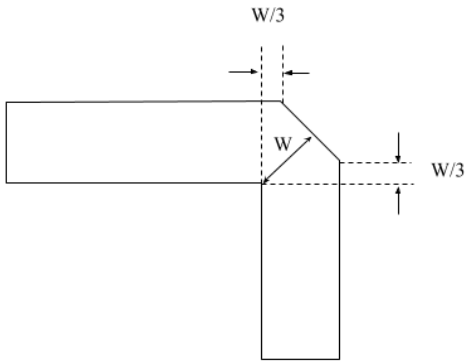

Figure 23: Mitered transmission line to reduce the discontinuity effect.

The dimension of each transmission line on a phase shifter network is shown in *Figure 24*.

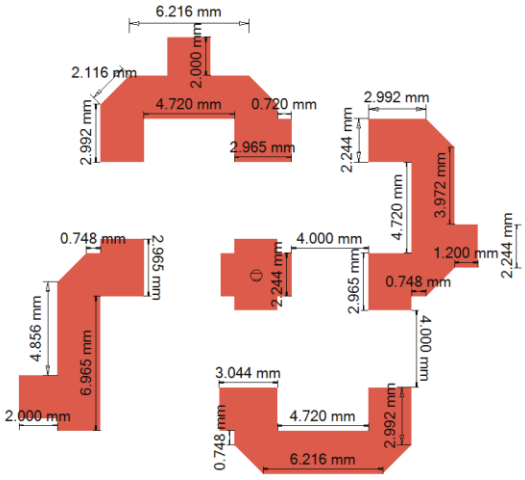

Figure 24: Dimensions of each transmission lines on a phase shifter

An increment of 90º phase shift is expected with an addition of each transmission line. The electrical length of each arm of the transmission line was calculated to be 7.13 mm to provide a phase increment of 90º. The ratio of the width of the transmission line to the height of the dielectric substrate is greater than one. Therefore, equations (10) and (11) were used to calculate the length of the transmission line. This electrical length could not be realized without leaving enough space around the transmission lines. The realized length of each arm of the transmission line is approximately 16.2425 mm (measured from center) which is about twice the calculated length. Due to the increment of realized transmission line length, the phase shift of about 205º (i.e. 155º) is expected with each additional transmission line.

Even though the expected phase shift may not be achieved, but the transmission lines in phase shifter network throughout this thesis will be referred as reference phase shift, 90º phase shift, 180º phase shift and 270º phase shift as shown in *Figure 22*.

3.2.2 Stub Matching

The impedance at each port of a four-way trace connecting the antenna was close to 50 Ω. When the microstrip traces of the phase shifter are placed on a substrate, the impedance is no longer 50 Ω. Hence, a single-stub matching technique is implemented to transfer the impedance of 50 Ω from the port at the four-way trace to the port of the phase shifter. The difference in Z-parameters at the four-way port and the phase shifter port is shown in *Figure 25*.

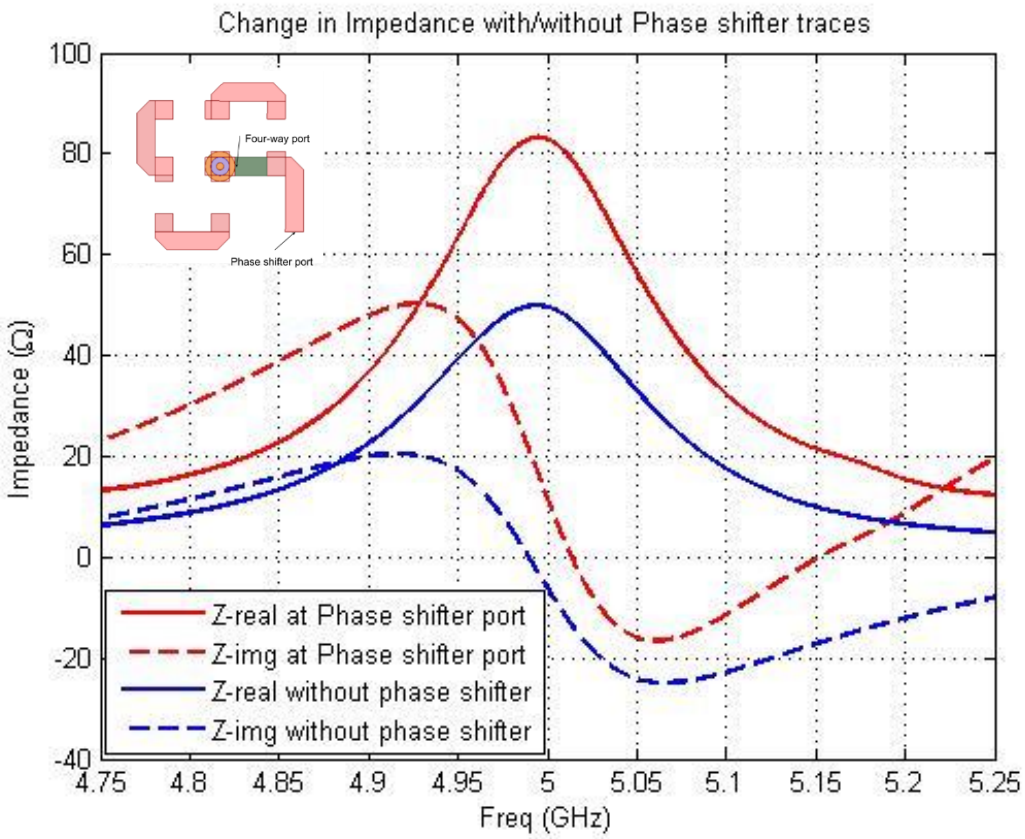

Figure 25 : Difference in z-parameter at the reference line junction and the phase shifter port.

The impedance at the four-way port where the reference line connects was found to be 49.53 – j5.885 Ω at 5 GHz, whereas the impedance at the phase shifter port was found to be 82.93 + j11.23 Ω. To transfer the impedance at the four-way port to the phase shifter port, equations (19) - (23) were used to roughly estimate the size and position of an open stub. It was difficult to determine the exact location and the size of the stub due to curved traces and involvement of coaxial cable. The size and position of an open stub was tuned in HFSS with multiple simulation and found to be of length 2 mm at 1.734 mm from the phase shifter port. The *Figure 26* shows that the transferred impedance is close to the impedance found before the placement of the phase shifter. The impedance at 5 GHz was found to be 53.63 - j10.68 Ω. The change of impedance is shown in *Table 5*.

Impedance at four-way port	49.53 – j5.885 Ω
Impedance at phase shifter port	82.93 + j11.23 Ω
Impedance after first stub placed	53.63 - j10.68 Ω

Table 5: Change in impedance due to placement of phase shifter network and single stub.

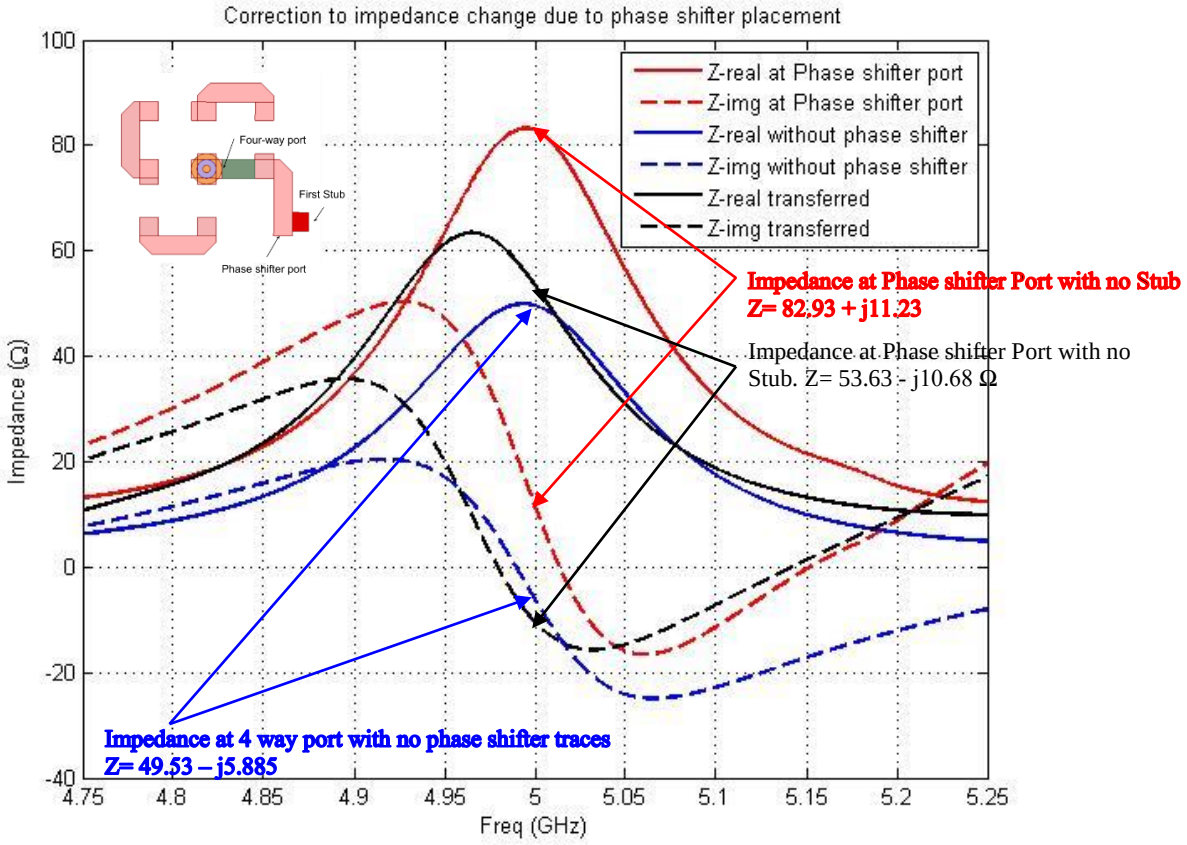

Figure 26: Impedance correction at the reference line junction

With the first stub in place, the impedance at the four-way port by the 90º phase shifter junction and the impedance at the phase shifter port was obtained from the simulation. The simulation was performed by removing the trace connecting the reference line and the four-way port, and connecting the traces leading through a 90º phase shift. The difference in the impedance values are shown in *Figure 27*. The impedance at the four-way port was found to be 49.56 – j0.1965 Ω whereas the impedance at the phase shifter port was found to be 37.92 – j6.417 Ω. A single open stub of length 2 mm was placed at 10.86

mm away from the load impedance i.e. the impedance at the four-way port. The simulation shows that the stub improved the impedance to 55.69 + j5.368 Ω. The improved impedance is shown in *Figure 28*. The impedance values are also shown in *Table 6*.

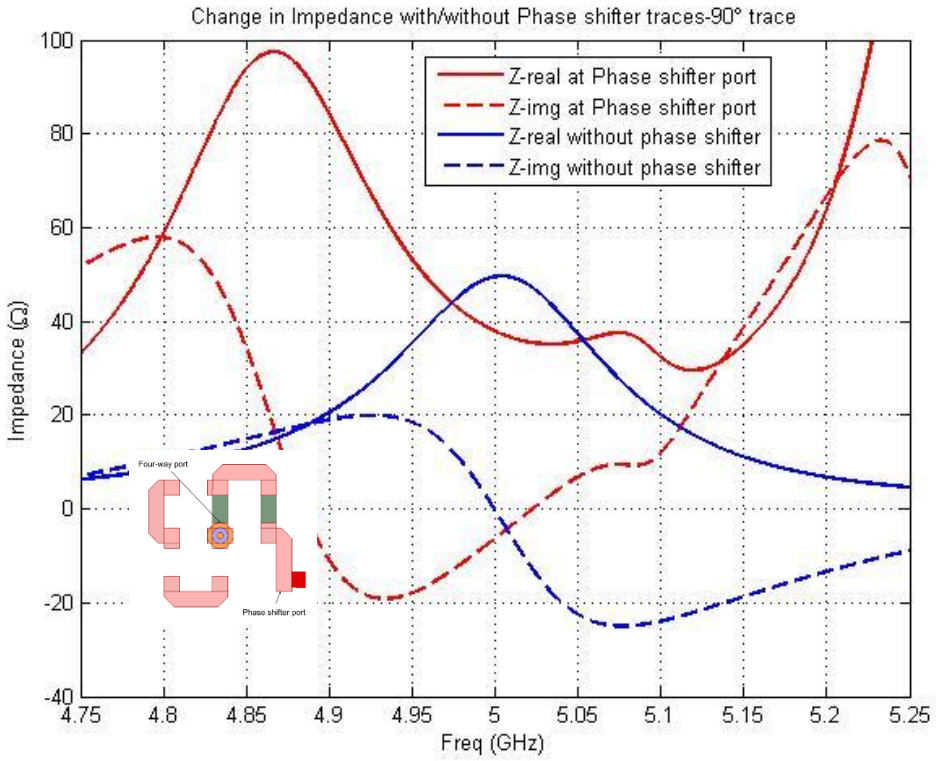

Figure 27: Difference in z-parameter at the 90º trace junction and the phase shifter port

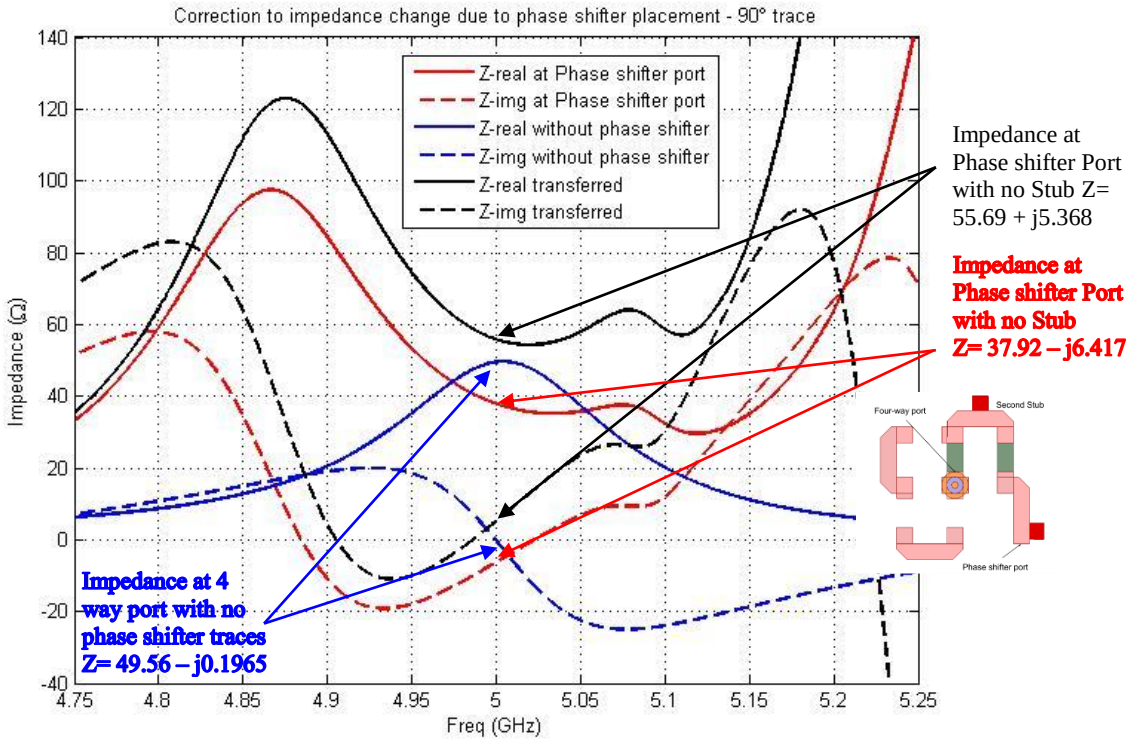

Figure 28: Impedance correction at the 90º trace junction

Impedance at four-way port	49.56 – j0.1965 Ω
Impedance at phase shifter port	37.92 – j6.417 Ω
Impedance after second stub placed	55.69 + j5.368 Ω

Table 6: Change in impedance due to placement of second stub.

Similarly, the impedance at the four-way port that connects the 180º phase shifter trace was found to be 49.71 – j0.3224 Ω. The impedance at the phase shifter port was changed to 55.91 + j9.99 Ω. The z-parameters for both ports are shown below in *Figure 29*.

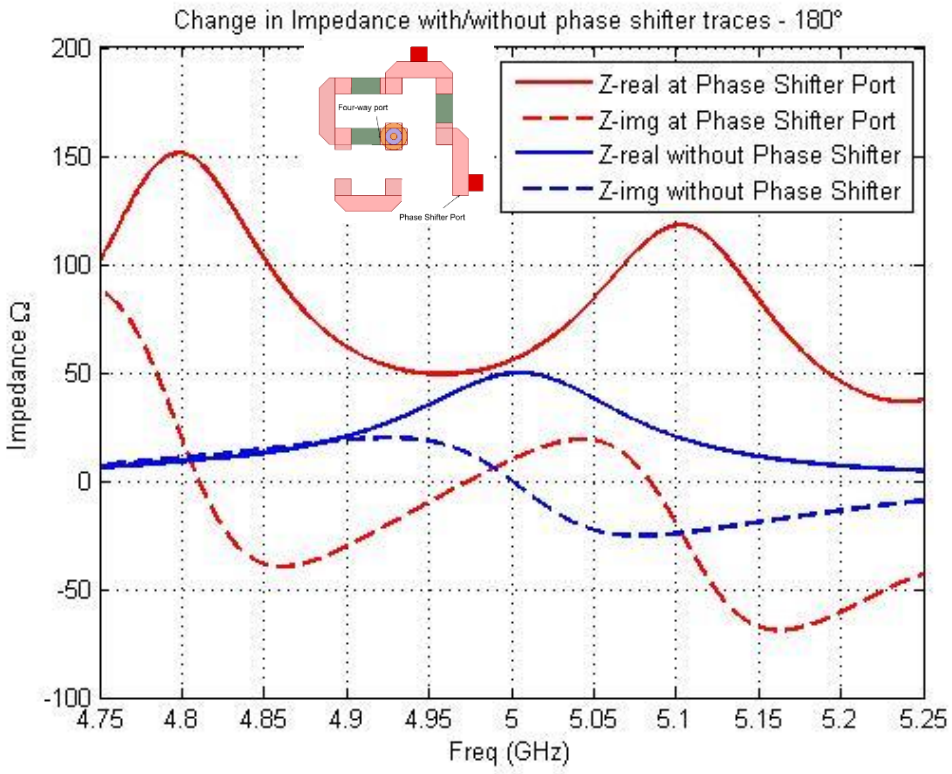

Figure 29: Difference in z-parameters at the 180º trace junction and the phase shifter port

To compensate for the impedance change, an open stub of 1.2 mm was placed 8.49 mm away from the load impedance. The transferred impedance value was found to be 57.94 – j2.78 Ω. The change in impedance is shown in *Table 7*.

Impedance at four-way port	49.71 – j0.3224 Ω
Impedance at phase shifter port	55.91 + j9.99 Ω
Impedance after third stub placed	57.94 – j2.78 Ω

Table 7: Change in impedance due to placement of third stub.

Due to the placement of an open stub, improvement was seen only on the reactance and not in resistance. However, the reflection coefficient at the resonance frequency improved by 3 dB. The S11 changed from 19 dB to 22 dB. A plot with transferred impedance is shown in *Figure 30*.

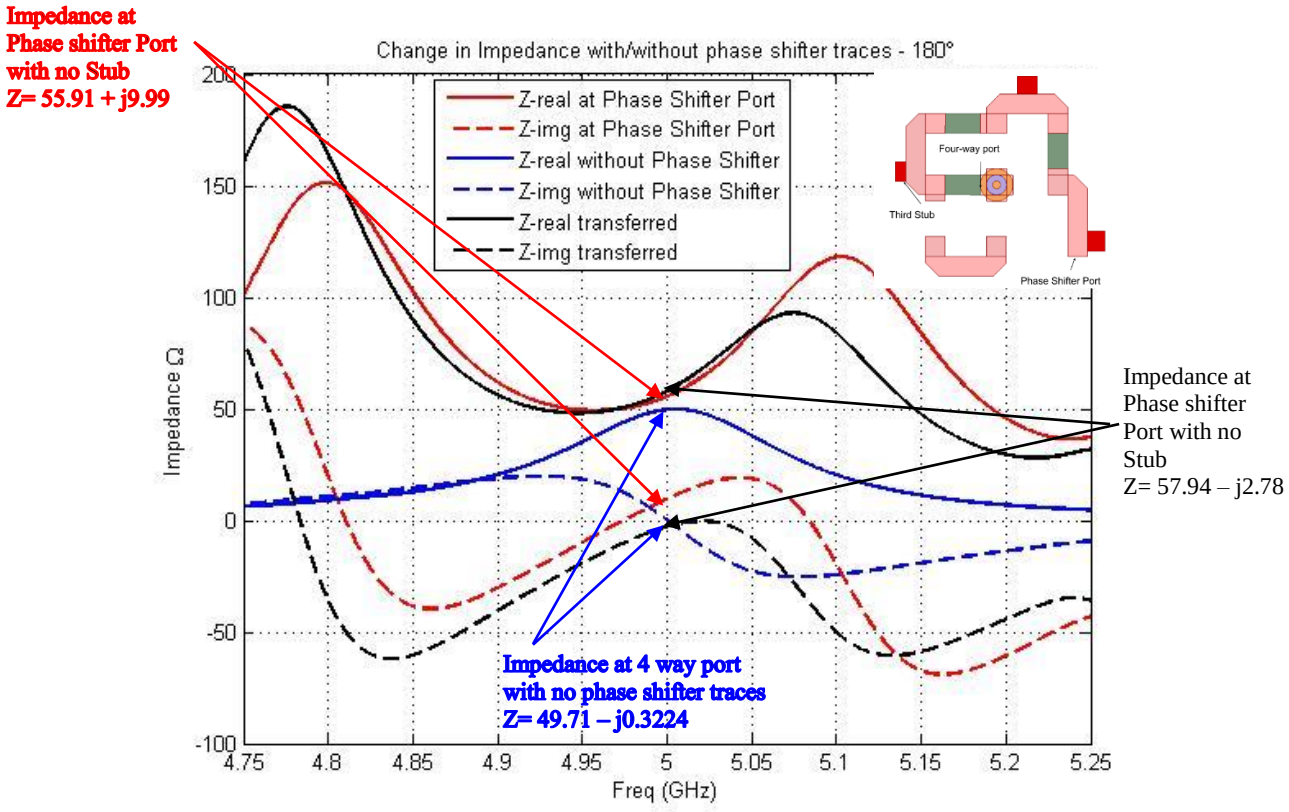

Figure 30: Impedance correction at the 180º trace junction

With all the stubs in place, the simulation was performed to measure the impedance at the phase shifter port. It was found that the impedance at the phase shifter port was found to be 60.7 – j15.6 Ω. There was a significant change in the impedance compared to the value measured at the four-way port. The impedance value at the four-way port before the placement of the phase shifter was 49.17 + j2.06. The difference in impedance is shown in *Figure 31*. To compensate for the change in impedance, an open stub of 0.8 mm was placed 5.12 mm away from the load. The new impedance was found to be 60.7 – j9.421 Ω. The plot for the changed impedance is shown in *Figure 32*. The impedance values are also shown in *Table 8*.

Impedance at four-way port	49.17 + j2.06 Ω
Impedance at phase shifter port	60.7 – j15.6 Ω
Impedance after fourth stub placed	60.7 – j9.421 Ω

Table 8: Change in impedance due to placement of fourth stub.

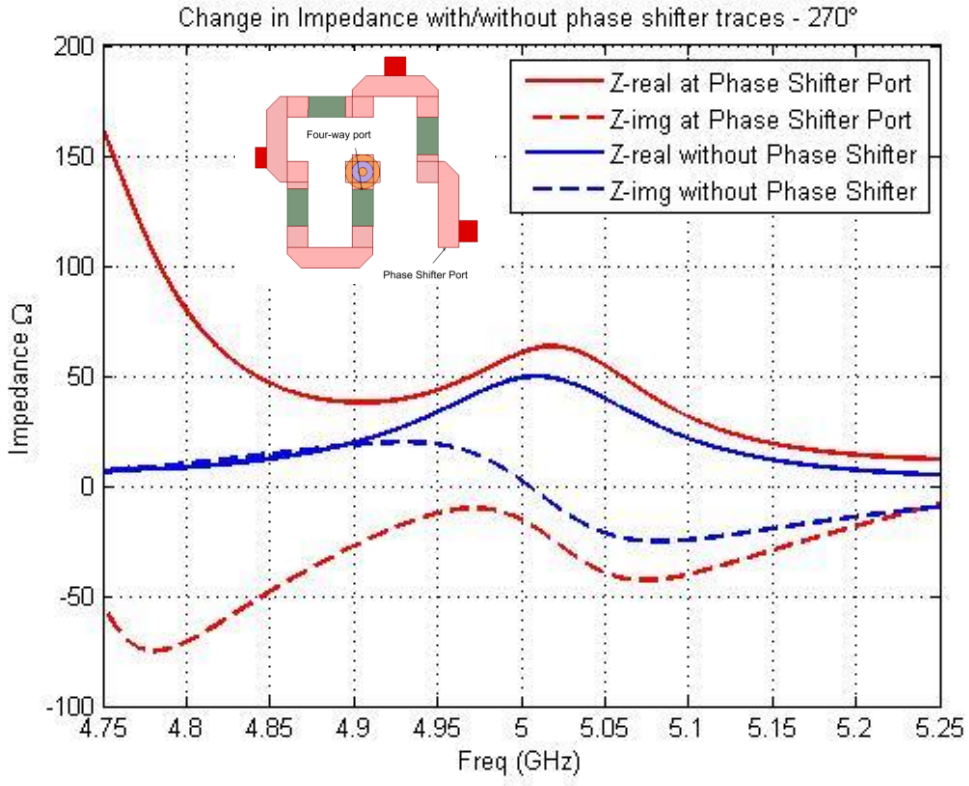

Figure 31: Difference in z-parameter at the 270º trace junction and the phase shifter port

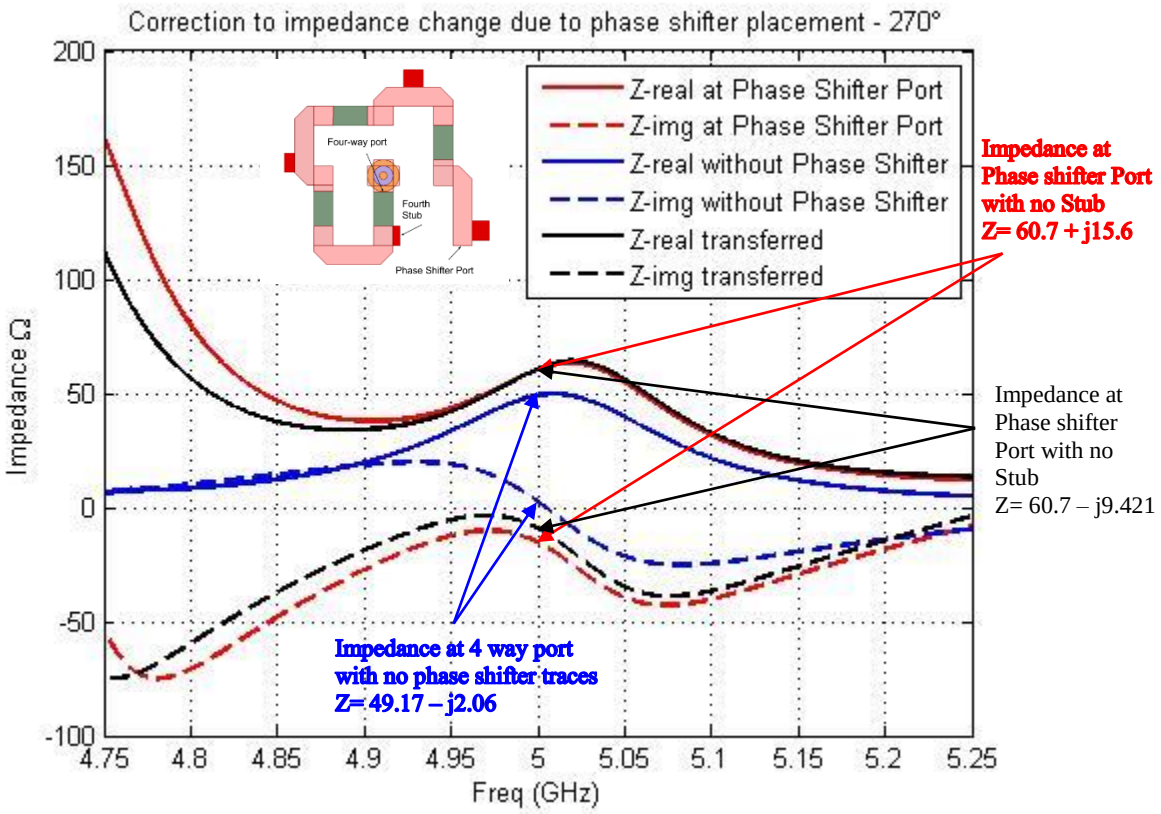

Figure 32: Impedance correction at the 270º trace junction

3.3 Single Antenna with Phase Shifter

The impedance measurements calculated previously were taken by routing the signal through different paths of a phase shifter network shown in *Figure 24*. The port was excited realizing a lumped port which can be assigned anywhere on the substrate, but to fabricate this antenna the port must be placed at the edge of the substrate. The phase shifter port used for previous measurements was extended to the edge. *Figure 33* shows a single antenna with various phase shift configurations. A trace of 22.36 mm was added to the phase shifter port to extend it to the edge.

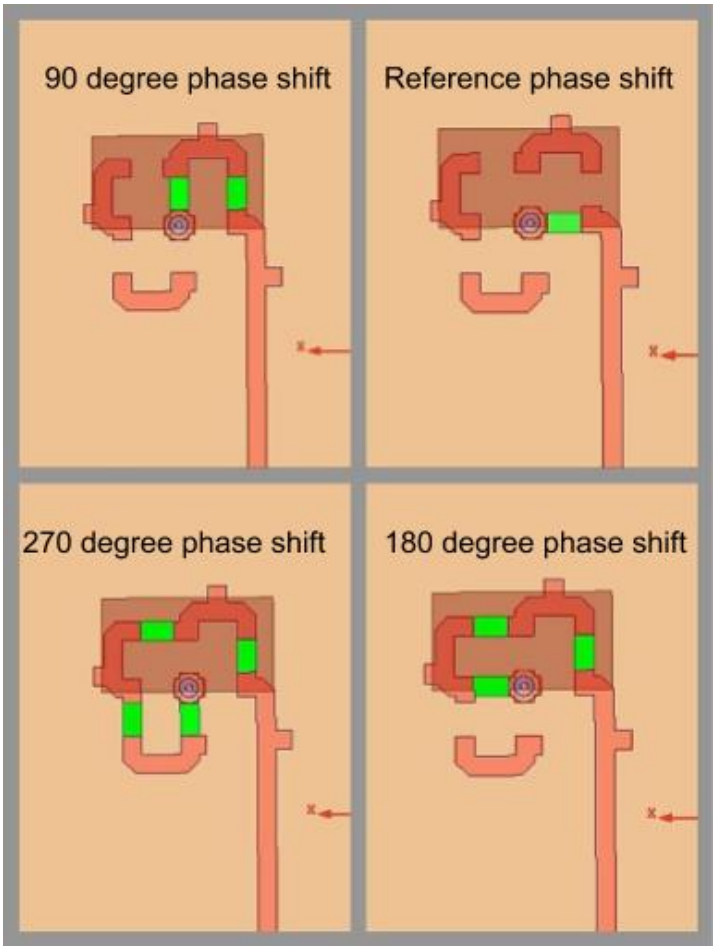

Figure 33: Single antenna with Clockwise phase configuration of 90º, Reference (0º), 180º and 270º.

The extension of the microstrip trace may affect the impedance at the port but a stub cannot be placed on this extended trace anymore. If a stub is placed to match a signal route for a 90º phase shift, the stub may have an adverse effect to the 180º phase shift route. The extended trace has a characteristic impedance of 50 Ω and hence, the extension should be just a continuation of a trace with a 50Ω input impedance. The impedance for each configuration is shown in the result section below.

3.4 Simulation Results

The *Table 9* below contains the simulation results for each phase configurations.

Phase Configuration	Impedance at the port (5 GHz)	S11 (5 GHz)	Max. Gain (5 GHz) 0º Azimuth	Max. Gain (5 GHz) 90º Azimuth
Reference Phase (0º)	52.32 + j15.39 Ω	-19.33 dB	5.43 dB	6.36 dB
90º Phase Shift	43.08 + j1.767 Ω	-19.3 dB	3.92 dB	5.23 dB
180º Phase Shift	37.31 – j5.737 Ω	-24.86 dB	1.93 dB	3.27 dB
270º Phase Shift	38.19 + j12.78 Ω	-16.13 dB	4.03 dB	5.08 dB

Table 9: Simulation result for single antenna with various phase configuration.

The figures corresponding to each of the above results are shown below.

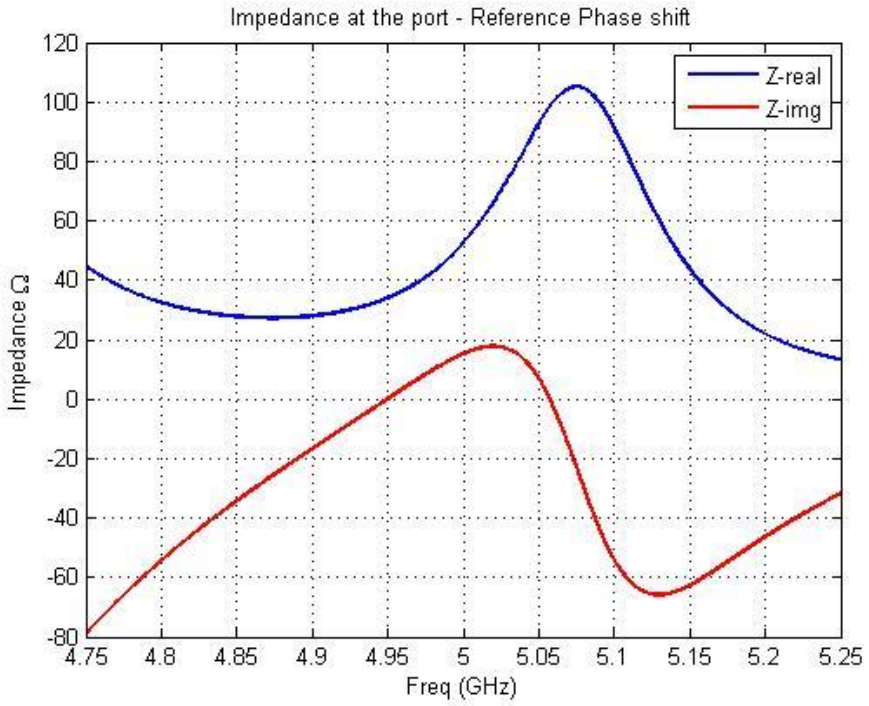

Figure 34: Single antenna port impedance with reference line phase configuration.

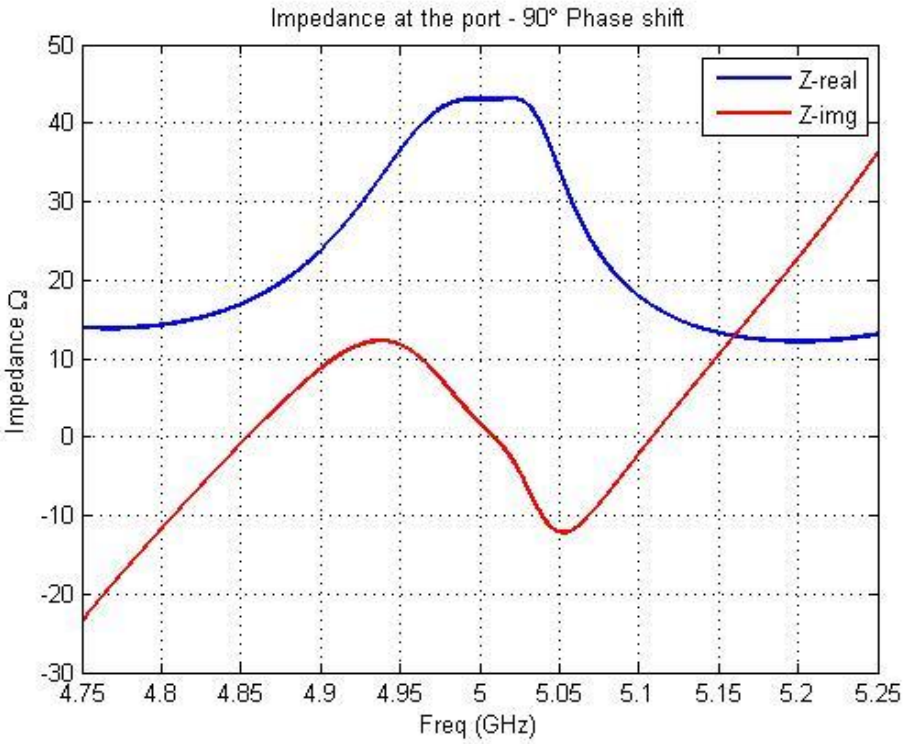

Figure 35: Single antenna port impedance with 90º phase configuration.

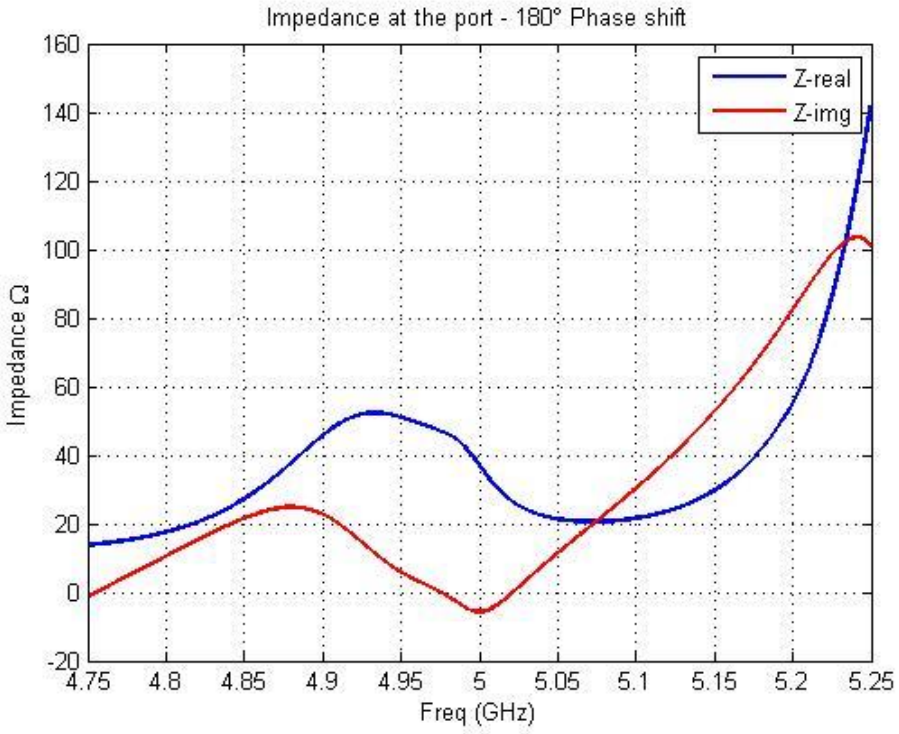

Figure 36: Single antenna port impedance with 180º phase configuration.

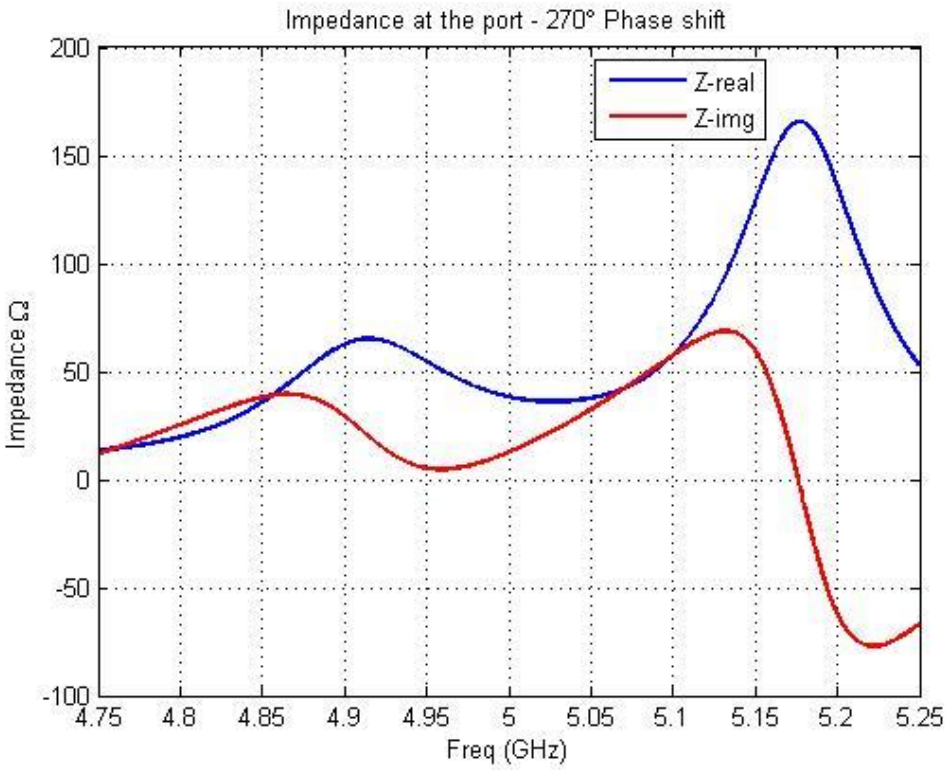

Figure 37: Single antenna port impedance with 270⁰ phase configuration.

The *Table 9* shows that the impedances at the port are not matched perfectly to 50 Ω. The mismatch in impedance can cause the signal to reflect to the source. The maximum power transfer occurs with a matched port. The *Figure 38* shows comparison of return loss for each phase configuration.

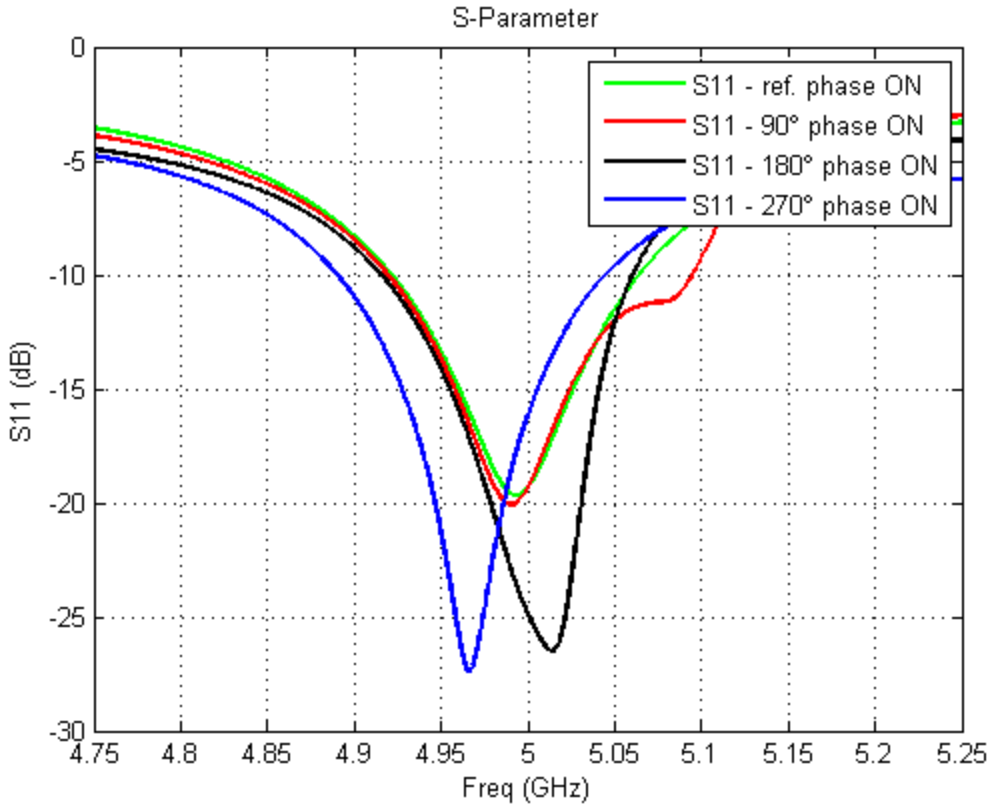

Figure 38: S11 of single antenna with various phase configuration.

Figure 39 and *Figure* 40 shows the two-dimensional radiation pattern of the antenna. The plots show that the gain is different for each phase configuration. This is because the resonant frequency for each phase configurations is not perfectly at 5 GHz. The pattern shape changes with phase configuration also suggest that there is mutual coupling between the antenna and the phase shift structure.

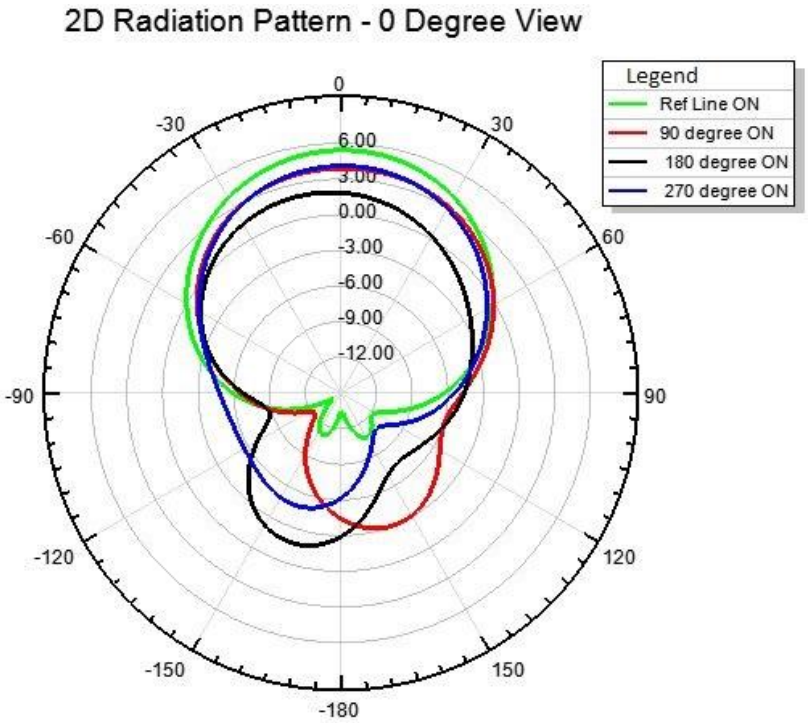

Figure 39: 2D radiation patter - 0º azimuth view

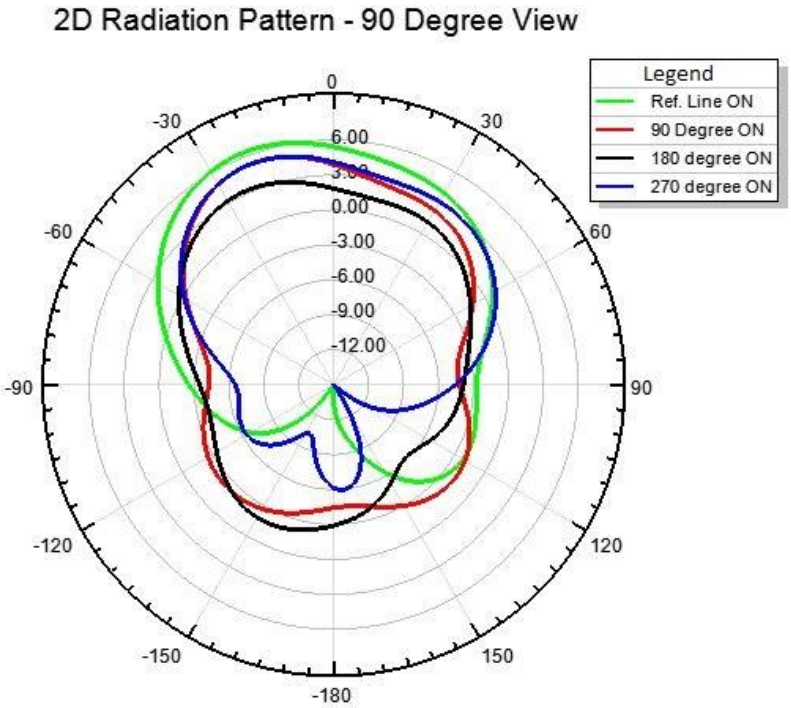

Figure 40: 2D radiation pattern - 90º azimuth view

The far-field intensity with respect to reference phase case are shown in *Figure 41* and*Figure* 42.

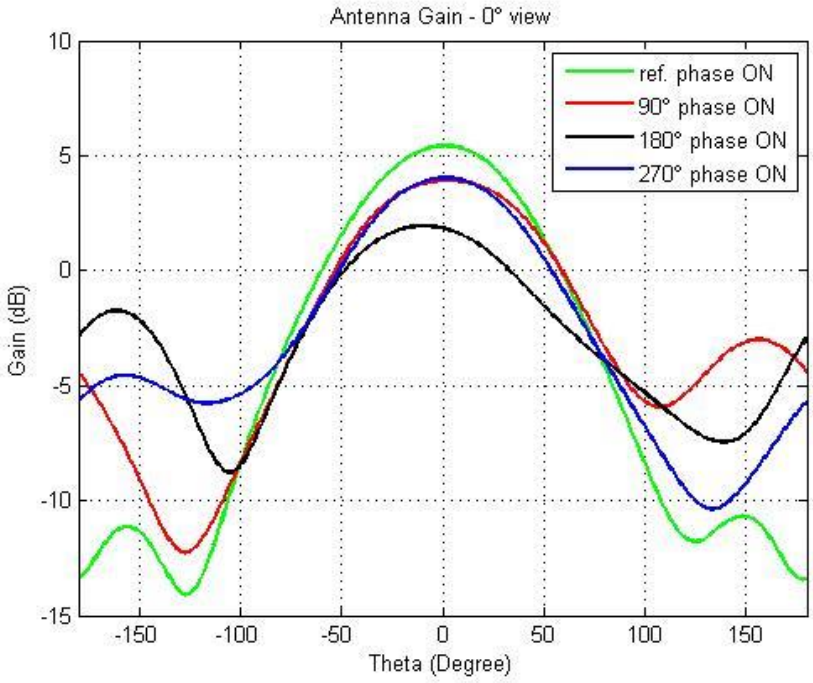

Figure 41: Antenna far-field intensity - 0º azimuth view.

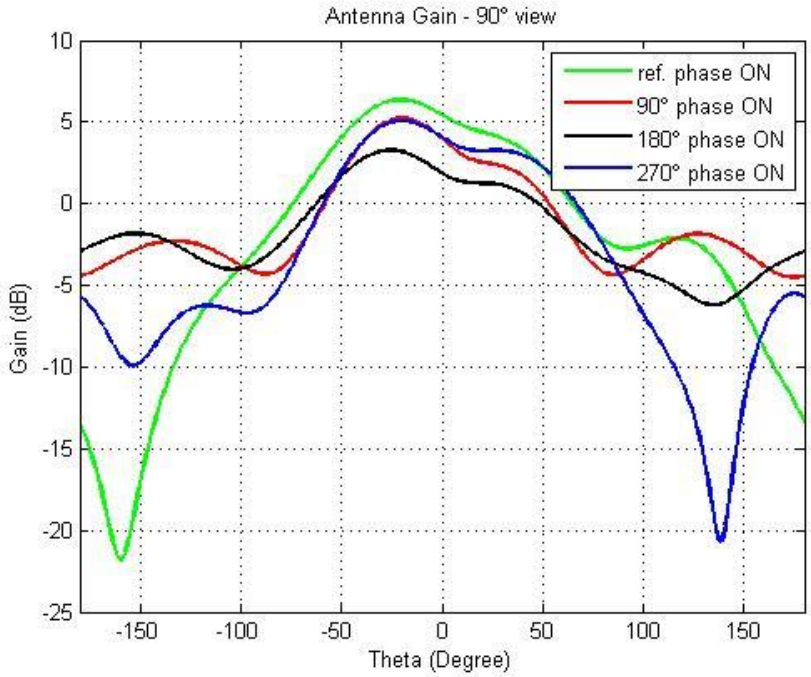

Figure 42: Antenna far-field intensity - 90º azimuth.

A three – dimensional radiation pattern for each phase shift options are shown in *Figure 43 -Figure* 46.

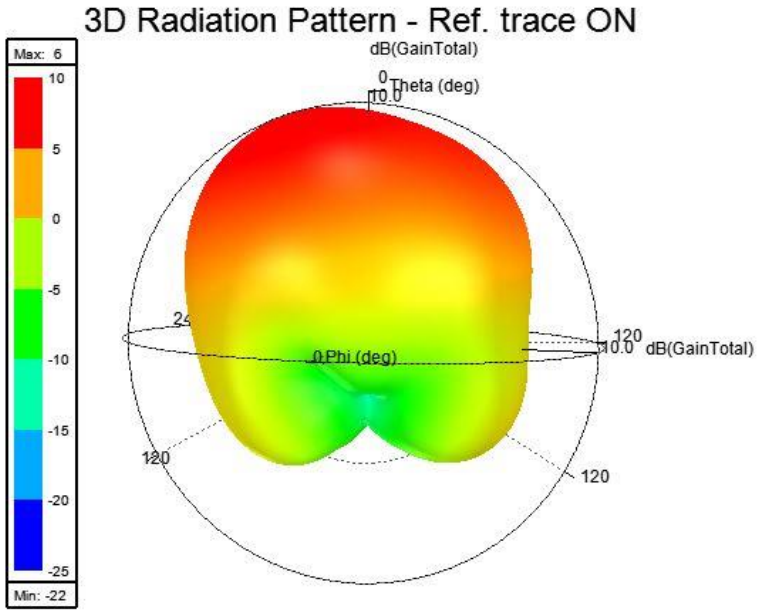

Figure 43: 3D radiation pattern with reference trace ON

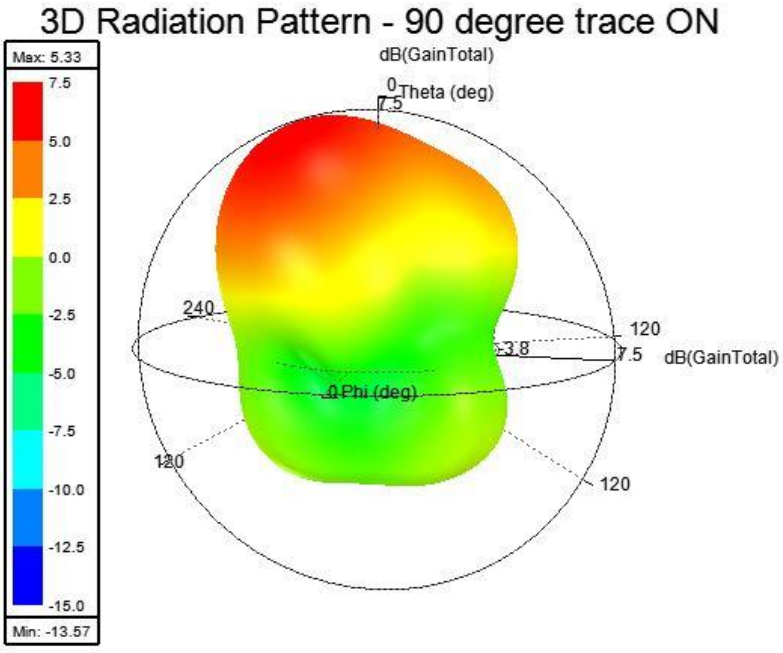

Figure 44: 3D radiation pattern with 90º trace ON

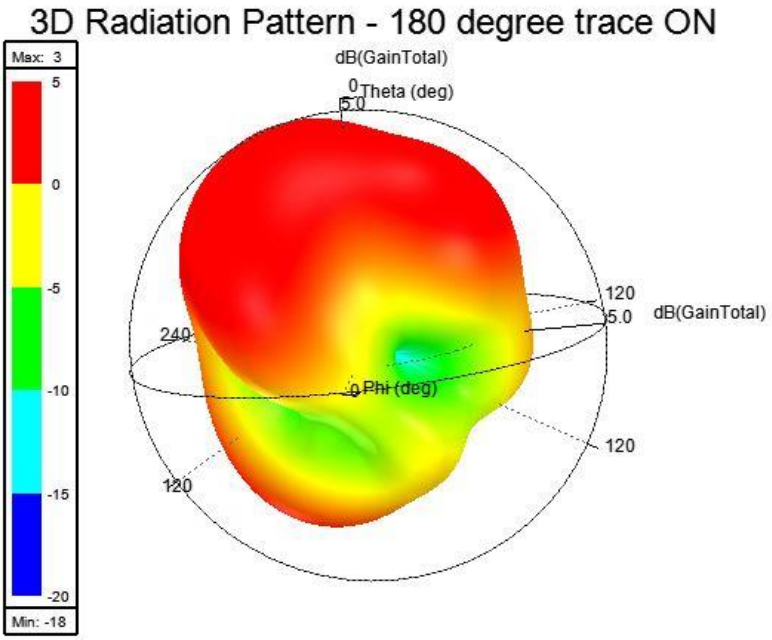

Figure 45: 3D radiation pattern with 180º trace ON.

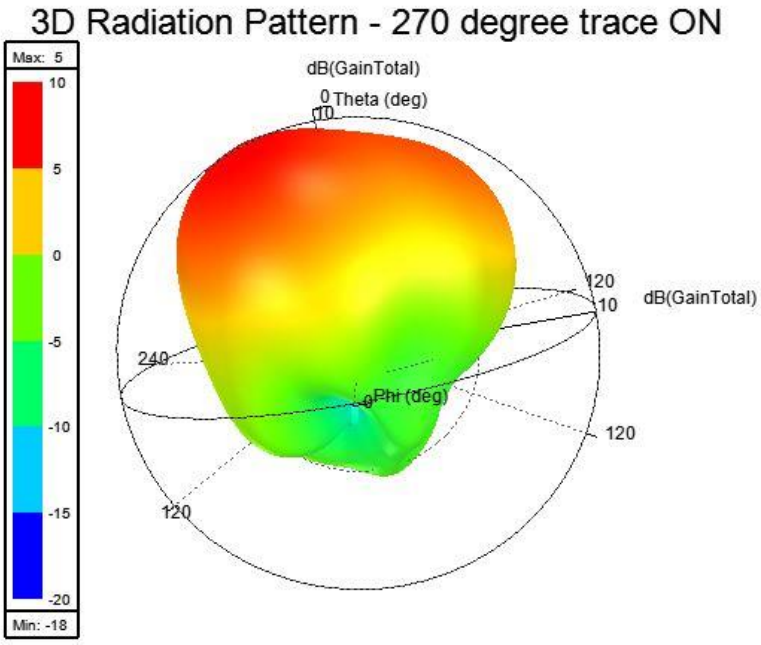

Figure 46: 3D radiation pattern with 270º trace ON.

The goal in designing a phase shifter is to provide a phase shift to the signal going into each antenna element. The design goal was to obtain a phase shift in an increment of 90º with the addition of each transmission line segment. As discussed before, a phase shift of about 155º can be achieved by adding transmission length using switches. However, the switches are not realized in simulation. A lumped resistor value of 1 Ω is used to replace the switches. If we add the length of the lumped component (4 mm) to the length of the transmission line, the overall length of each transmission line will be about 24.2425 mm. This length will provide a calculated phase shift of about 306º (i.e. 54º).

Figure 47 shows phase shift for each phase shift configuration for return loss. The measurement of phase is not possible on a forward gain signal (like S21) because the antenna is just a single port system and S21 can only be requested during simulation on a two-port network.

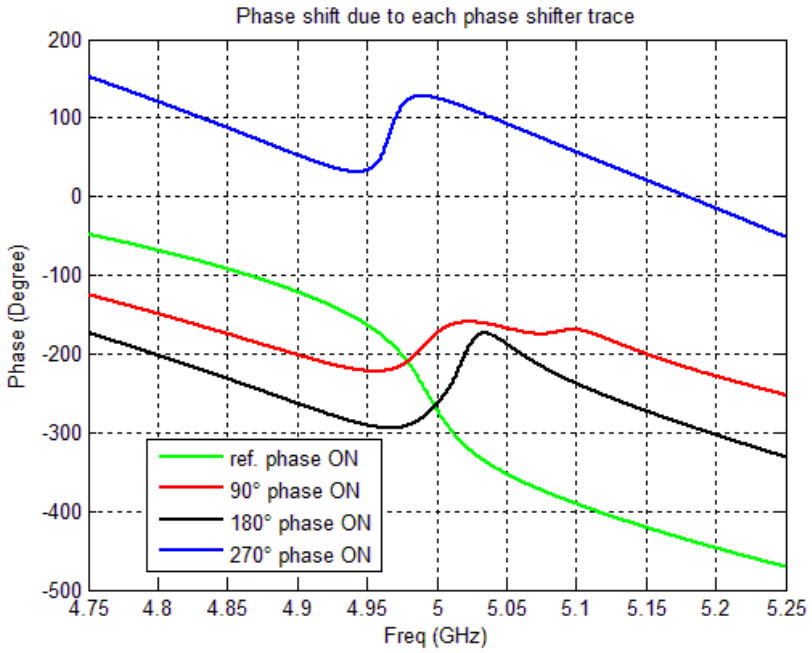

Figure 47: Phase shift due to each phase shifter trace plotted using raw data

Figure 47 shows that the phase values are not within a range of 0º to 360º. Therefore, the data is adjusted to fit the phase curve within this range as shown in *Figure 48*. The maximum phase value for the reference phase is assumed to be 360º and the phase values for the 270º trace are shifted by 360º. Furthermore, the data is converted to obtain positive numbers for change in phase.

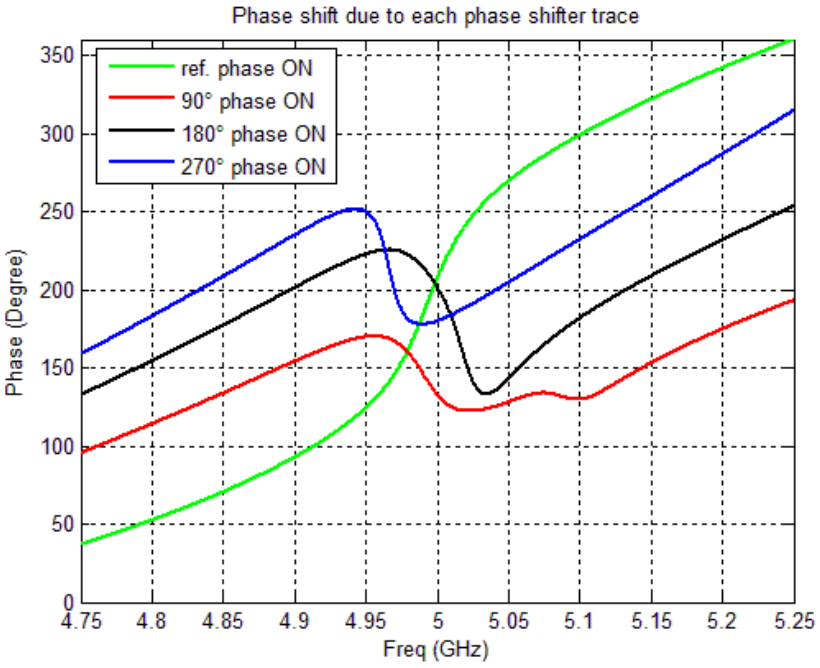

Figure 48: Adjusted Phase Shift due to each phase shifter trace

Figure 49 shows a linear change in phase before and after the resonance region. This plot was obtained by finding the difference in phase for each additional transmission line with respect to the reference transmission line. An average phase change was calculated for all positive and negative changes in phase. It was found that the changes in phase for the positive side were 56.16º, 96.31º, and 117.48º, respectively, for 90º, 180º, and 270º traces. Similarly, for the negative side, the changes in phase were found to be 146.38º, 108.4º, and 58.68º respectively for 90º, 180º, and 270º traces.

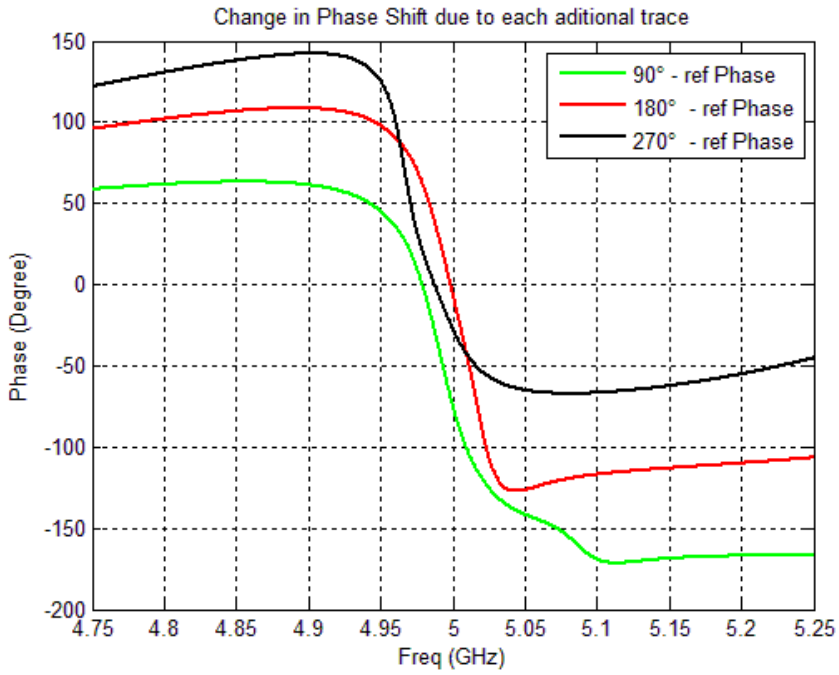

Figure 49: Change in phase shift due to each additional trace.

3.5 Corporate feed design

A corporate feed network is designed to feed a four-element antenna array. A similar feeding network is designed in [26] to feed a conformal microstrip phased array antenna. In this feed system, the lengths from the main feed point to each port are equal. Due to equal lengths, the corporate feed does not introduce additional phase shift to the signal going into the phase shifter network. The corporate feed network designed for our antenna is shown in

Figure 50.

The microstrip line labelled “a” connects the phase shifter network. The width of “a” is same as the width of the transmission line used for the phase shifter network shown in *Figure 24.* The microstrip lines “a” and “d” are of equal dimension and they have an impedance of 50 Ω. The transmission line “c” branches out into two paths, each with 100

Ω impedance. A quarter-wave transformer is used to connect “a” and “c”. The impedance of the quarter-wave transformer is found using equation (18). The impedance required to transfer 50 Ω impedance to 100 Ω was found to be about 70 Ω.

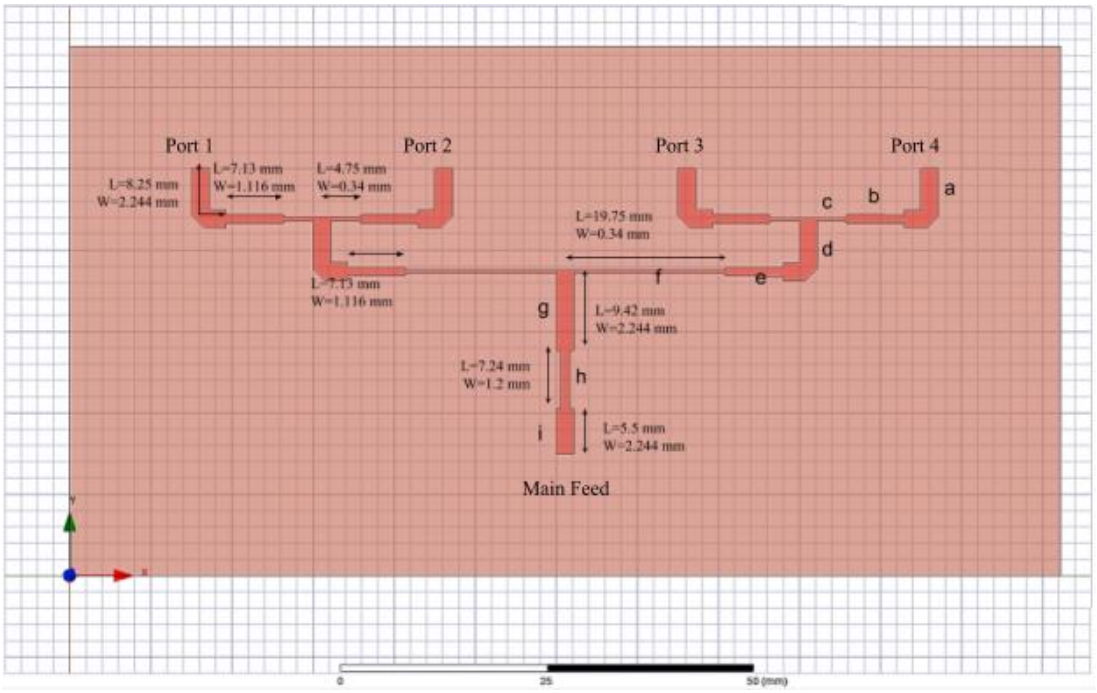

Figure 50: Corporate feed network.

Similarly, the impedance of 50 Ω at “d” was transferred to 100 Ω at “f” using a quarter wave transformer “e”. The microstrip line “g” is a 50 Ω transmission line. It branches out equally on two sides, each with 100 Ω impedance, to provide equal power assuming all port sees 50 Ω. The impedance at the junction of “g” and “h” was slightly off from 50 Ω. Therefore, a quarter wave transformer was used to transfer an impedance of 50 Ω at “i”. The length and width of “i” was tuned in HFSS using a parametric sweep.

This corporate feed network was simulated in HFSS. *Figure 51* shows the return loss at the man port and all other ports of the feeding network. It shows that the return loss at the feed port is found to be -11.53 dB. The return losses at the output ports are found to

be -18.05 dB, -8.5 dB, -7.96 dB, and -17.59 dB respectively. The middle ports show smaller return loss values. This is likely due to mutual coupling.

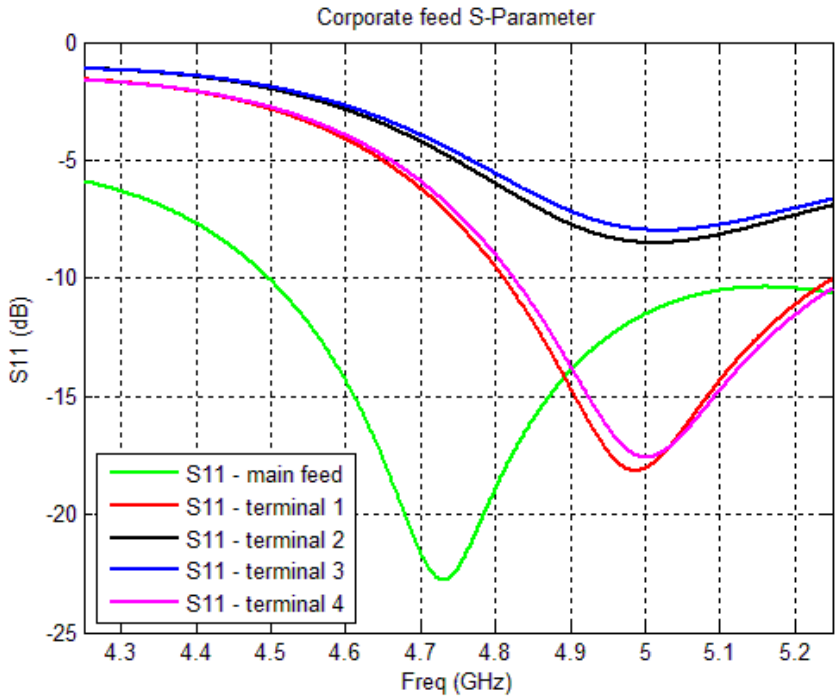

Figure 51: S11 for the corporate feed network.

3.6 Phased Array Antenna

3.6.1 Design

The Phased Array Antenna consist of four patch antenna elements, phase shifter networks, and a corporate feed network. Each antenna element in the array has the same dimension as the single antenna discussed above. The length of each antenna element is 11.37 mm and the width is 20.78 mm. The antenna elements are placed on a substrate of length 80.1128 mm and width 161.7784 mm. The antenna elements are placed one half-wavelength apart center to center and a space of one quarter-wavelength is established between the antenna element and the edge of the substrate. A ground plane is placed on the

other side of the dielectric substrate. A Rogers RT/Duroid 6000 [23] is used as a dielectric material. The height of the dielectric substrate is 1.524 mm and the relative permittivity is 6.15.

The phase shifter for the antenna is placed on a different dielectric substrate. The phase shifter is connected to the corporate feed network as shown in *Figure 52*. The corporate feed and the phase shifter lay on one side of the substrate while the other side has a ground plane.

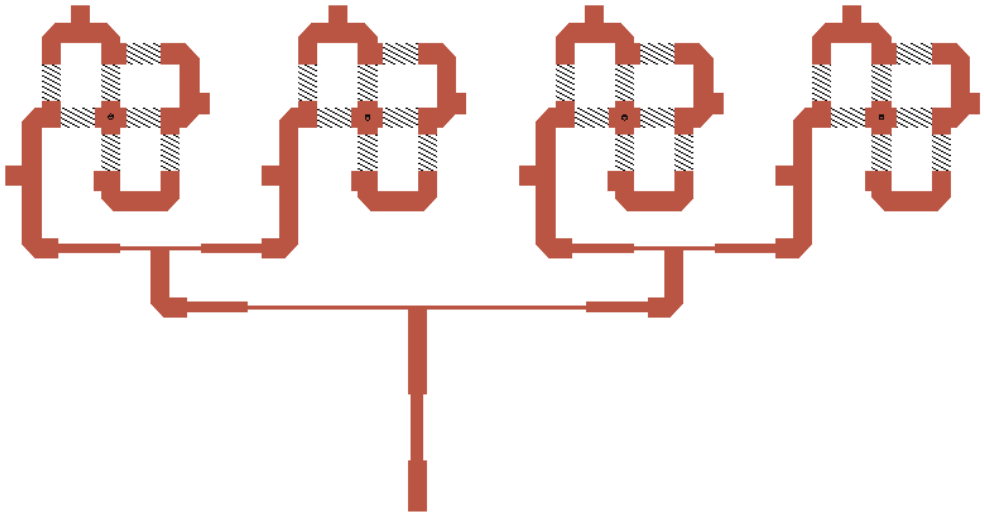

Figure 52: A corporate feed network connected to a phase shifter.

The board with this feeding network is connected to the board with the antenna elements using coaxial cable. The two ground planes are connected by the outer conductor of the coaxial connector that feeds each antenna element. The short 5 mm cable that connects these two boards is designed in HFSS with 50Ω impedance. The inner conductor has a radius of 0.45 mm. The outer conductor has a radius of 1.8425 mm. The dielectric material used between the two conductors is Polyethylene. This material has a dielectric constant of 2.25. The impedance of the coaxial cable is determined using equations (6) and equation

(7). The top view and side view of the antenna array are shown in *Figure 53* and *Figure* 54 respectively.

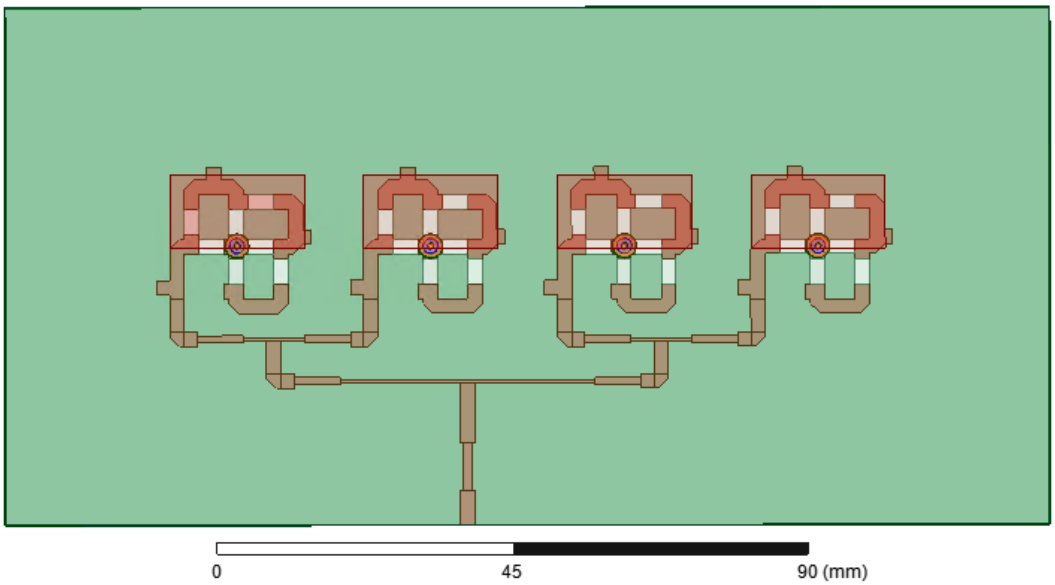

Figure 53: Antenna Array – top view.

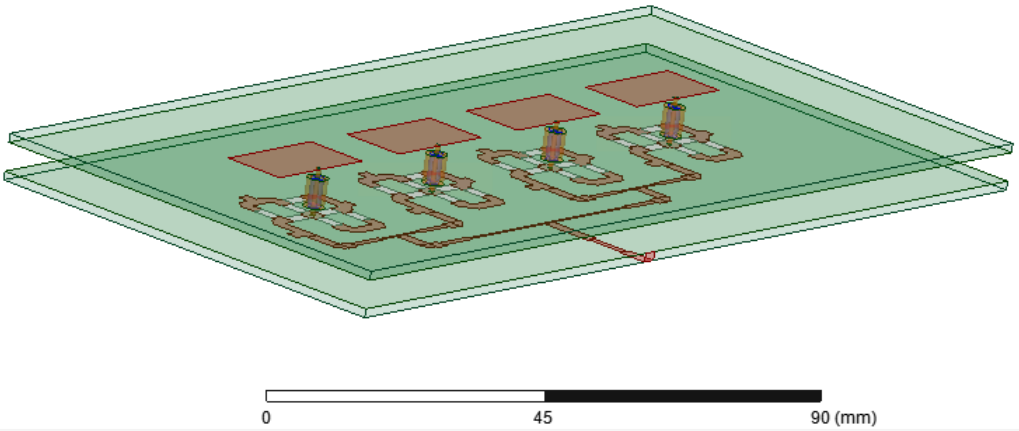

Figure 54: Antenna Array – side view.

3.6.2 Simulation Results

The antenna array is placed on a Perfectly Matched Layer radiation boundary for simulation. The simulation is performed without implementing switches between the transmission line on a phase shifter network. A lumped component is used to connect these transmission lines to produce a desired phase shift. The simulation is performed to obtain beam steering at three different angles. The first simulation is performed by exciting the first antenna with a reference phase, second antenna with 90º, third with 180º, and the fourth with 270º. This is shown in *Figure 55*. This phase configuration should provide a maximum beam steering in the negative x-direction (end-fire direction).

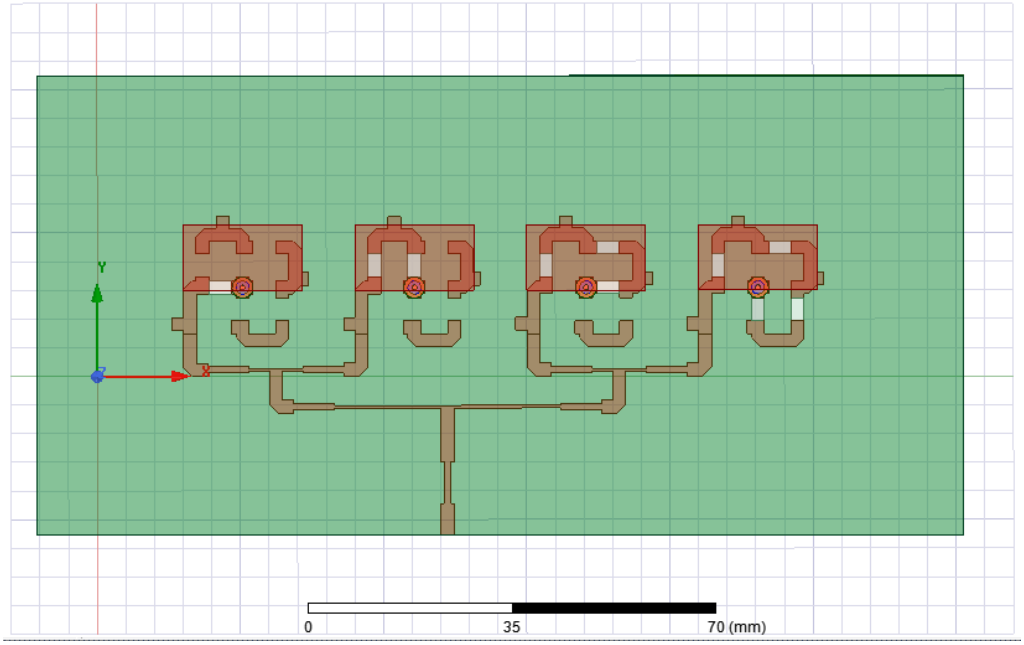

Figure 55: Antenna excitation with 0º, 90º, 180º, and 270º phase shift to each antenna element.

The simulation results are shown from *Figure 56* to *Figure* 59. The simulation results show that the return loss at 5 GHz is about 18 dB. The smaller return loss value is due to impedance mismatch. The impedance is found to be 32.37 – 6.22i Ω at the port as shown in *Figure 57*.

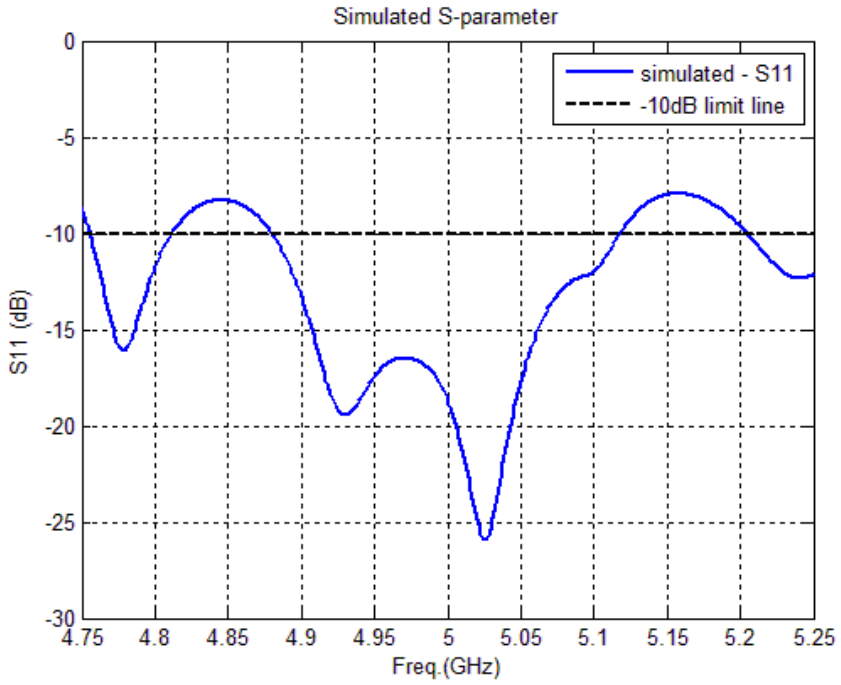

Figure 56: S11 of the antenna array feed port with ascending (0º, 90º, 180º, and 270º) phase shift.

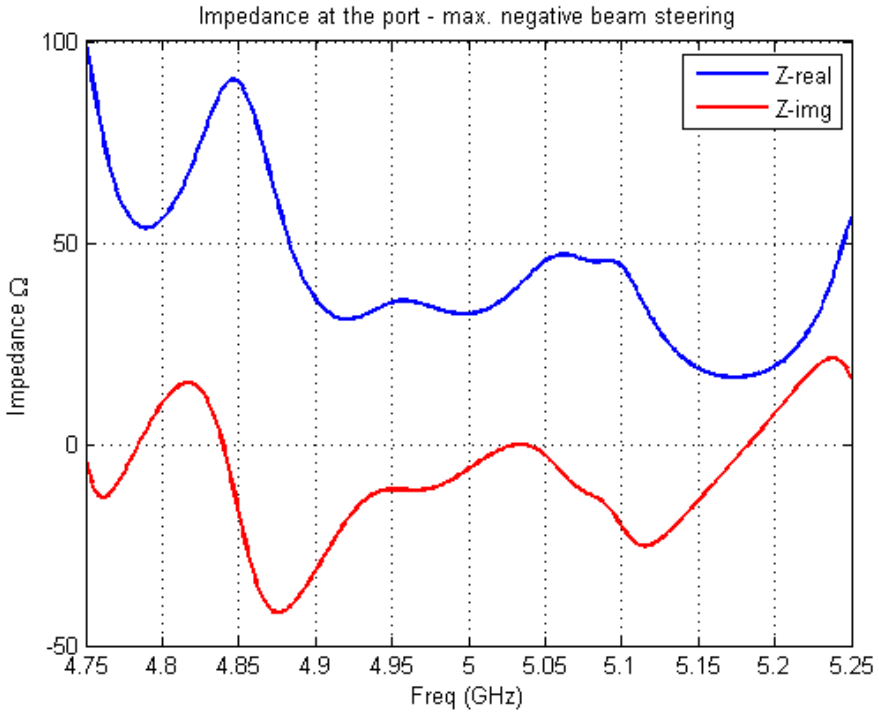

Figure 57: Impedance at the feed port for ascending phase shift.

Figure 58 and *Figure* 59 show the two-dimensional and three-dimensional radiation patterns of the antenna respectively. These radiation pattern shows that the maximum lobe occurred around -45º.

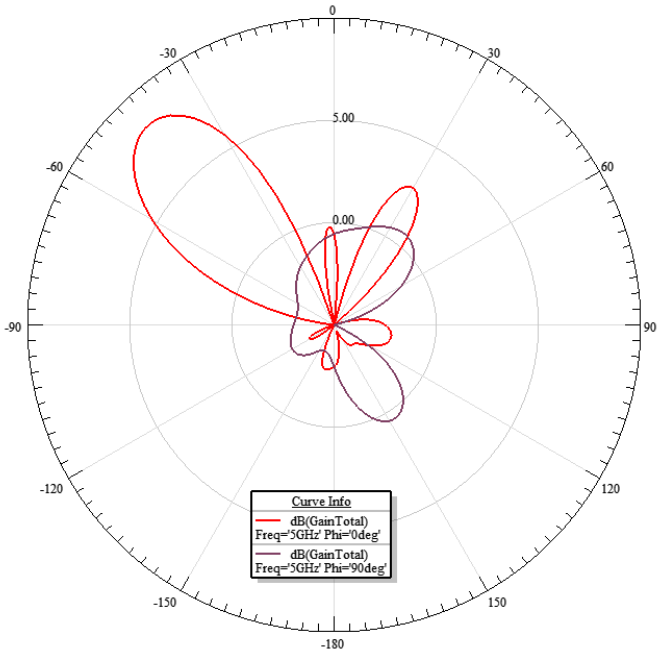

Figure 58: 2D Radiation Pattern – elevation with ascending phase shift

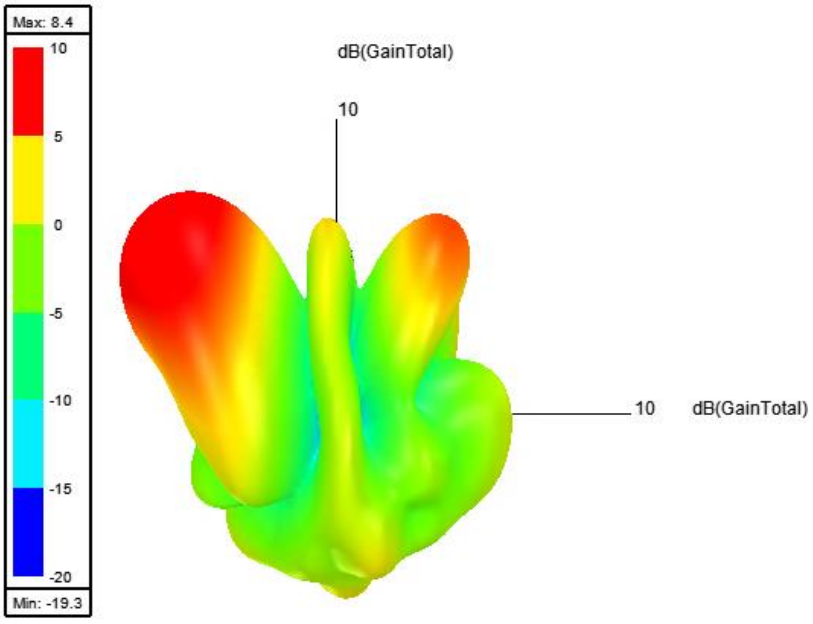

Figure 59: 3D Radiation Pattern with ascending phase shift

The second simulation was performed by exciting the antenna element with the reversed phase configuration as shown in *Figure 60*. This phase configuration should produce a maximum beam steering in the positive x-direction.

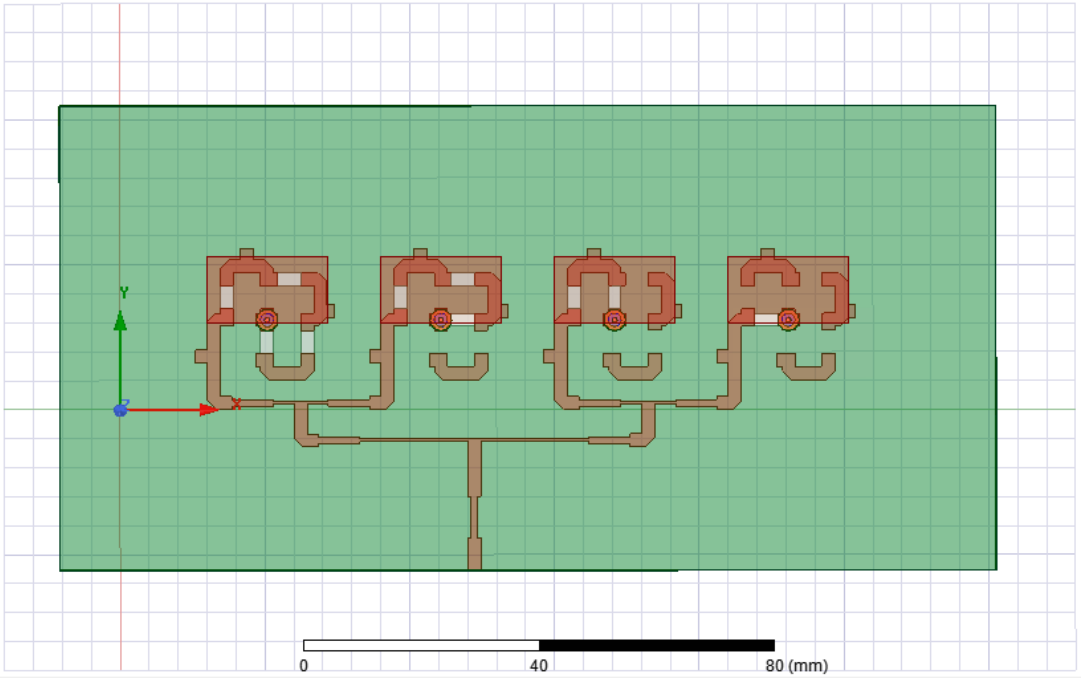

Figure 60: Antenna excitation with 270º, 180º, 90º, and 0º phase shift to each antenna element.

The simulation results are shown below from *Figure 61* to *Figure* 64. The return loss at 5 GHz is still about 18 dB. The Z-Parameter plot in *Figure 62* shows that the impedance at the center frequency is 45.46 – 10.52i **Ω**. *Figure 63* shows that the maximum lobe on positive side occurred at +45º.

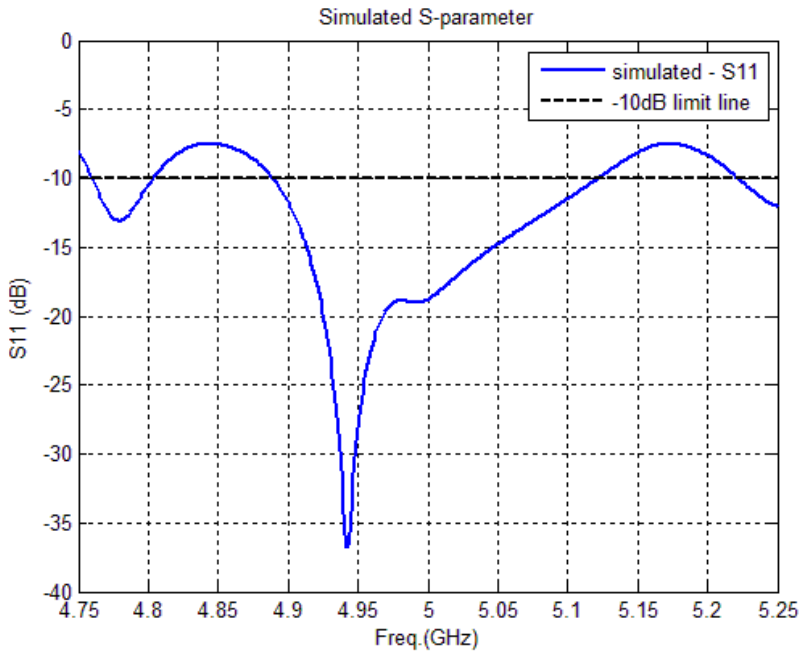

Figure 61: S11 of the antenna array with descending (270º, 180º, 90º, and 0º) phase shift.

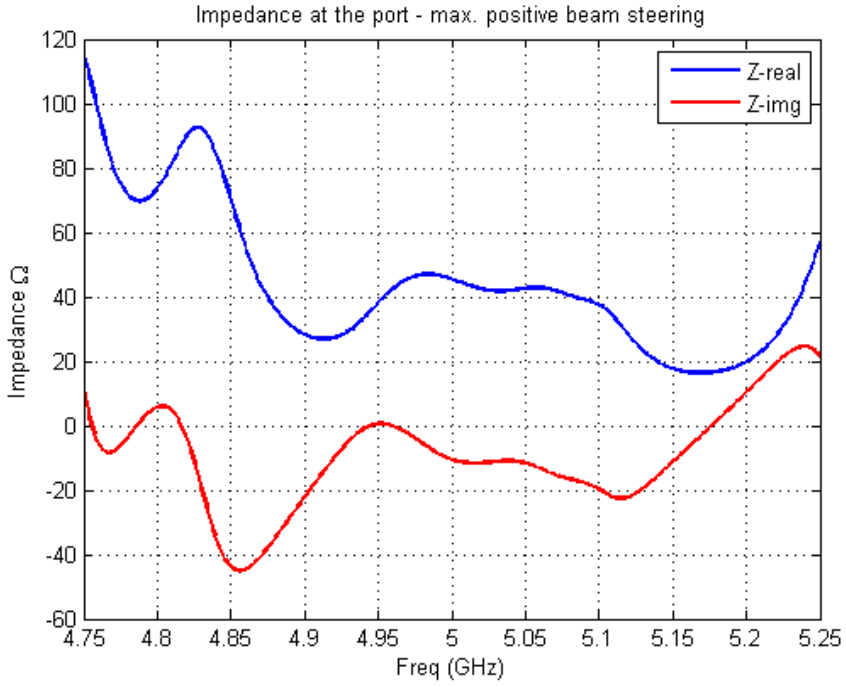

Figure 62: Impedance at the antenna port for descending phase shift.

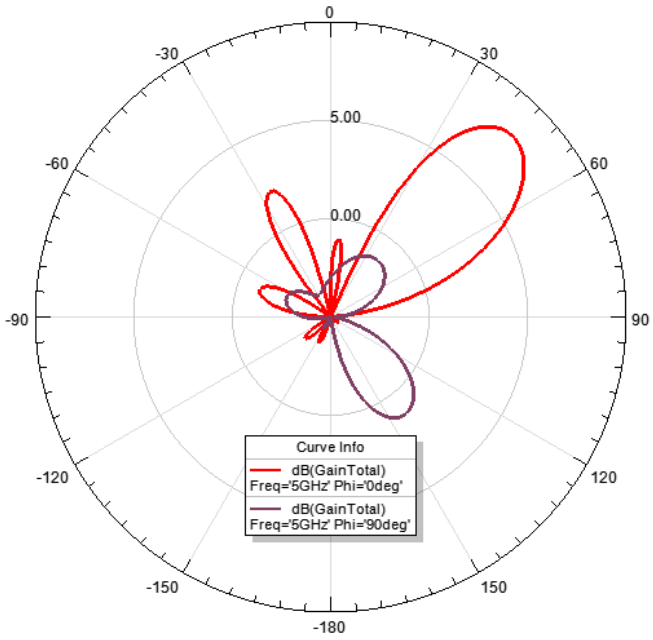

Figure 63: 2D Radiation Pattern - elevation with descending phase shift

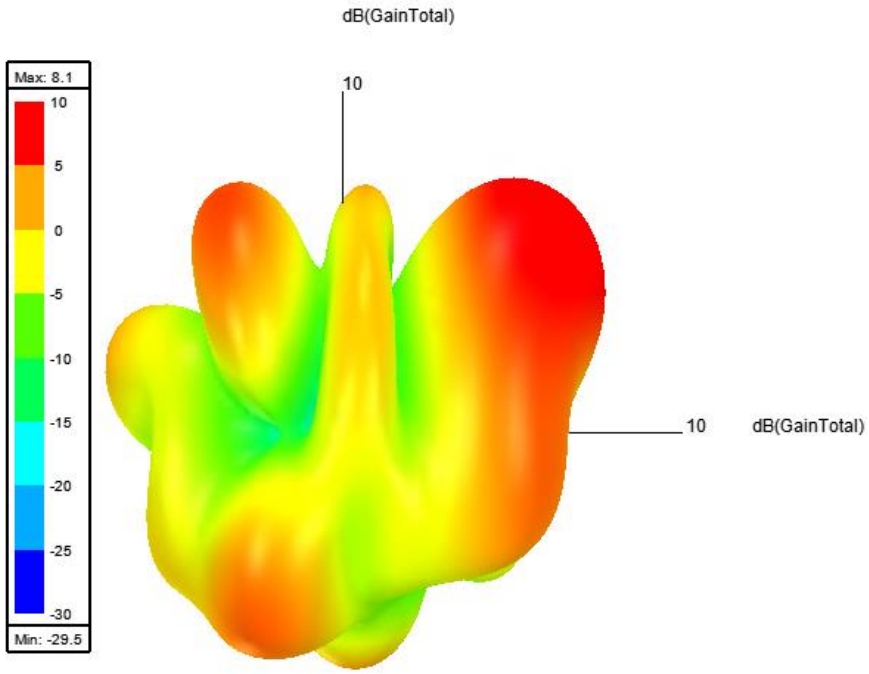

Figure 64: 3D Radiation Pattern with descending phase shift

Similarly, the third simulation was performed by exciting each antenna element with its reference phase as shown in *Figure 65*. Since there is no phase shifting on the signals going into any of the antenna elements, the beam steering should not happen. This antenna should produce a broadside beam.

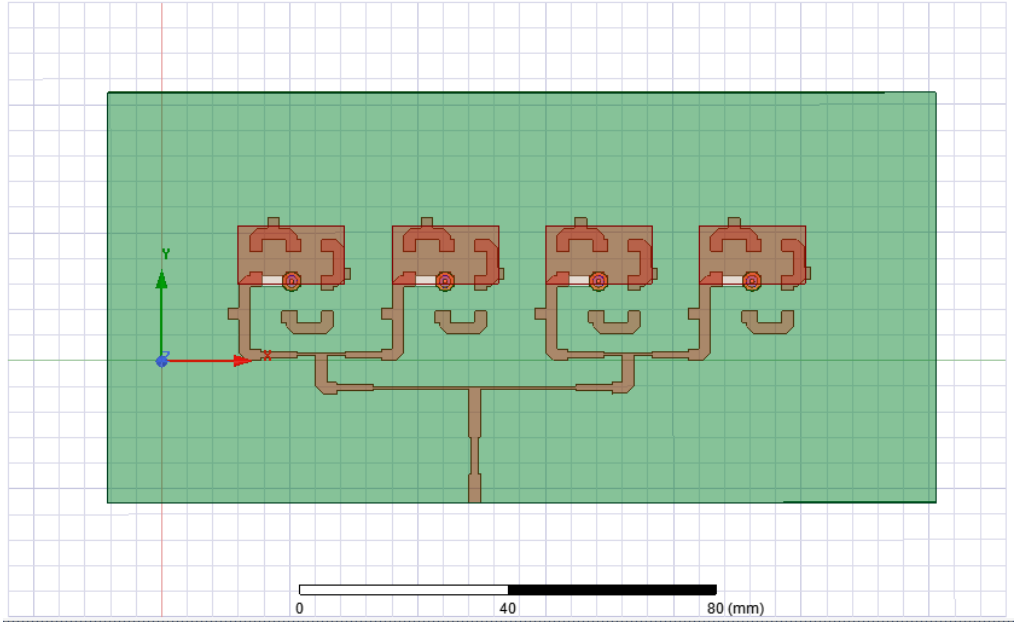

Figure 65: Antenna excitation with 0º phase shift to each antenna element

The simulation result for the 0º phase shift is presented in *Figure 66* – *Figure* 69. The return loss at 5 GHz is found to be about 15 dB. The impedance at 5 GHz is 46.58 +7.8i Ω as shown in *Figure 67*. *Figure 68* and*Figure* 69 show that the antenna beam is transmitted at an angle of 0º.

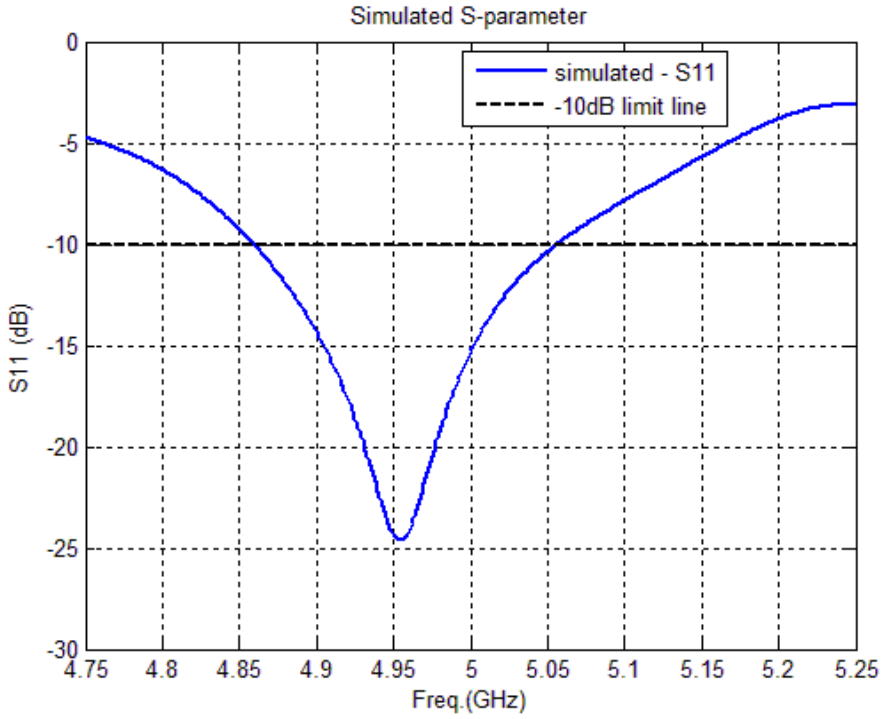

Figure 66: S11 of the antenna array with 0º phase shift.

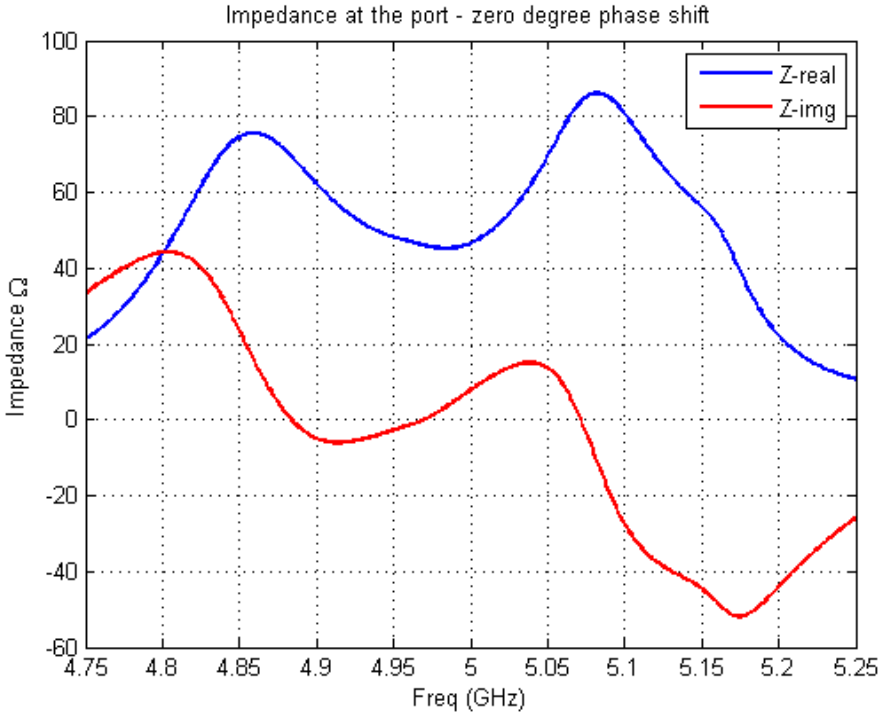

Figure 67: Impedance at the antenna port for 0º phase shift.

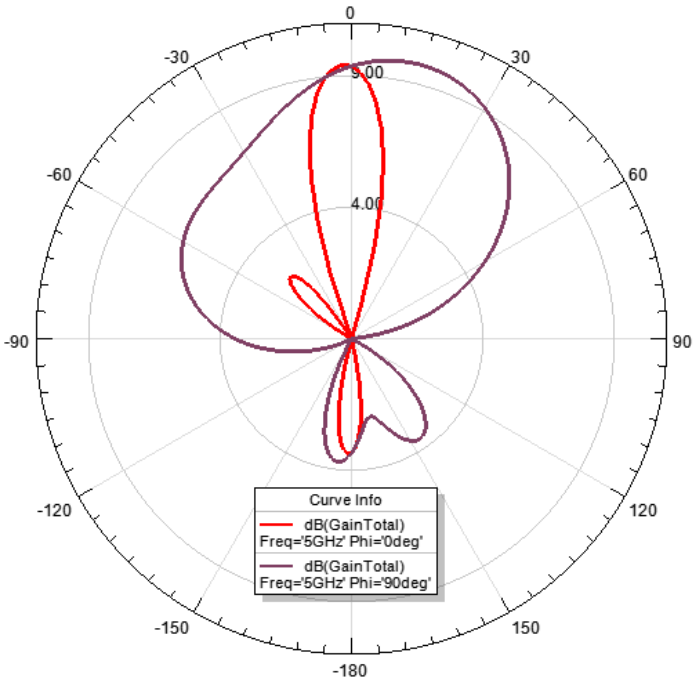

Figure 68: 2D Radiation Pattern - elevation with 0º phase shift.

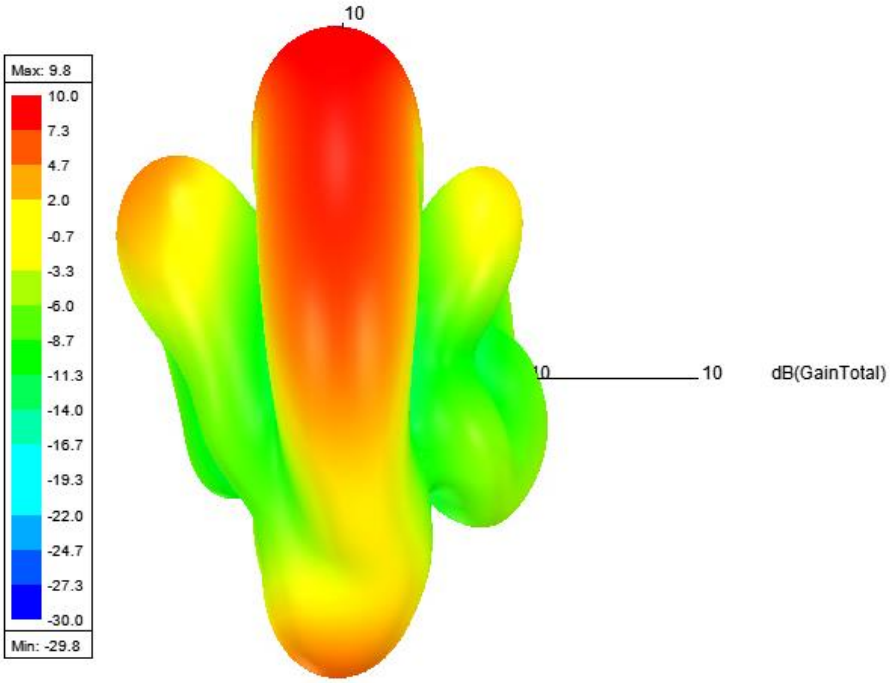

Figure 69: 3D Radiation Pattern with 0º phase shift

The *Table 10* summarizes the simulation result for the antenna array.

	S11 (dB)	Z (Ω)	Gain (dB) (5 GHz) 0º Azimuth	Direction (beam center)	HPBW 0º Azimuth
Equal Phase Shift (0º)	-15	46.58 +7.8i	9.8	0º	21º
Ascending Phase shift (0º, 90º,180º, 270º)	-18	32.37 – 6.22i	8.4	-45º	30º
Descending Phase Shift (270º, 180º, 90º, 0º)	-18	45.46 – 10.52i	8.1	+45º	30º

Table 10: Simulation result for three different phase configurations in an antenna array.

Figure 70 and *Figure* 71 show the combined return loss and two-dimensional radiation pattern respectively for all three phase configurations.

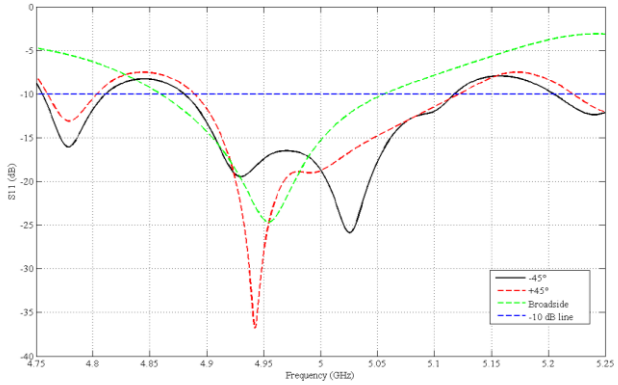

Figure 70: Combined return loss for different phase configuration

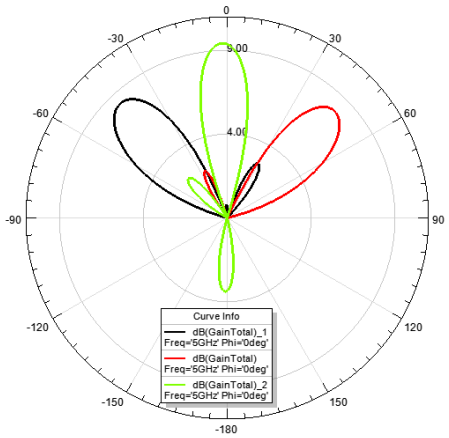

Figure 71: Combined 2D radiation pattern for three different phase excitations.

3.6.3 Mutual Coupling

The return loss for each antenna above was shifted above and below the center frequency. This may have caused due to the interaction between the antenna elements. Each of the antenna elements are isolated from other antenna elements to observe the changes in S11 and impedance of the antenna. Each antenna shown in *Figure 72* to *Figure* 75 were simulated and the results are presented.

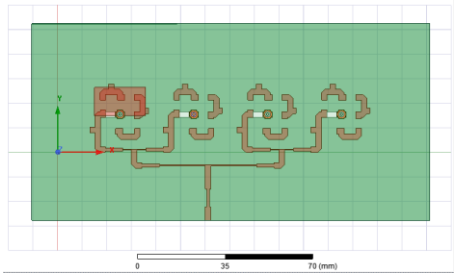

Figure 72: Setup with first antenna element with other ports terminated with 50 Ω.

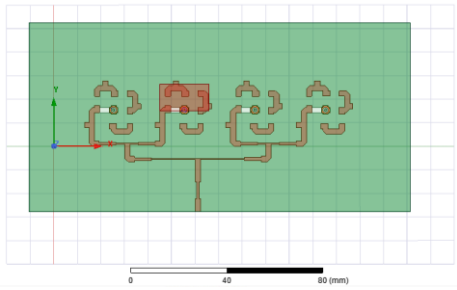

Figure 73: Setup with second antenna element with other ports terminated with 50 Ω.

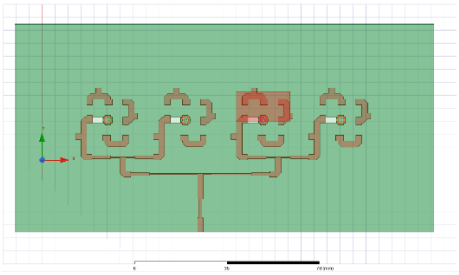

Figure 74: Setup with third antenna element with other ports terminated with 50 Ω.

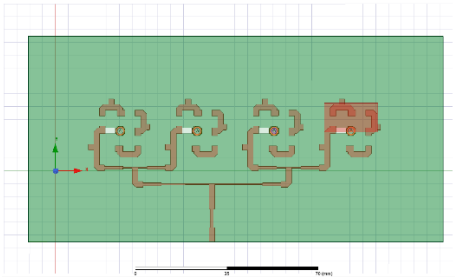

Figure 75: Setup with fourth antenna element with other ports terminated with 50 Ω.

The impedance plot for each of these antennae are shown below in *Figure 76 to Figure* 79.

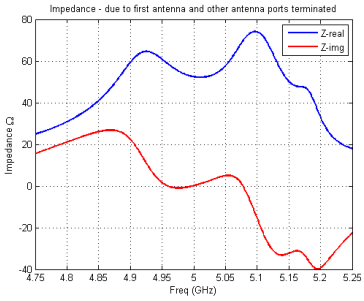

Figure 76: Impedance with only first antenna

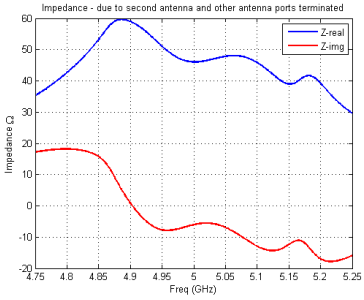

Figure 77: Impedance with only second antenna

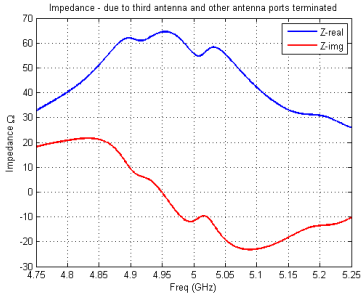

Figure 78: Impedance with only third antenna

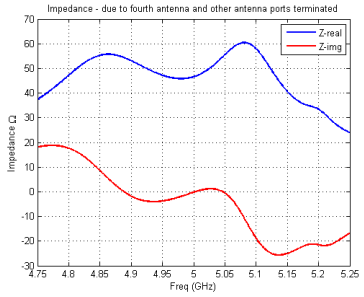

Figure 79: Impedance with only fourth antenna

The combined S11 plot for all four antennae is shown in *Figure 80*.

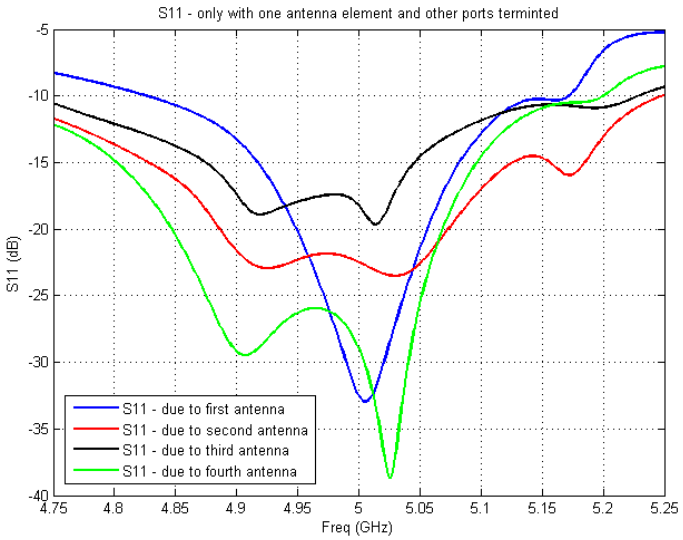

Figure 80: S11 for each isolated antenna.

Table 11 below shows the actual value of S11 and impedance at center frequency.

	S11 (dB)	Impedance (Ω)
First antenna only	-32.51	52.42+j0.13
Second antenna only	-22.48	46.04-j6.052
Third antenna only	-18.27	55.67-j11.67
Fourth antenna only	-28.97	46.57-j0.2

Table 11: S11 and Impedance for each antenna elements isolated from other elements

The above simulation suggests that the shift in center frequency occurred due to mutual coupling between antenna elements. The impedance for each isolated antenna elements is found to be closer to 50 Ω in each case. The return loss plot for each case is centered around the center frequency of 5 GHz.

3.7 Phase Control Design

During simulation the switches between the microstrip lines are replaced by lumped components. The phase shifting in the actual antenna will be achieved by changing the

length of microstrip lines using switches. These switches will then be controlled by a micro controller.

The RF switch most suitable for this antenna array would be a Mercury Wetted Switch [13]. This switch exhibits low capacitance at off-state and low resistance in on-state. It also establishes metal-to-metal contact as it uses Mercury to connect two conductors. The switch can turn on and off by manipulating a DC control signal through a single pin. *Figure 81* shows the open state of the switch. In this switch, 30 and 32 are Mercury droplets attached to two conductors. A dielectric oxide coating 28 is applied to gate member 24. So, when the control voltage is applied to a high resistive gate member 24, the mercury droplets expand and make contact as shown in *Figure 82* [13].

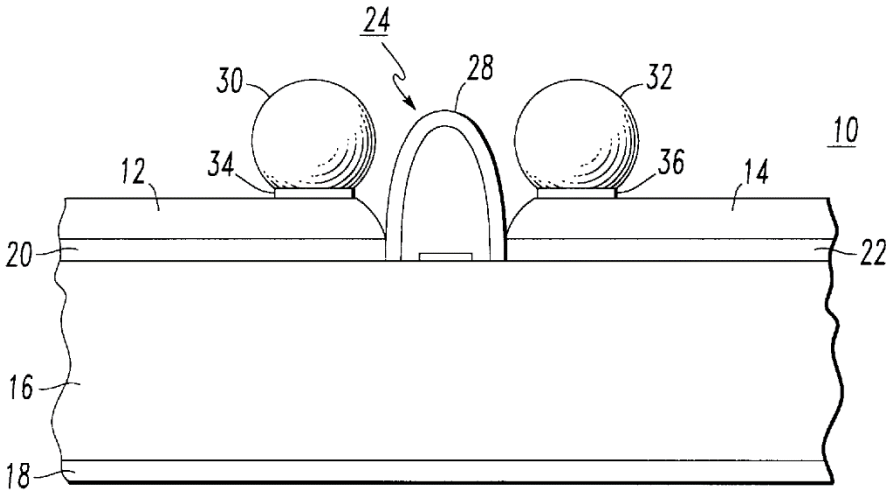

Figure 81: Open state of Mercury Wetted switch [13].

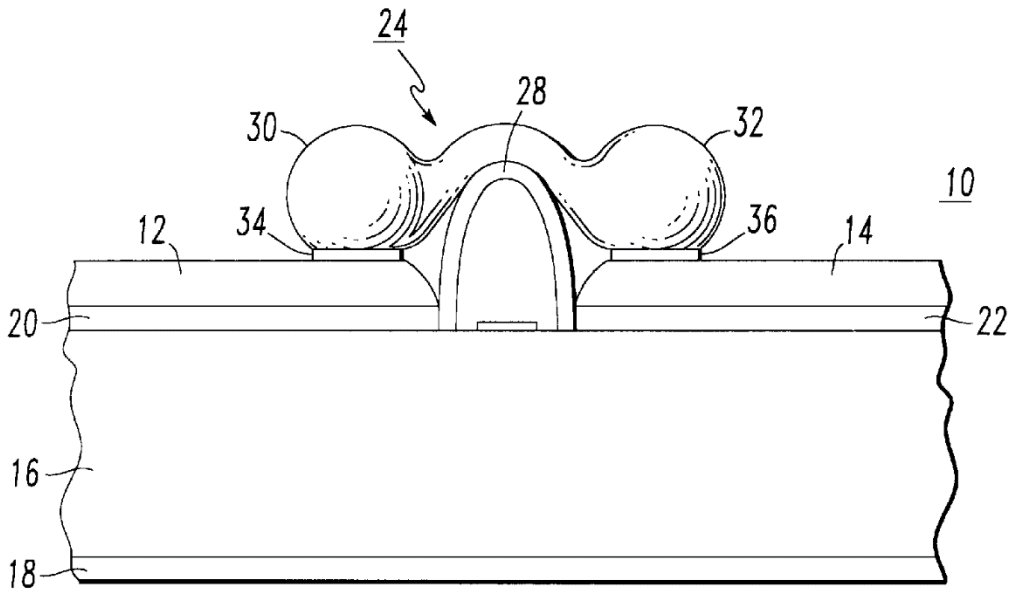

Figure 82: Closed state of Mercury Wetted switch [13].

This switch requires only one pin to turn it ON and OFF. This switch is helpful in RF circuits as it requires a fewer number of control lines. The interference due to control lines can be reduced by realizing these switches in the antenna array. However, this switch was not available to realize in the antenna. Therefore, a different switch was used in this project. As an alternative to mercury-wetted switches, a 3mm x 3mm, PE4246 RF switch by Peregrine Semiconductor is used in this project. This is a Single-Pole, Single-Throw (SPST) switch with low insertion loss and operates at +3 volts [27]. This is a Complementary-Metal Oxide Semiconductor (CMOS) switch with 6 pins. The pin configuration is shown in *Figure 83*.

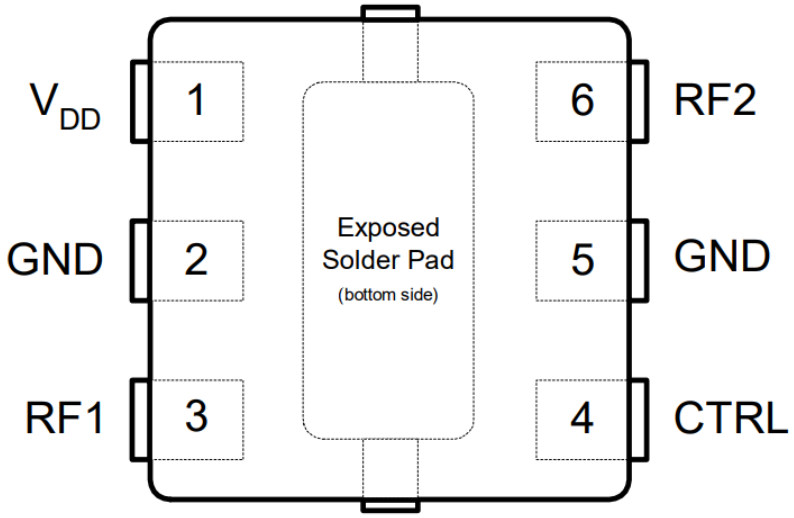

Figure 83: PE4246 PIN Configuration.

In this switch, Pin 3 and Pin 6 are two RF terminals, Pin 2 and Pin 5 are grounds, Pin 1 is power supply to the switch and Pin 4 is the control. In our design, the ground pin 2 and 5, and the exposed solder pad are connected. A bypass capacitor is used as close as possible to the V_{DD} pin to short potential AC signals going into the switch. A 0.1µF capacitor [28] is used. The capacitor has a dimension of 1.25mm x 2mm and a thickness of 0.7mm. The V_{DD} pin and the CTRL pin are connected. So, when the switch receives power, there is a connection between RF1 and RF2. When the power to the switch is cut, RF1 isolates from RF2.

These 3mm x 3mm switches are placed between the microstrip lines within 4 mm spaces. The switch pads are drawn as shown in *Figure 84*.

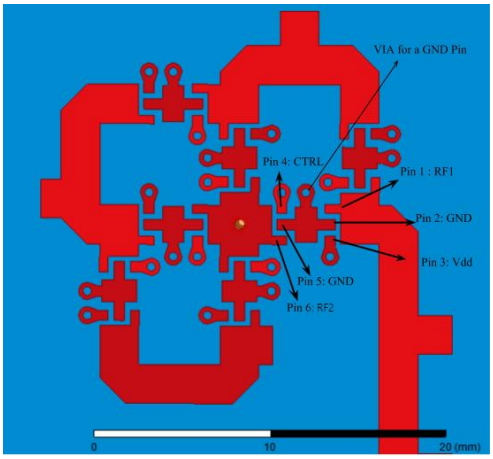

Figure 84: Switch pads drawn between microstrip lines.

The switch pads connected to the circular features are the via that are connected to the other side of the board. The other side of the board is shown in *Figure 85*.

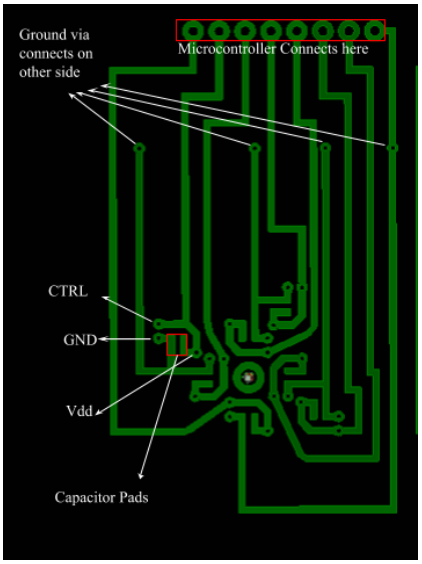

Figure 85: Control lines and via

Each antenna element has seven switches to control the phase shift. Each of the switches is connected to the microcontroller to turn the switch ON and OFF. Each side of the board is shown in *Figure 86* and *Figure* 87 respectively. The board has only a partial ground plane

on the control line side. This ground plane is connected to the ground on the board with antenna with an external wire. The whole antenna is shown in *Figure 88*.

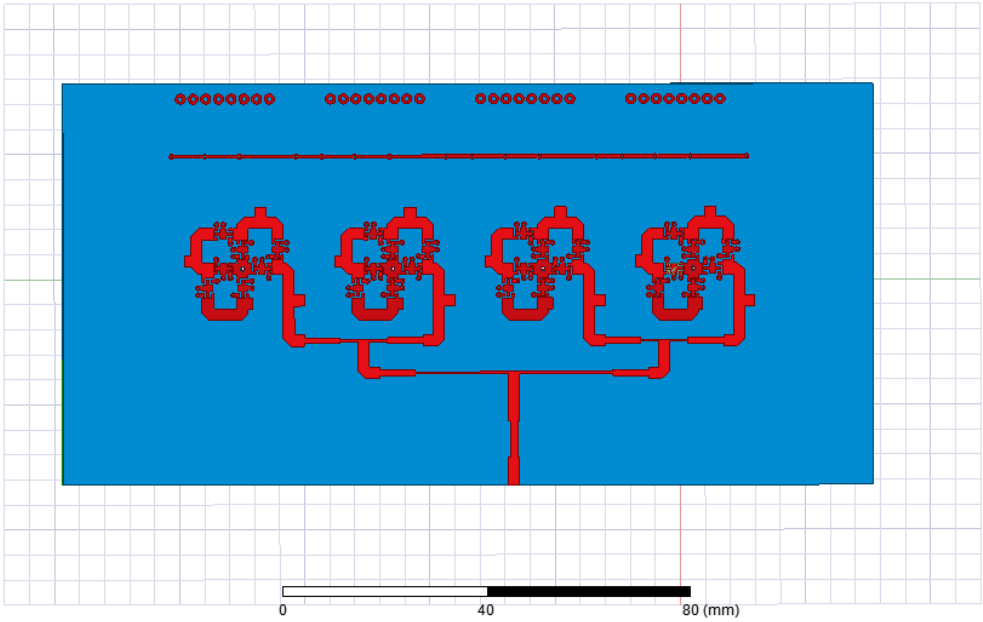

Figure 86: Antenna board with Corporate feed network (top side).

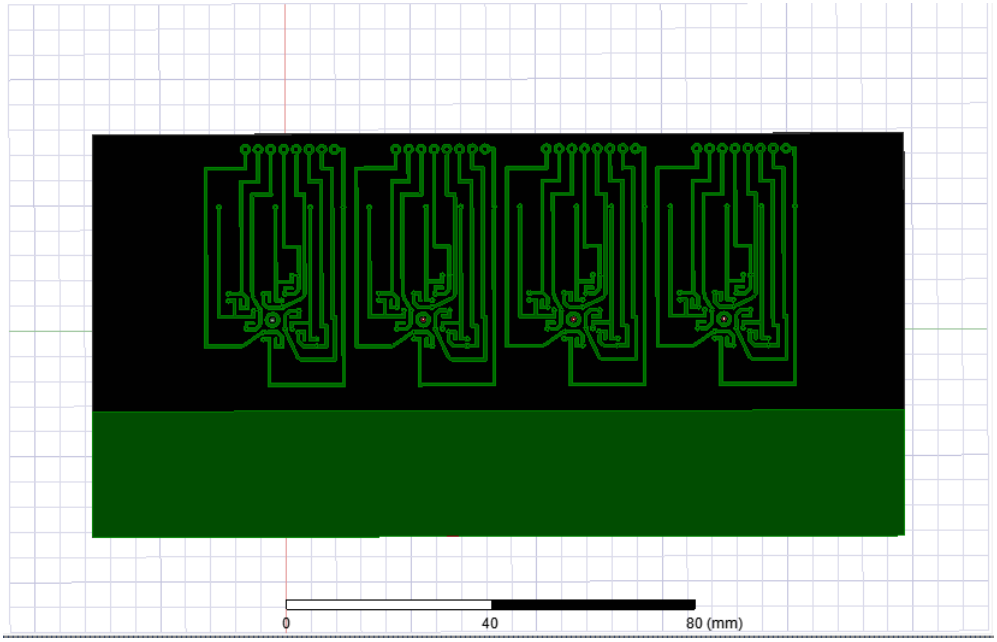

Figure 87: Antenna Board with Control lines (bottom side)

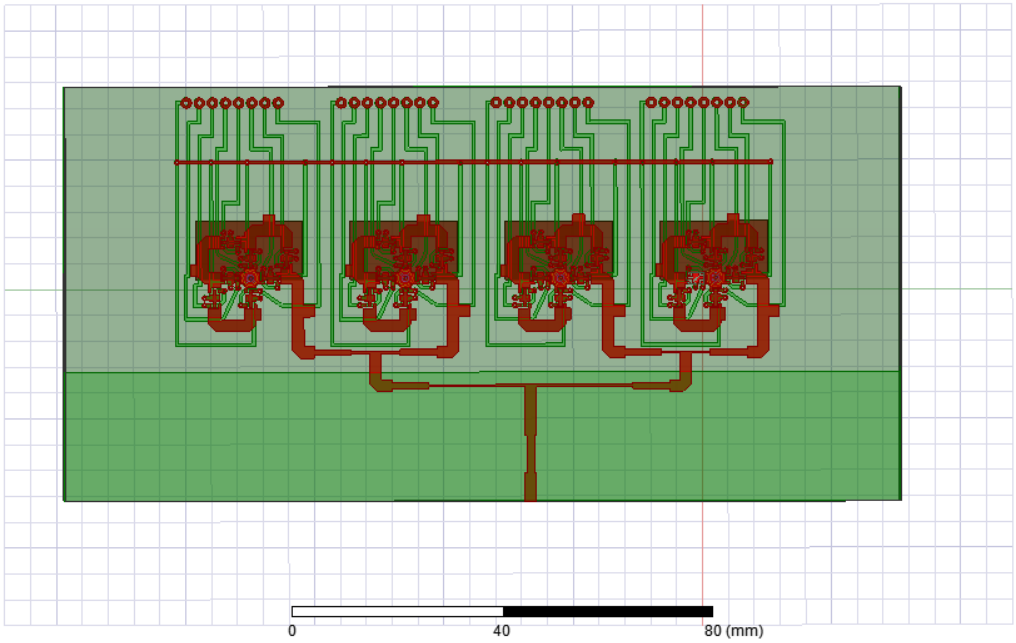

Figure 88: Antenna as a whole

Since the power pin (V_{DD}) and Control pin (CTRL) are connected, both pins are supplied with 3.3 Volts from an output of an Arduino. An Arduino digital pin provides 5 Volts. Therefore, a resistor divider is used to divide 5 volts, so that only 3.3 volts goes to the switch. To obtain an output voltage of about 3.3 volts, a 200 kΩ and 360 kΩ resistor are used in resistor divider circuit. The antenna array with the control circuit is shown in *Figure 89*.

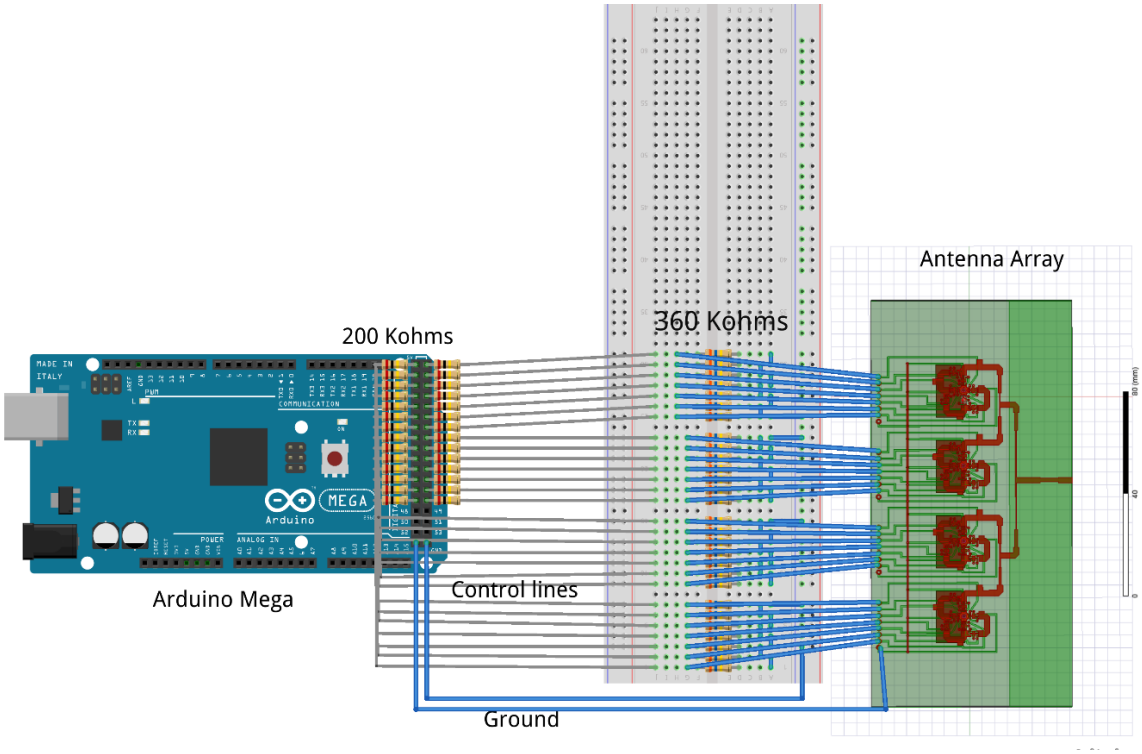

Figure 89: Antenna array with control circuit.

CHAPTER 4: ANTENNA FABRICATION

The antenna models developed in HFSS are built to predict performance. The HFSS models are exported as machine readable Gerber files. The Gerber files are used by a milling machine to cut the copper top according to the design. The antennae are fabricated in RT/Duroid 6006 / RO4360G2 type material. A single antenna was first built. *Figure 90* shows the board with an antenna patch.

Figure 90: Fabricated single antenna

The phase shifter sides of the antennas for all fixed phase shifts are shown in *Figure 91*. Each of the phase shifters from left to right is expected to achieve a phase shift of 0º, 90º, 180º and 270º of phase shift.

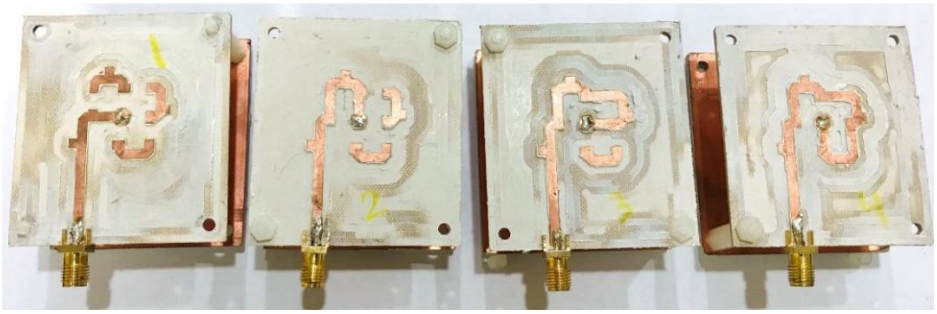

Figure 91: Phase shifter sides of fabricated antennas.

An SMA connector is soldered at the input end of the phase shifter as shown in *Figure 91*. The antenna and phase shifter boards are connected with a semi-rigid coaxial cable. The outside diameter of the coaxial cable is 0.865 inches and the inner conductor diameter is 0.0201 inches. During simulation, antenna boards were separated 5mm apart. However, the fabricated antenna and the phase shifter boards have a separation of 20 mm. This separation was necessary to solder the coaxial cable to the ground plane.

A single antenna was built to measure the phase shift due to change in microstrip lines. The antenna shown in *Figure 90* and *Figure* 91 were found to be inadvertently fabricated with the wrong dielectric material when tested. Therefore, a single antenna was built again with the right material. The antenna is shown in *Figure 92*.

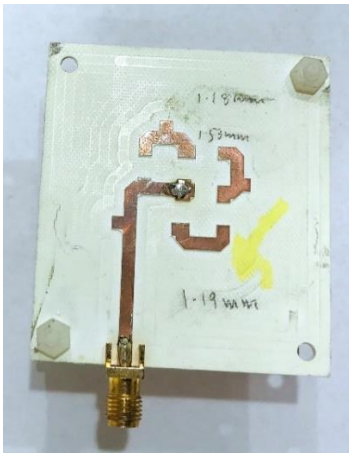

Figure 92: Fabricated single phase shifter on Rogers/Duroid 6006.

Another antenna had to be built when the antenna in *Figure 92* was found resonating at an undesired frequency. The milling machine scrapped too much dielectric material and cause the antenna to resonate at an undesired frequency. The new antenna is shown in *Figure 93*.

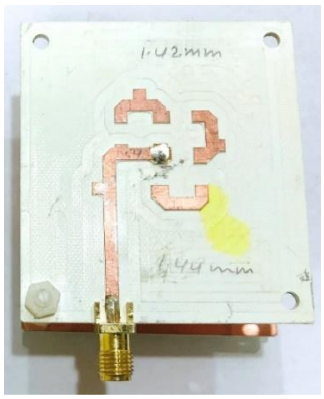

Figure 93: Fabricated single antenna #2 on Rogers/Duroid 6006

The same problem occurred with the antenna shown in *Figure 93* as well. The antenna array was sent to a vendor for fabrication. Each side of the antenna array is shown in *Figure 94* to *Figure* 97.

Figure 94: Fabricated antenna – array side.

Figure 95: Fabricated antenna – ground plane side.

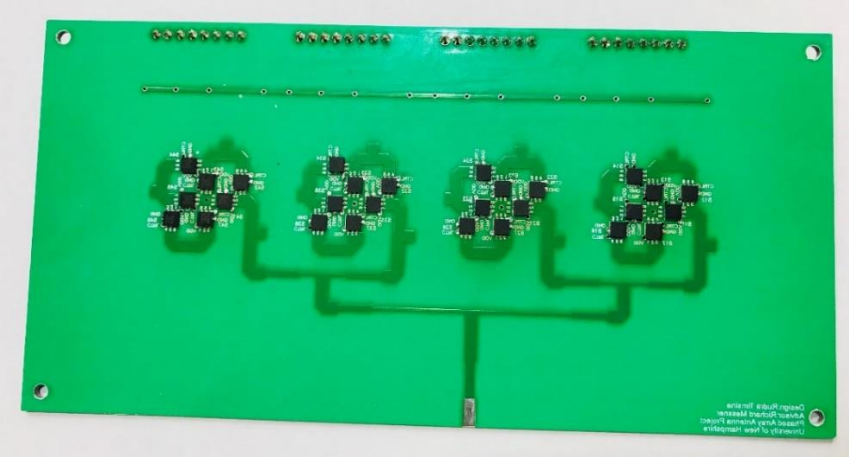

Figure 96: Fabricated Phase Shifters – phase shifter side.

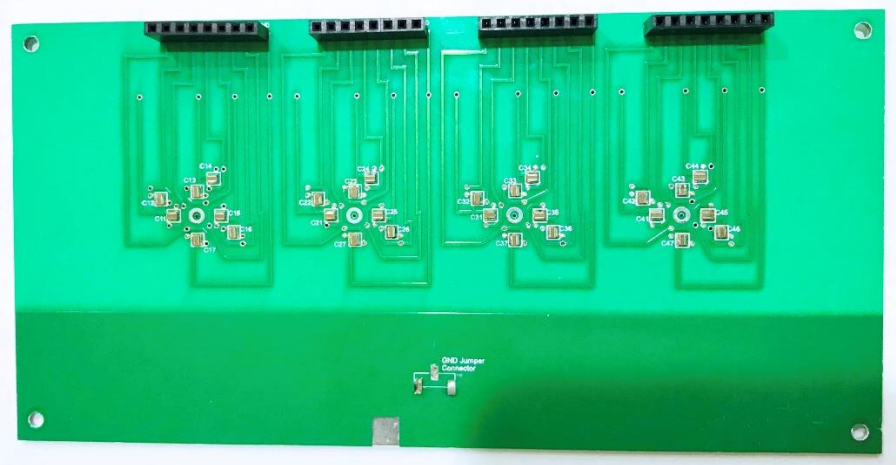

Figure 97: Fabricated Phase Shifters – Control side.

The antenna boards shown above are assembled as shown in *Figure 98* and *Figure* 99.

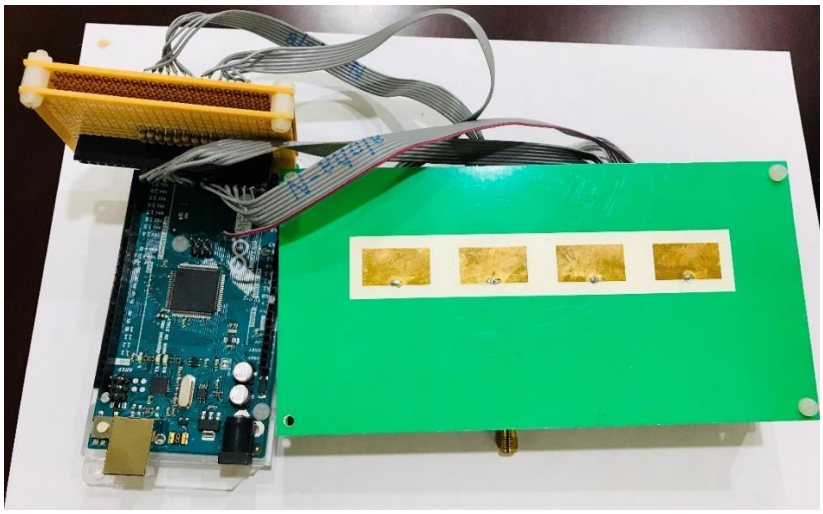

Figure 98: A complete antenna – array side.

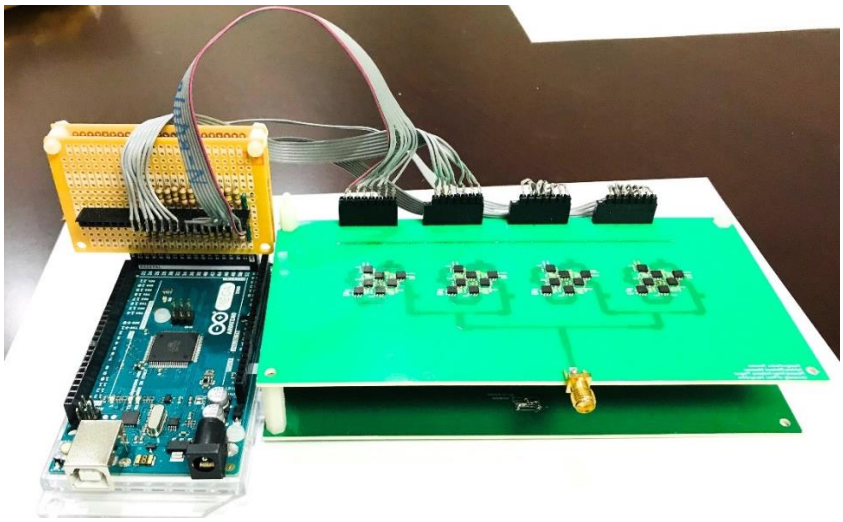

Figure 99: A complete antenna – phase shifter side.

The antenna was tested to find out whether a switch would work. A single switch was excited and the continuity on the microstrip lines connected by the switch was tested. It failed the continuity test. Other errors were also found later in the board that contributed to defective antenna. The phase shifter board had only partial ground plane which was connected to the other ground plane with a copper wire. The microstrip line for phase shifter

network was without ground plane underneath. The copper wire was not suitable for high frequency (5 GHz in this case). Therefore, more antennae were built using a milling machine. Microstrip transmission lines were used to replace the switches. Three antennae were built to form beam at three different angles. The array side of the antenna is shown in *Figure 100*.

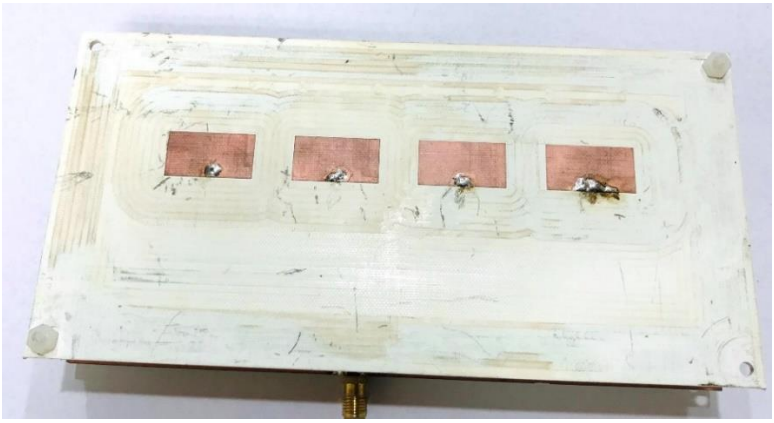

Figure 100: Fabricated antenna – array side (without switches).

The antenna with reference phase i.e. equal delay to each array element is shown in *Figure 101*. *Figure 102* and *Figure* 103 show ascending and descending phase shifting.

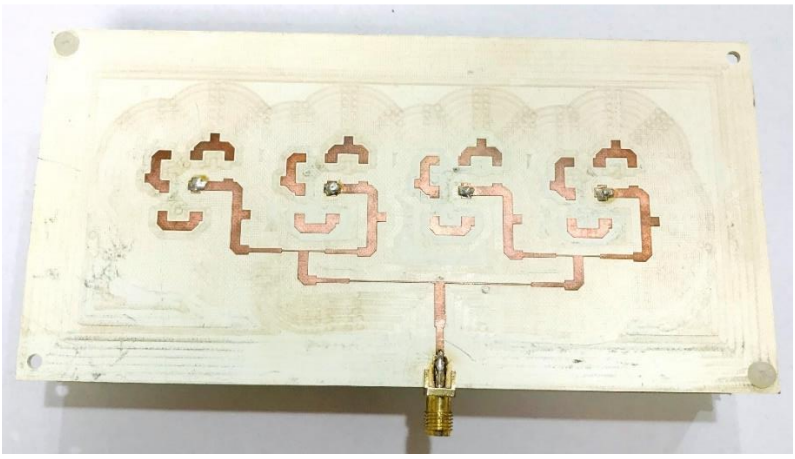

Figure 101: Fabricated Antenna – reference phase shift.

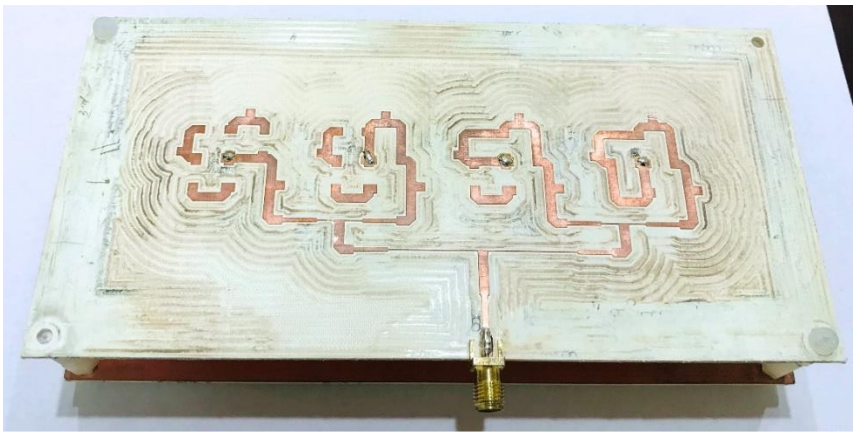

Figure 102: Fabricated antenna – ascending phase shift.

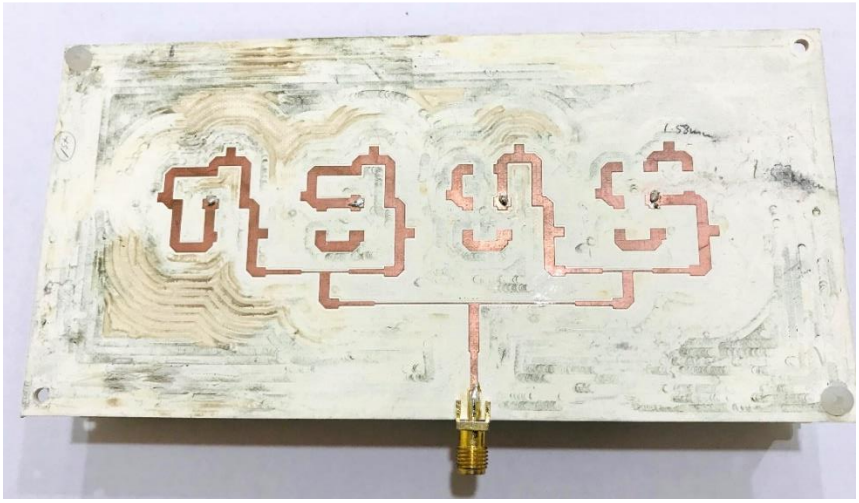

Figure 103: Fabricated antenna – descending phase shift.

CHAPTER 5: RESULTS

The antenna array was tested for return loss and radiation pattern. The return loss is measured using a Vector Network Analyzer and the radiation pattern was measured in a far-field anechoic chamber. First, the single antenna was measured for the return loss. As discussed in Chapter 4, a dielectric material was inadvertently used to build the first single antenna with fixed phase shift networks. The return loss values incorrect for each of these antennae are shown in *Figure 104* to *Figure* 107.

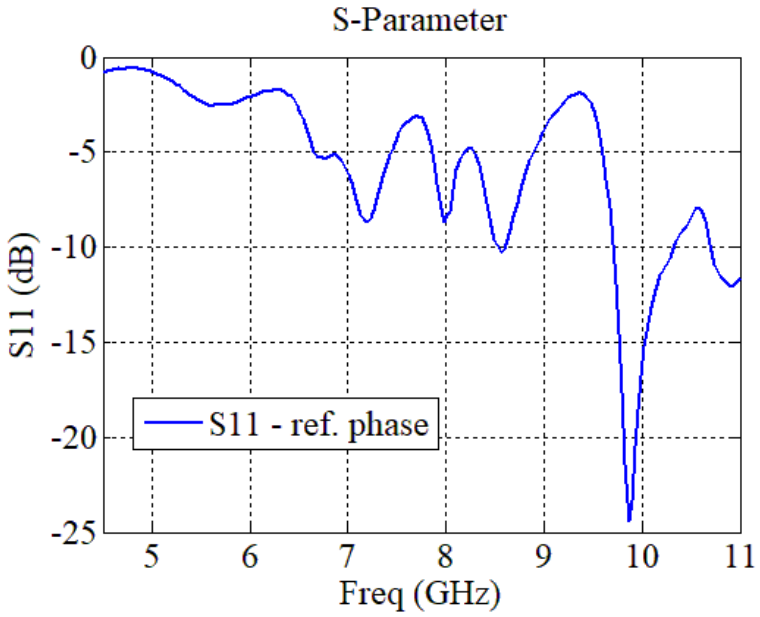

Figure 104: Single antenna return loss – reference phase (wrong dielectric).

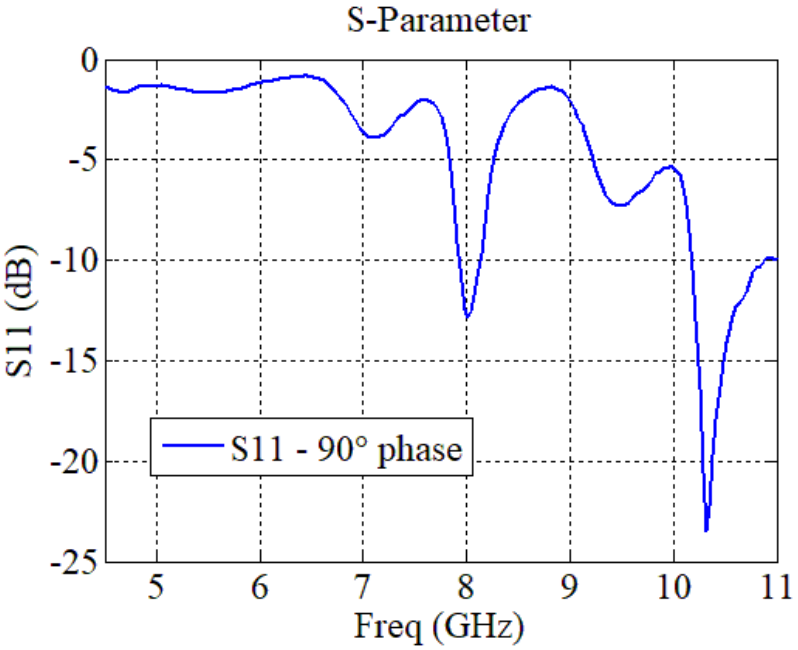

Figure 105: Single Antenna return loss - 90º phase (wrong dielectric).

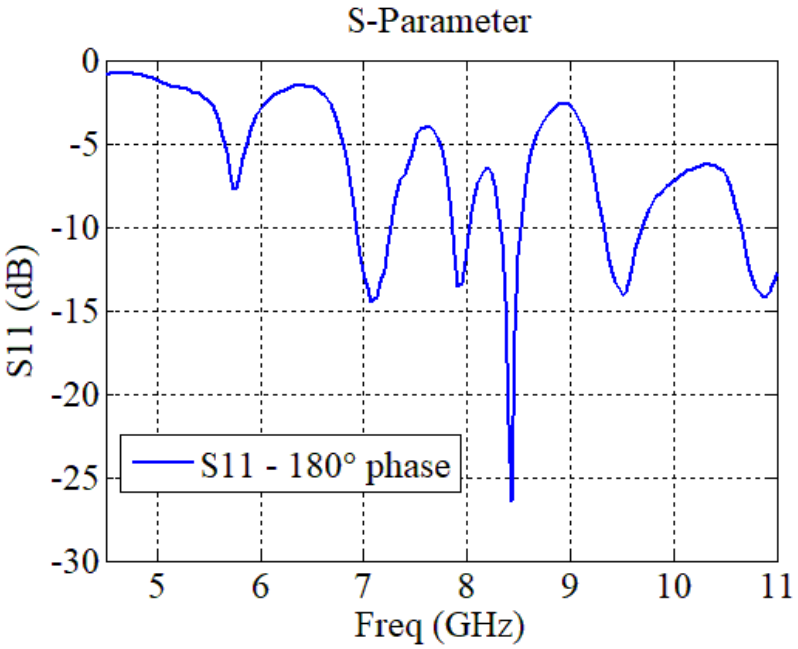

Figure 106: Single Antenna return loss - 180º phase (wrong dielectric).

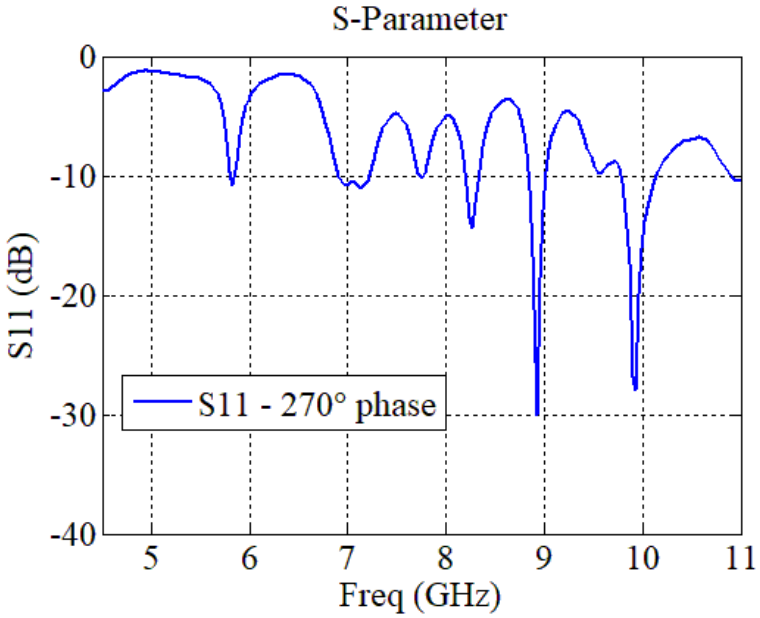

Figure 107: Single Antenna return loss - 270º phase (wrong dielectric).

It is clear from these figures that the antenna and the feed structure is not resonating at 5 GHz. It was known only after testing that the dielectric material was not the proper one. Thus, the correct dielectric material was subsequently used to realize another antenna. This time only one antenna was built to make sure that the antenna resonates at the right frequency. The return loss for this antenna is shown in *Figure 108*.

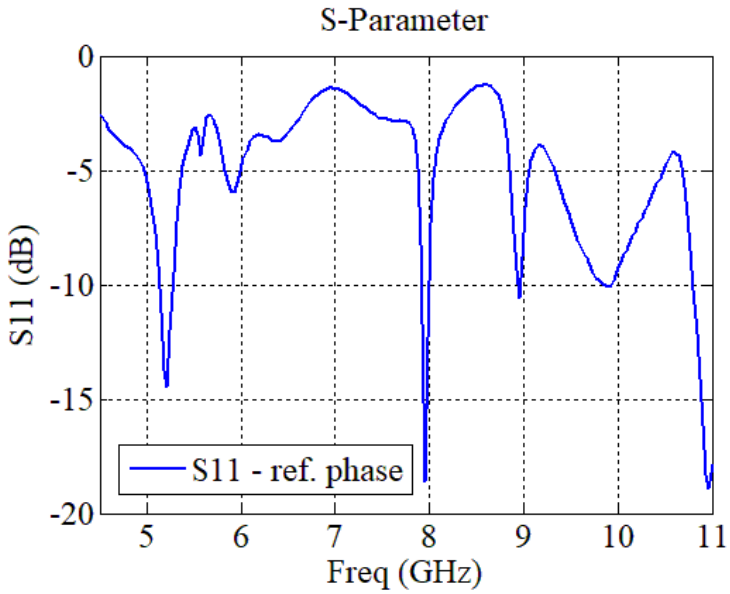

Figure 108: Single antenna return loss – reference phase.

Figure 108 shows that the antenna is still not resonating at 5 GHz. The closest resonance is at 5.215 GHz. The antenna was investigated to find issues during fabrication. It was found that the milling machine scraped too much dielectric and made it thinner. The antenna was simulated with a dielectric thickness of 1.524 mm, but the realized antenna has the dielectric thickness of 1.18 mm. The copper patch area was elevated which introduced air as a second dielectric material at the edge of the antenna. This may have caused a fringing effect. Due to this effect, the resonance frequency shifted. Another antenna was built again with the same dielectric material. The return loss for this antenna is shown in *Figure 109*.

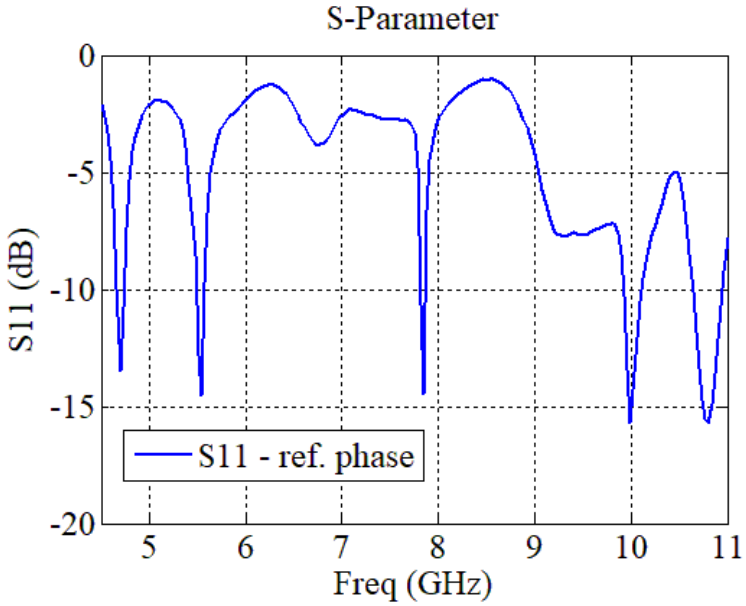

Figure 109: Single antenna return loss – reference phase.

This antenna is also not resonating at the right frequency. As we can see from *Figure 109*, the antenna is resonating at a frequency of 4.695 GHz with very narrow bandwidth (0.1 GHz). Another resonance occurred at 5.5 GHz with a bandwidth of about 1.2 GHz. This time, the thickness of the antenna was 1.43 mm. Several efforts were made to fix the milling

machine from scraping off too much dielectric. Since the problem was not resolved, the same antennae built above with the wrong dielectric were tested to measure phase shift. The phase shift due to each length of the transmission line is shown in *Figure 110*.

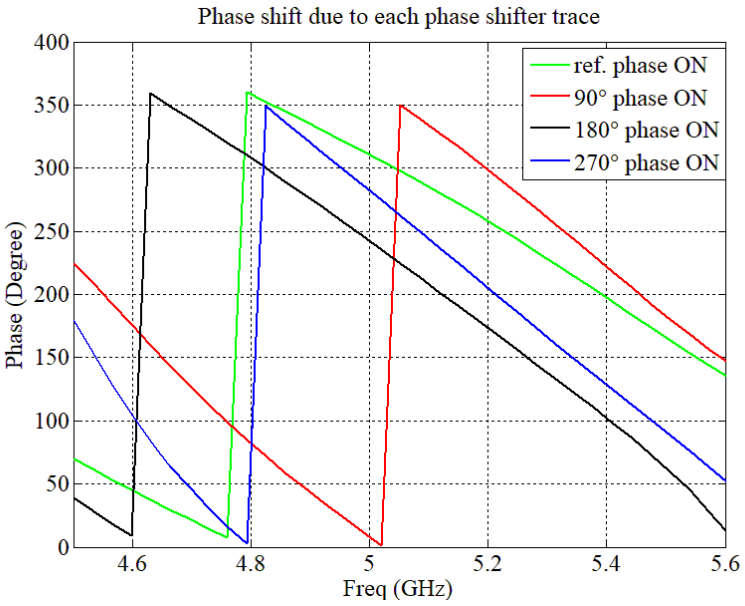

Figure 110: Measured Phase shift due to each phase shifter trace.

The change in phase shift is shown in *Figure 111*.

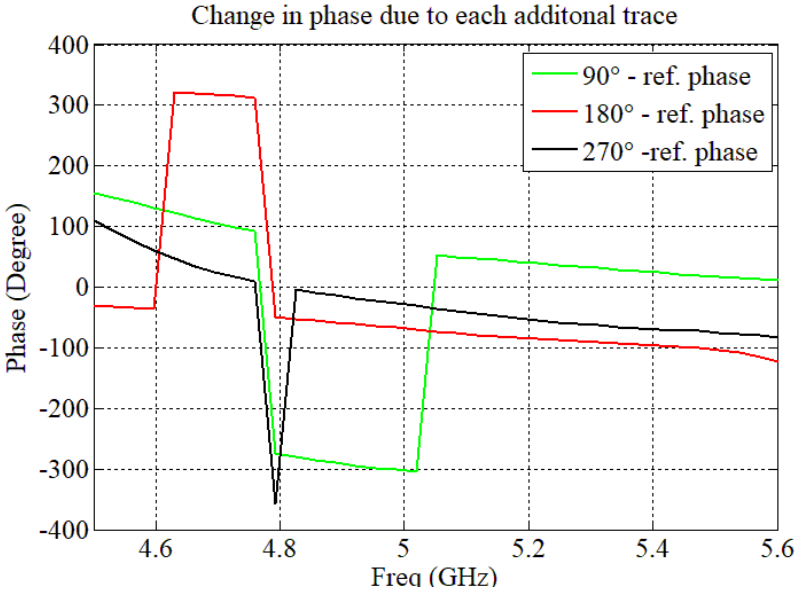

Figure 111: Change in phase shift due to each additional trace

Next, the phased array antenna was tested. As mentioned above in the fabrication section, the antenna array with assembled switches did not pass the continuity test, so this antenna was not tested for radiation pattern and return loss. The antenna array with hardline microstrip line placed in the switch spaces was tested instead. The return losses measured with a VNA yielded the following results:

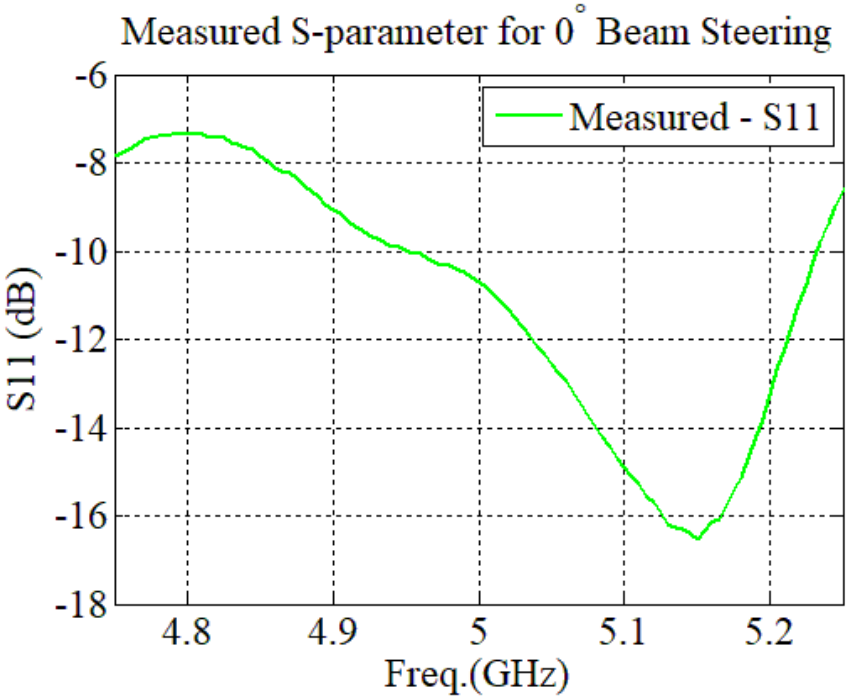

Figure 112: Measured return loss for 0º beam steering antenna.

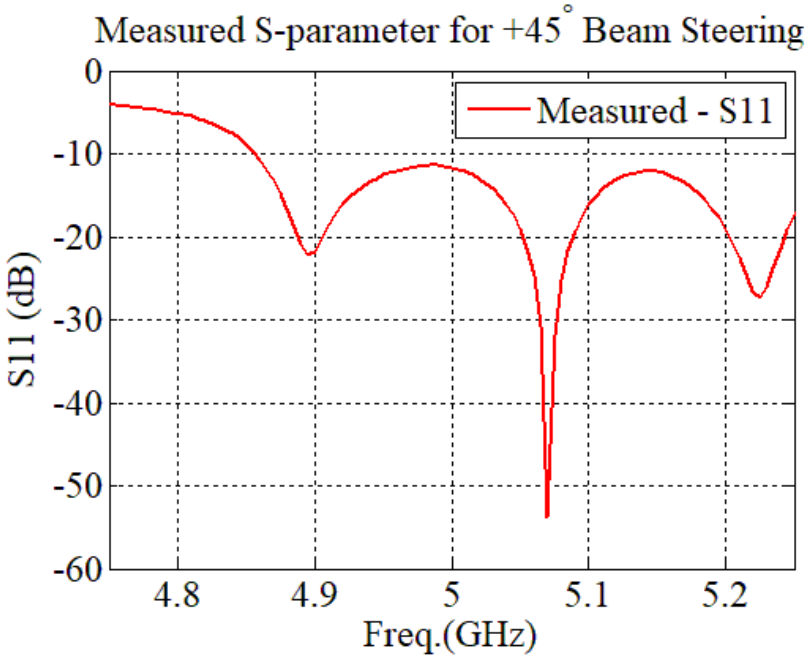

Figure 113: Measured return loss for +45º beam steering antenna.

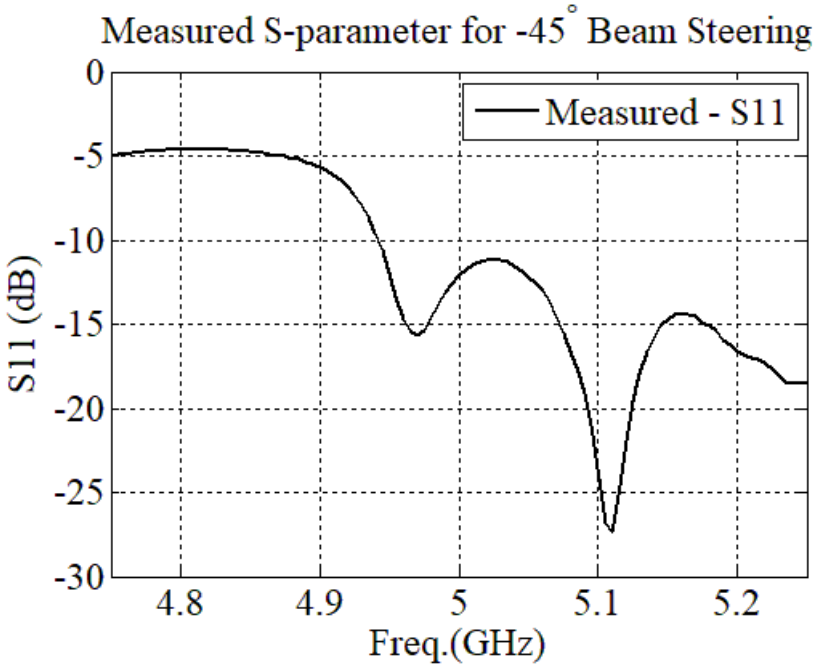

Figure 114: Measured return loss for -45º beam steering antenna.

Figure 112 to *Figure* 114 shows that the resonance frequency is shifted towards a higher frequency. For the broadside beam antenna, the resonance frequency is at 5.15 GHz, 5.07 GHz for +45º beam antenna, and 5.1 GHz for -45º beam antenna. The error in resonance frequency may have occurred due to fabrication error. The following figures shows a comparison between simulated and measured return loss for all three antennae.

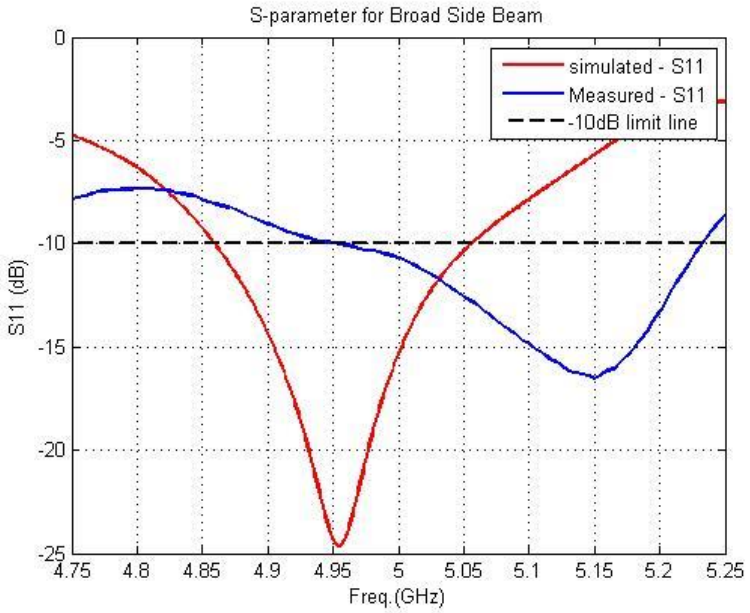

Figure 115: Measured and Simulated return loss for broad side beam antenna.

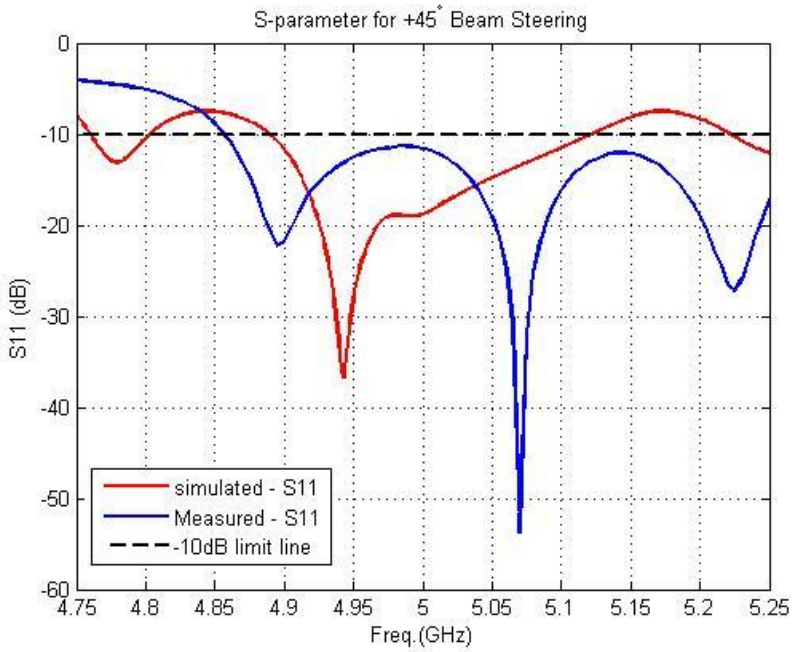

Figure 116: Measured and Simulated return loss for +45º beam steering antenna.

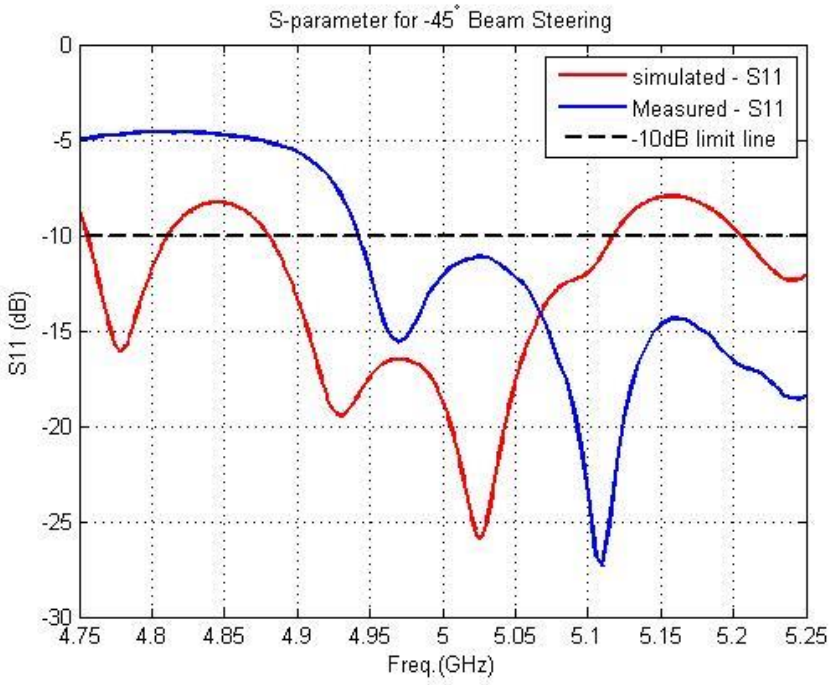

Figure 117: Measured and Simulated return loss for -45º beam steering antenna.

Figure 118 shows the comparison of return loss between three antennae.

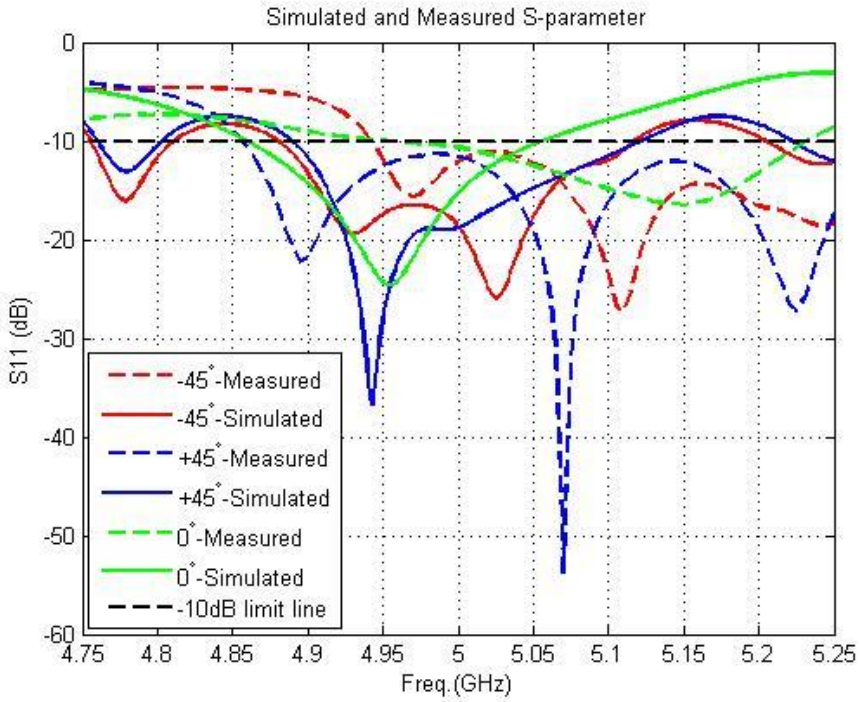

Figure 118: Measured and Simulated return loss for all three-antenna array.

The radiation patterns for these antennae were measured in a far-field anechoic chamber. The measurement setup inside the chamber is shown in *Figure 119*.

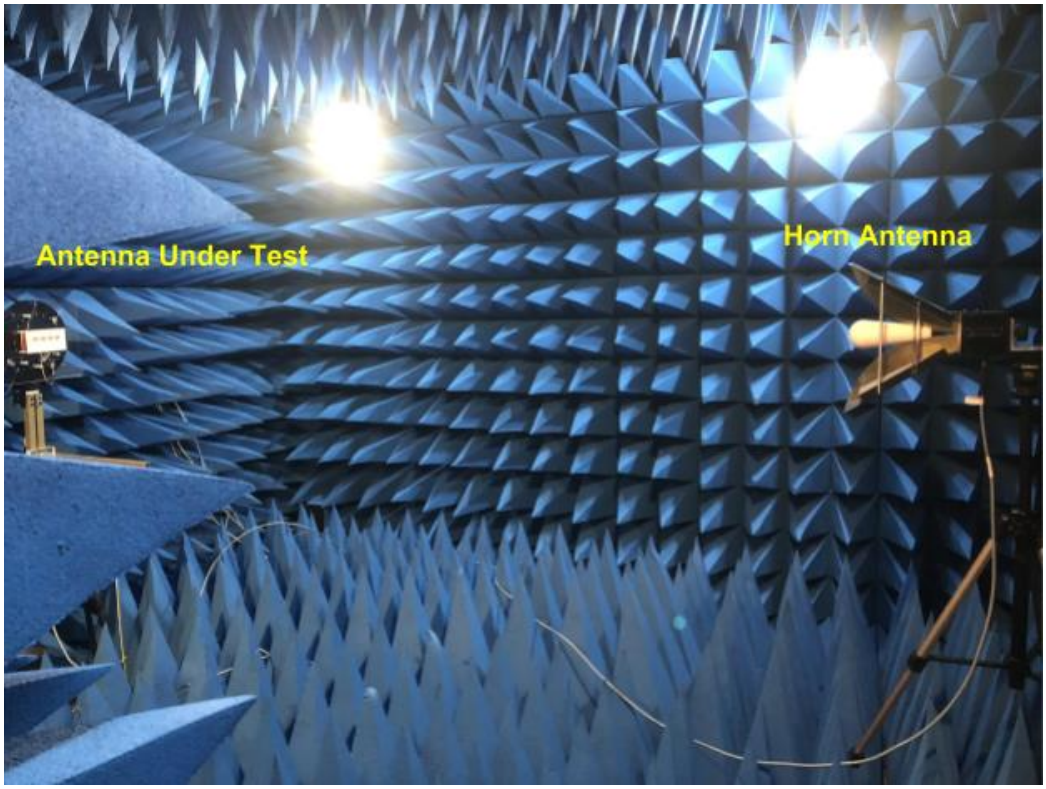

Figure 119: Measurement setup inside an anechoic chamber.

In this setup, the horn antenna is used as a transmit antenna and the antenna under test is used as a receive antenna. The horn antenna is connected to the transmitter port of the VNA and the test antenna is connected to the receiver port. The loss on the cable that connects the VNA port and the antenna is accounted in the radiation pattern results. To obtain an accurate result, the horn antenna must point at the center of the antenna array. The antenna port for the test antenna is not at the center. Hence, a mount was built so that the horn antenna points at the center of the antenna array. The mount is shown in *Figure 120*. *Figure 121* shows the laser light pointed from the horn antenna.

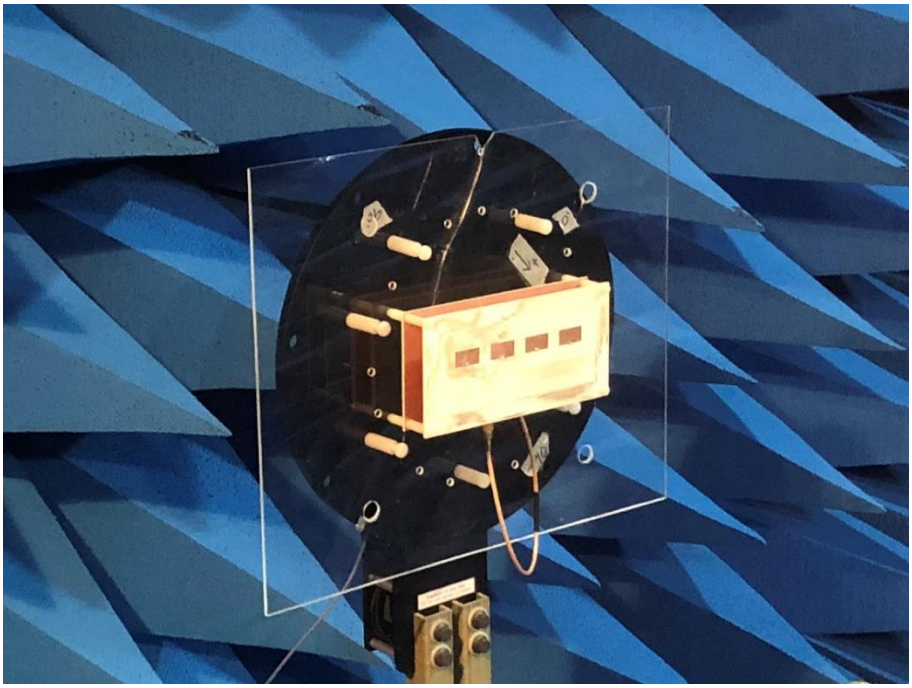

Figure 120: Antenna mount

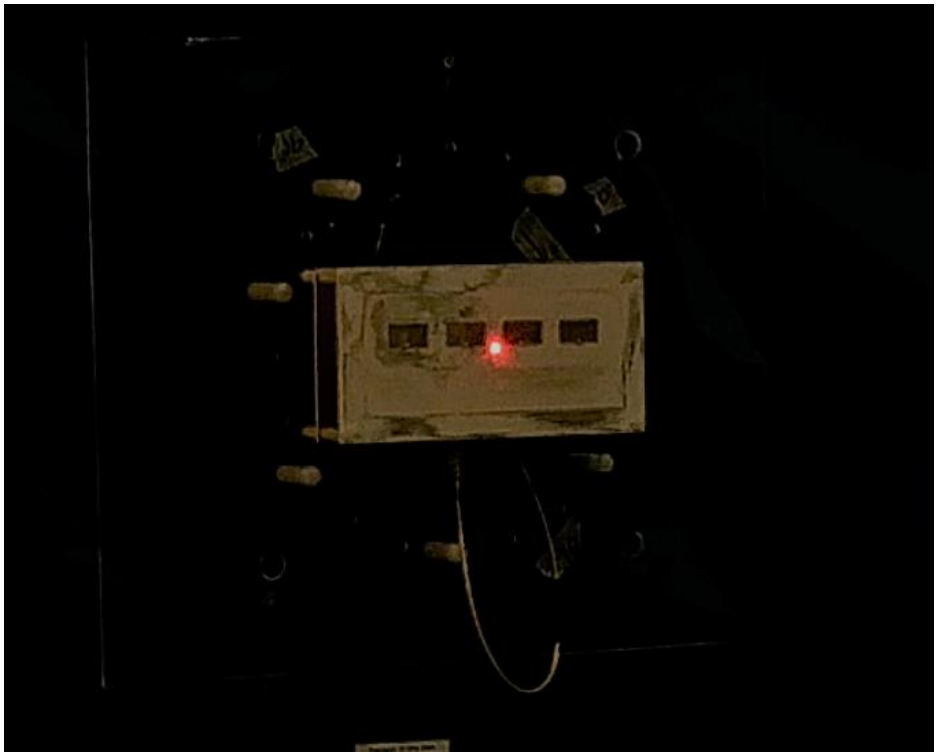

Figure 121: Antenna centered with horn antenna.

The test antenna was rotated horizontally (i.e. in azimuth angle) from 0º to 360º in increments of 1º. The signal power received by the test antenna for each angle was recorded. The testing of the three antennae produced the following radiation patterns shown in *Figure 122* to *Figure* 124.

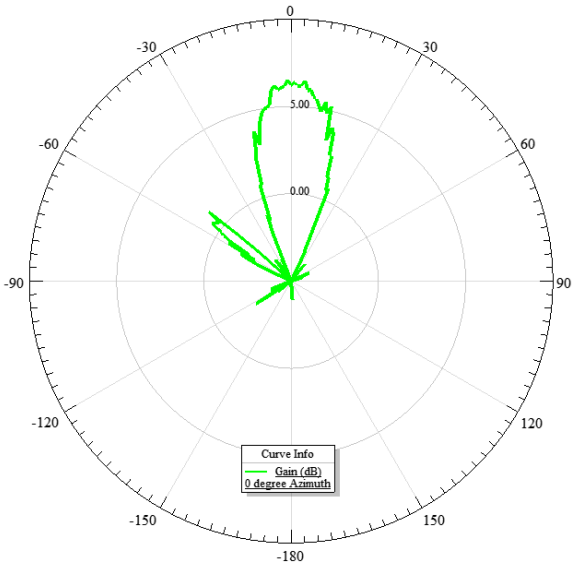

Figure 122: 2D radiation pattern for broadside beam antenna.

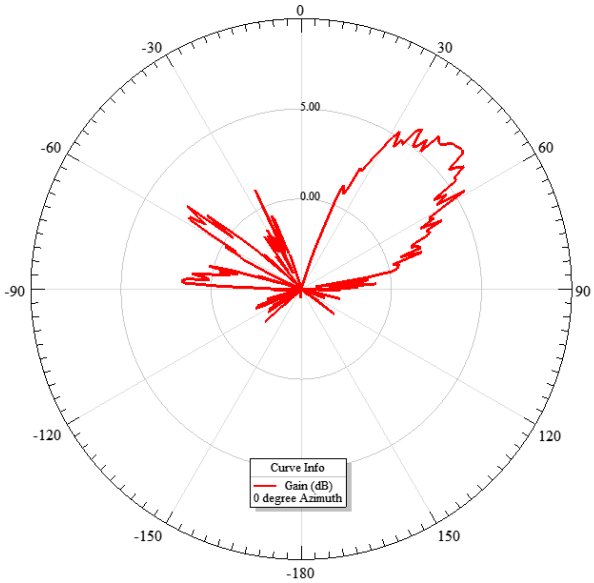

Figure 123: 2D radiation pattern for +45º beam antenna.

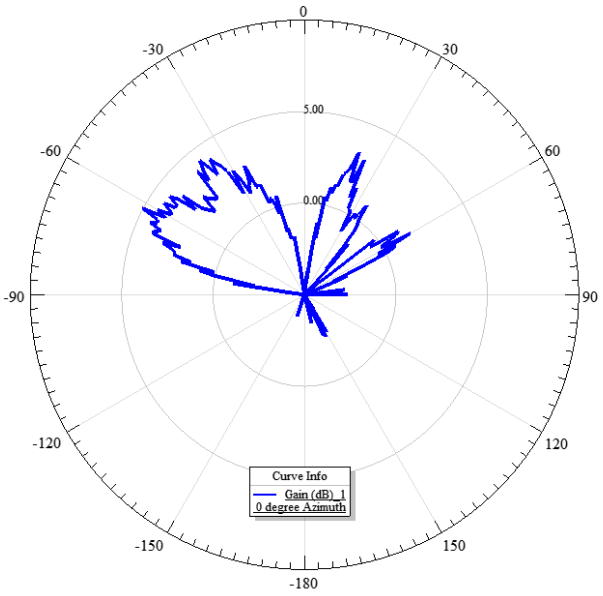

Figure 124: 2D radiation pattern for -45º beam antenna.

The antenna with a broadside beam has a center at 0º. The peaks of the main lobe of the other two antennae are at -51º and 49º, respectively. The comparison between the measured and simulated results are shown in *Figure 125* - *Figure* 127.

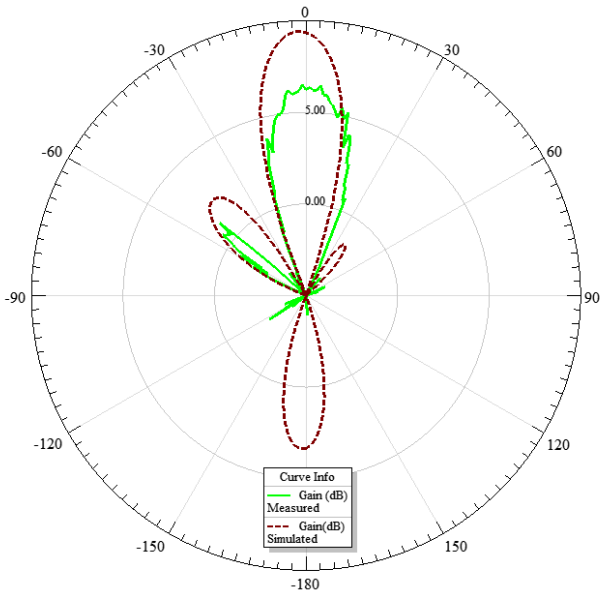

Figure 125: Measured and Simulated 2D radiation pattern – broadside beam.

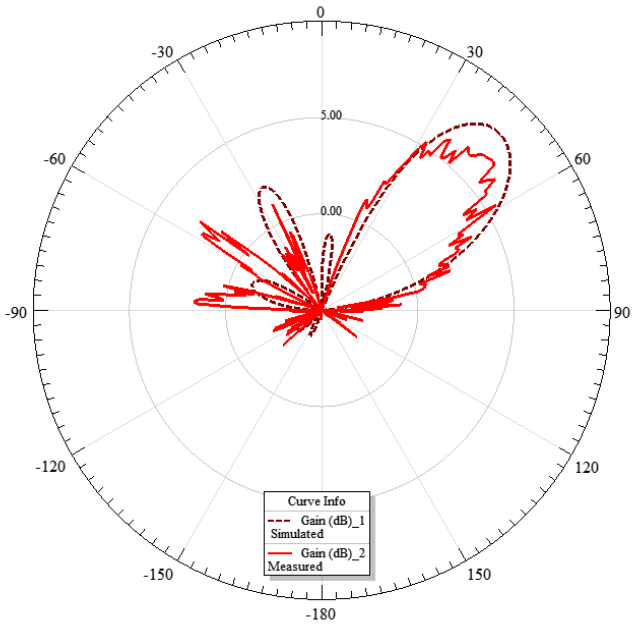

Figure 126: Measured and Simulated 2D radiation pattern, 45º beam

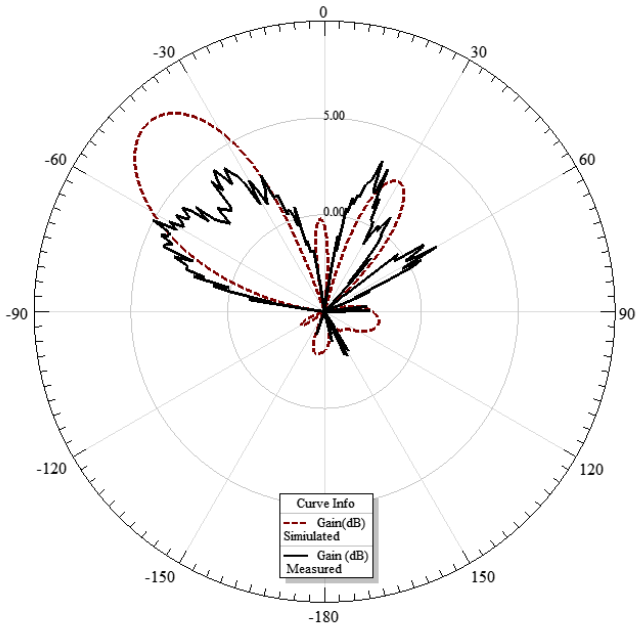

Figure 127: Measured and Simulated 2D radiation pattern, -45º beam

The direction of the measured radiation pattern aligned well with the simulated result. The measured gain is found to be 2-3 dB less than the simulated gain. This is because of the shift in resonance frequency. The measured radiation patterns do not look as smooth as the simulated pattern. This is because the test antenna was rotated around the azimuth plane using a stepper motor. The irregular pattern is due to the movement of the motor.

Figure 128 shows the measured and simulated radiation patterns for all three antennae together.

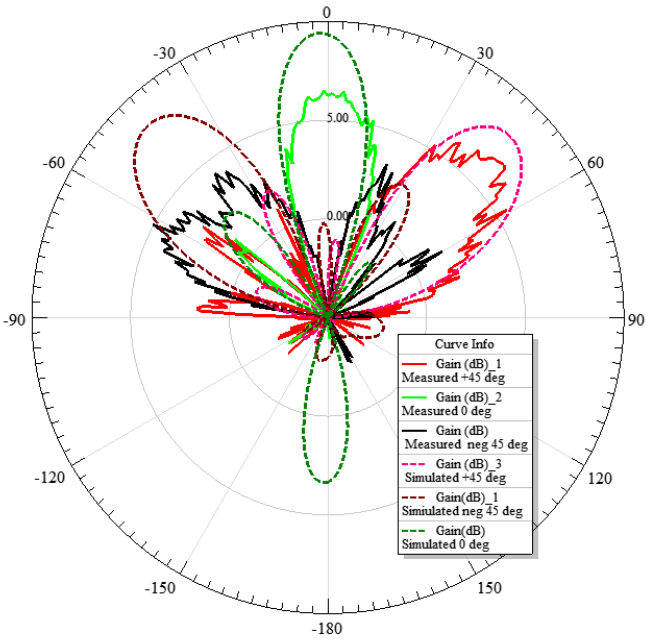

Figure 128: Measured and Simulated 2D radiation patterns for all three antennae.

The *Table 12* summarizes the measured and simulated results for all three antennae array.

Measurement at 5 GHz	Equal Phase shift (0^o)	Ascending Phase shift (0^o, 90^o,180^o, 270^o)	Descending Phase Shift (270^o, 180^o, 90^o, 0^o)
S11 (dB) Simulated	-15	-18	-18
S11(dB) Measured	-11	-12	-13
Gain (dB) 0^o Azimuth Simulated	9.8	8.4	8.1
Gain (dB) 0^o Azimuth Measured	6.49	3.53	6.8
Direction (beam center) Simulated	0^o	-45^o	45^o
Direction (beam Center) Measured	0^o	-51^o	49^o
HPBW 0^o Azimuth Simulated	21^o	30^o	30^o
HPBW 0^o Azimuth Measured	28^o	57^o	30^o
Bandwidth (BW) Simulated	199 MHz	247 MHz	248 MHz
Bandwidth (BW) Measured	256 MHz	342+ MHz	398+ MHz

Table 12: Measured and Simulated results

As discussed earlier, the phase shift obtained due to addition of each transmission line in a phase shifter network could not be measured precisely with the return loss signal. The change in phase shift due to addition of each microstrip line segment was not uniform. The non-uniform phase change applies to both simulated and measured results. The direction of maximum and minimum beam steering for both measured and simulated result was found to be close to $\pm 45^o$. A Matlab simulation was performed to obtain the phase shift that provides these beam steering angles. It was found that a uniform increment of 120^o phase shift would provide a beam steering from -45^o to 45^o. Therefore, a uniform phase shift close to 120^o was achieved with our phase shifter. The Matlab code in Appendix A produced a plot shown in *Figure 129.* The simulation in Matlab was performed with point sources using equation (52). The Matlab simulation produced an array patterns plot. The simulation did not consider the mutual coupling between antenna elements. Therefore, the measured plots are not in close agreement with the Matlab simulation. The antenna would have

provided a beam steering close to ±60º, if a uniform phase shift of 90º was achieved. This is shown in *Figure 130*.

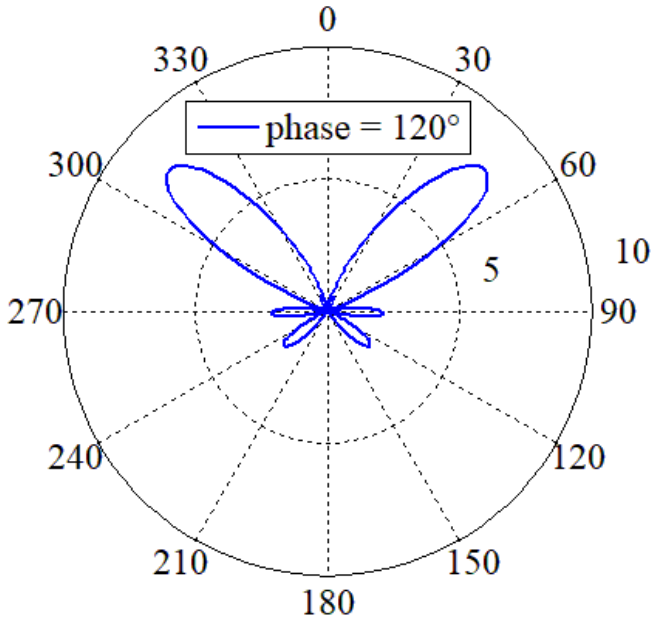

Figure 129: Matlab Simulation with 120º uniform phase shift increments.

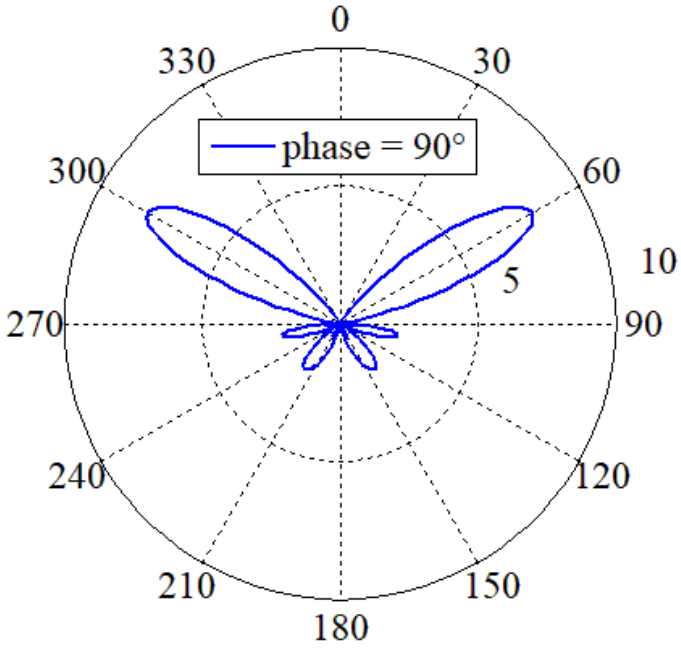

Figure 130: Matlab Simulation with 90º uniform phase shift increments.

CHAPTER 6: CONCLUSION AND FURURE WORK

6.1 Conclusion

In conclusion, the HFSS simulated and measured results for the antenna radiation pattern agree with each other in their general features. Both measured and simulated radiation patterns are steered in directions that were predicted in the design. The phase shift obtained from addition of each transmission line did not quite agree with what was expected. The hypothesis was to obtain a phase shift of 90º, 180º and 270º with respect to the reference phase shift. An effort was made to realize these phase shifts but, in the design, realized there was no space left to place the switches. The tight space between the transmission lines in phase shifter network would introduce more undesirable coupling. Therefore, the microstrip lines were made longer and the propose phase shift was therefore not obtained. A longer transmission line may have produced a phase shift in an increment of 120º to obtain a beam steering of ±45º. Also, the measurement of phase shift was performed by looking at the return loss signal. The actual phase difference may be different if it was measured in a forward signal. This measurement was not possible in a single port network system. A lack of time domain reflectometer also limited us from measuring the phase shift directly.

Nevertheless, the measured results for antenna performance correlated well with the simulated results. The realized antenna was able to make a beam steering of ±45º. A similar approach can be applied to achieve a compact in phase shifter for other applications requiring a steerable beam pattern. This method of phase shifting is useful for antenna arrays for small electronic devices that have area constraints. The phase shifter has a potential use in diverse applications requiring MIMO and beam steering technologies. This

compact design can replace bulky and costly Butler matrices discussed in chapter 1. This allows the design to be implemented in small electronic devices we use in everyday life.

6.2 Future Work

There are a few improvements to the phased array antenna left for the future due to limited time to implement in this thesis. The phased array antenna shown in Chapter 4 with a micro-controller to control the individual switches did not work properly due to lack of ground plane on the phase shifter board. The design and fabrication with a multi-layer board would have solved this problem. The shift in center frequency was found on measured and simulated antenna results due to mutual coupling. This could be improved placing a meta-material between antenna elements. Both of these could be addressed in future work.

The technique implemented in this project to obtain phase shift can be applied to applications at other frequency bands. This method of phase shifting has a potential use for 5G technology, beam steering applications. The size of the antenna can be reduced significantly at 5G frequencies. The antenna also has a potential use as a sensor in an imbedded system. The beam steering ability of the antenna is very useful for scanning objects in the far-field region of the antenna. The single port phased array antenna has a possible use in a scanning radar system as well. Any of these areas would be interesting areas for further investigation and design. It is hoped that some new student will take some of these ideas for future work and improve upon this initial design.

REFERENCES

[1] G. Morrison, "cnet.com," CNET, 11 May 2016. [Online]. Available: https://www.cnet.com/news/atsc-3-0-what-you-need-to-know-about-the-future-of-broadcast-television/. [Accessed 02 12 2018].

[2] N. D. Volkow, "Effects of Cell Phone Radiofrequency Signal Exposure on Brain Glucose Metabolism.," *JAMA: the journal of the American Medical Association,* vol. 305, no. 8, p. 808, 2011.

[3] E. Morgan, "Prepare For Change," 1 December 2018. [Online]. Available: https://prepareforchange.net/2018/12/01/cell-phone-radiation-leads-to-cancer-says-u-s-ntp-in-final-report/. [Accessed 2 December 2018].

[4] K. Sarabandi and F. Wang, "Phased Array of large refglectors for deep-sapce communication," *IEEE Transcations on Aerospace and Electronic Systems,* vol. 43, pp. 251-261, 2007.

[5] T. Kinghorn, I. Scott and E. Totten, "Recent advances in airborne phased array radar systems," in *IEEE International Symposium on Phased Array Systems and Technology (PAST)*, Waltham, MA, 2016.

[6] H. Ren, J. Shao, R. Zhou, B. Arigong, H. K. Kim, C. Li and H. Zhang, "A compact phased array antenna system based on dual-band Butler matrices," in *IEEE Radio and Wireless Symposium*, Austin, TX, 2013.

[7] M. S. R. Bashri, T. Arslan and Z. Wei, "A Dual-band Linear Phased Array Antenna for WiFi and LTE Mobile Applications," in *Loughborough Antennas and Propagation Conference (LAPC)*, Loughborough, 2015.

[8] S. I. Latif, D. A. Nelson and V. La, "An on-body conformal printed array antenna at mmWave frequencies for healthcare applciations," in *17th International Symposium on Antenna Technology and Applied Electromagnetics (ANTEM)*, Montreal, QC, 2016.

[9] Y. Huang, J. Bao, X. Li and Y. Du, "A 4-bit switched line phase shifter based on MEMS switches," in *10th IEEE International Conference on Nano/Micro Engineered and Molecular Systems*, Xi'an, 2015.

[10] J. Zhang, S. Cheung and Q. Zhu, "Design of 180 degree - switched-line pahse shifter with constant phase shift using CRLH TL," in *2014 IEEE Antennas and Propagation Society International Symposium (APSURSI)*, Memphis, TN, 2014.

[11] K. Y. Kapusuz and U. Oguz, "Millimeter wave phased array antenna for modern wireless communication systems," in *10th European Conference on Antennas and propagation (EuCAP)*, Davos, 2016.

[12] F. Huang, W. Chen and M. Rao, "Switched beam antenna array based on butler matrix for 5g wireless communication," in *IEEE International Workshop on Electromagnetics Appliation and Student Innovation Competition (iWEM)*, Nanjing, 2016.

[13] H. C. Nathanson, T. J. Smith, J. C. B. Freidhoff, F. W. Hopwood, J. E. Degenford and J. D. Adam, "Mercury Wetted Switch". United States Patent US5912606A, 18 August 1998.

[14] C. A. Balanis, in *Antenna Theory: Analysis and Design*, New Delhi, India, Wiley India, 2009, pp. 27-29.

[15] J. D. Kraus, in *Antennas*, McGraw Hill, 1988, pp. 20-23.

[16] M. Hafsal, "VLSI and Embedded System Technical Library," [Online]. Available: http://vetechlib.blogspot.com/2009/08/polarization.html. [Accessed 22 March 2017].

[17] R. Ludwig and G. Bogdanov, "RF Circuit Design: Theory and Application," Pearson Prentice Hall, 2009, pp. 40-97.

[18] S. A. Schelkunoff, "The electromagnetic theory of coaxial transmission lines and cylindrical shields," *The Bell System Technical Journal,* vol. 13, no. no. 4, pp. 532-579, Oct. 1934.

[19] K. L. Kaiser, "Transmission lines and Matching," in *Transmission Lines, Matching, and Crosstalk*, CRC Press, 2005, pp. 3-70 - 3-72.

[20] W. L. Stutzman and G. A. Thiele, "Resonant Antennas: Wires and Patches," in *Antenna Theory And Design*, John Wiley & Sons, Inc., 1998, pp. 164-224.

[21] C. Wolff, "Radar Basics," November 1998. [Online]. Available: http://www.radartutorial.eu/06.antennas/Phased%20Array%20Antenna.en.html. [Accessed 22 April 2017].

[22] M. Kopp, An Introduction to HFSS: Fundamental Principles, Concepts, and Use, Pittsburg, PA: Ansoft, LLC, 2009.

[23] "RT/duroid® 6006/6010LM High Frequency Laminates," Rogers Corporation, 2017. [Online]. Available: https://www.rogerscorp.com/documents/612/acs/RT-duroid-6006-6010LM-Laminate-Data-Sheet.pdf. [Accessed 23 October 207].

[24] "RO4360G2™ Laminates," Rogers Corporation, [Online]. Available: https://www.rogerscorp.com/acs/products/56/RO4360G2-Laminates.aspx. [Accessed 06 12 2018].

[25] M. T. Ali, T. A. Rahman, M. R. Kamarudin and M. N. M. Tan, "A planar antenna array with seperated feed line for higher gain and sidelobe reduction.," *Progress In Electromagnetics Research C*, vol. 8, pp. 69-82, 2009.

[26] R. Munson, "Conformal Microstrip Antennas and Microstrip Phased Arrays," *IEEE Transactions on Antennas and Propagation*, vol. 22, no. 1, pp. 74-78, 1974.

[27] P. Semiconductor, "8," 2003-2010. [Online]. Available: https://www.psemi.com/pdf/datasheets/pe4246ds.pdf. [Accessed 2018 November 2018].

[28] Digi-Key, "Digi-Key Corporation," [Online]. Available: https://www.digikey.com/product-detail/en/murata-electronics-north-america/LLL216R71E104MA01L/490-4346-1-ND/1022490. [Accessed 14 November 2018].

ABBREVIATIONS

PAA: Phased Array Antenna

MEMS: Micro-electro Mechanical Switches

HPBW: Half Power Beam Width

DC: Direct Current

RF: Radio Frequency

VSWR: Voltage Standing Wave Ratio

HFSS: High Frequency Structural Simulator

FEM: Finite Element Method

PEC: Perfect Electric Conductor

PML: Perfectly Matched Layer

RLC: Resistor Inductor Capacitor

2D: Two Dimensional

3D: Three Dimensional

mm: Milli-Meter

SPST: Single-Pole Single-Throw

CMOS: Complementary-Metal Oxide Semiconductor

BW: Band-Width

SISO: Single Input Single Output

APPENDIX A

```
%%%%%%%%%%%%%%%%%%%%%%%%%%%%%%%%%%%%%%%%%%%%%%%%%%%%
%This code produces a beam steering polar plot
%with given phase shift.
%%%%%%%%%%%%%%%%%%%%%%%%%%%%%%%%%%%%%%%%%%%%%%%%%%%%
clear all
%Center Frequency 5 GHz
center_f=5*10^9;
%Speed of light
c=3*10^8;

%5001 points between 4.75 GHz - 5.25 GHz
f=linspace(4.75e9,5.25e9,5001);
%Wave length
lamda=c./f;
%wave number
beta=2*pi./lamda;
%distance between antenna element
d=c/(2*center_f);

%for 90 degree phase shift
%PhaseShift=270;%90 is same as 270
%for 120 degree phase shift
PhaseShift=240;%120 is same as 240
phase=[PhaseShift,PhaseShift,PhaseShift]*pi/180;
theta=linspace(-1*pi,pi,360);
R=2; %far field distance (arbitrary distance)
E=exp(-1i*beta*R)/(4*pi*R); %electric field

beta_d=beta*d;

%Array Factor
AF=1+exp(1i*(beta_d'*cos(theta)+phase(1)))+exp(2*1i*(beta_d'*cos(theta)
+phase(2)))+exp(3*1i*(beta_d'*cos(theta)+phase(3)));

polar(theta,AF(2501,:))
angle=(phase(1))*180/pi;
view([90 -90]);
text=['phase = ',num2str(360-angle),char(176)];
legend(text);
```